National Library of Canada
Canadian Theses Service
Ottawa, Canada
K1A 0N4

Bibliothèque nationale du Canada
Services des thèses canadiennes

CANADIAN THESES

THÈSES CANADIENNES

NOTICE

The quality of this microfiche is heavily dependent upon the quality of the original thesis submitted for microfilming. Every effort has been made to ensure the highest quality of reproduction possible.

If pages are missing, contact the university which granted the degree.

Some pages may have indistinct print especially if the original pages were typed with a poor typewriter ribbon or if the university sent us an inferior photocopy.

Previously copyrighted materials (journal articles, published tests, etc.) are not filmed.

Reproduction in full or in part of this film is governed by the Canadian Copyright Act, R.S.C. 1970, c. C-30.

AVIS

La qualité de cette microfiche dépend grandement de la qualité de la thèse soumise au microfilmage. Nous avons tout fait pour assurer une qualité supérieure de reproduction.

S'il manque des pages, veuillez communiquer avec l'université qui a conféré le grade.

La qualité d'impression de certaines pages peut laisser à désirer, surtout si les pages originales ont été dactylographiées à l'aide d'un ruban usé ou si l'université nous a fait parvenir une photocopie de qualité inférieure.

Les documents qui font déjà l'objet d'un droit d'auteur (articles de revue, examens publiés, etc.) ne sont pas microfilmés.

La reproduction, même partielle, de ce microfilm est soumise à la Loi canadienne sur le droit d'auteur, SRC 1970, c. C-30.

THIS DISSERTATION HAS BEEN MICROFILMED EXACTLY AS RECEIVED

LA THÈSE A ÉTÉ MICROFILMÉE TELLE QUE NOUS L'AVONS REÇUE

Canada

NL-339 (r.86/06)

THE UNIVERSITY OF ALBERTA

PHOTOLUMINESCENCE STUDIES OF CARBON IN SEMI-INSULATING GALLIUM ARSENIDE

by

(C) TEH CHIN KHUAN

A THESIS

SUBMITTED TO THE FACULTY OF GRADUATE STUDIES AND RESEARCH

IN PARTIAL FULFILMENT OF THE REQUIREMENTS FOR THE DEGREE

OF DOCTOR OF PHILOSOPHY

IN

SOLID STATE PHYSICS

DEPARTMENT OF PHYSICS

EDMONTON, ALBERTA

SPRING 1987

Permission has been granted to the National Library of Canada to microfilm this thesis and to lend or sell copies of the film.

The author (copyright owner) has reserved other publication rights, and neither the thesis nor extensive extracts from it may be printed or otherwise reproduced without his/her written permission.

L'autorisation a été accordée à la Bibliothèque nationale du Canada de microfilmer cette thèse et de prêter ou de vendre des exemplaires du film.

L'auteur (titulaire du droit d'auteur) se réserve les autres droits de publication; ni la thèse ni de longs extraits de celle-ci ne doivent être imprimés ou autrement reproduits sans son autorisation écrite.

ISBN 0-315-37666-X

Letter of Permission

The undersigned hereby grant permission to TEH CHIN KHUAN to include any relevant material from the papers that she has coauthored with us in her thesis entitled PHOTOLUMINESCENCE STUDIES OF CARBON IN SEMI-INSULATING GALLIUM ARSENIDE.

F. L. Weichman

.....

Dr. F.L. Weichman

Tin Chin Che

.....

Dr. C.C. Tin

Date: March 16, 1987

THE UNIVERSITY OF ALBERTA

RELEASE FORM

NAME OF AUTHOR: TEH CHIN KHUAN

TITLE OF THESIS: PHOTOLUMINESCENCE STUDIES OF CARBON IN SEMI-INSULATING GALLIUM ARSENIDE

DEGREE FOR WHICH THESIS WAS PRESENTED: DOCTOR OF PHILOSOPHY

YEAR THIS DEGREE GRANTED: SPRING 1987

Permission is hereby granted to THE UNIVERSITY OF ALBERTA LIBRARY to reproduce single copies of this thesis and to lend or sell such copies for private, scholarly or scientific research purposes only.

The author reserves other publication rights, and neither the thesis nor extensive extracts from it may be printed or otherwise reproduced without the author's written permission.

(SIGNED) .....

PERMANENT ADDRESS:

SUNGAI RAYA ESTATE

BATU PAHAT, JOHORE

MALAYSIA

DATED 16TH OF MARCH, 1987

THE UNIVERSITY OF ALBERTA

FACULTY OF GRADUATE STUDIES AND RESEARCH

The undersigned certify that they have read, and recommend to the Faculty of Graduate Studies and Research for acceptance, a thesis entitled PHOTOLUMINESCENCE STUDIES OF CARBON IN SEMI-INSULATING GALLIUM ARSENIDE submitted by TEH CHIN KHUAN in partial fulfilment of the requirements for the degree of DOCTOR OF PHILOSOPHY in SOLID STATE PHYSICS.

Frank L. Weichman
.....
Supervisor

D.G. Hughes
.....

S.R. Morrison
.....

A.P. Roscoe
.....

A. Kalnins
.....

Alain Roth
.....
External Examiner

Date: March 16, 1987

DEDICATED

TO

MY MOTHER

AND TO THE

LOVING MEMORY OF MY FATHER

Abstract

In undoped liquid-encapsulated Czochralski-grown semi-insulating gallium arsenide (LEC SI GaAs), carbon forms an acceptor level, C_{As}, which is responsible for the ~1.49 eV donor-acceptor (D-A) pair radiative recombination at low temperatures. We have measured the decay and the line-shape of the photoluminescence signals at and near the D-A emission peak for temperatures ranging from 4.1 to 34 K, for several samples of LEC SI GaAs with different carbon concentrations, to study the effects of the different carbon concentrations on the photoluminescence signal.

Detailed analysis shows that a competitive process exists between the band-to-acceptor (B-A) and D-A emissions. The results also show that the D-A emission due to carbon can be explained by a hydrogenic model involving Coulomb interaction between D-A pairs of separation R, with the most probable D-A transition occurring for $200 < R < 1300$ Å.

The photoluminescence decay has been found to follow a double exponential law at the early stage of the decay but follows a power-law of the form $L(t) \propto t^{-p}$ at a later stage. Analysis of the temperature dependence of the exponential components gives two activation energies of ≃5.7 and ≃15 meV. We propose that these two activation energies are associated with two different donor levels at ≃5.7 and ≃21 meV from the conduction band.

For a photoluminescence decay curve whose time constant follows the Arrhenius relation, we have shown that a new

method of analysis that involves measuring the differential luminescence signal as a function of temperature is simpler than using a non-linear least-squares method.

The exponent, p, of the power-law decay is found to be both temperature (T) and concentration dependent of the form $p = -1 + \beta T$, where β is proportional to the concentration of the acceptors, C_{As}, in the temperature range $18 < T < 30$ K.

Several mechanisms were considered to account for both the exponential and the power-law behaviors. We propose that the most likely mechanism is a thermal detrapping process followed by thermalization into lower energy states through a hopping mechanism.

Acknowledgements

The author would like to thank the following who have made contributions, in one way or another, to the process that culminates in the writing of this thesis:

Dr. F.L. Weichman, my thesis supervisor, for his guidance, understanding and patience,

Dr. J.E. Bertie of the Chemistry Department for allowing the use of the FTIR equipment,

Tin Chin Che, my husband, for his encouragement and moral support,

my mother, brothers and sisters, for their encouragement and support during my time of need,

Dr. Roelof Bult, of Cominco Ltd., Electronic Materials Division, Trail, British Columbia, for providing the samples,

Department of Physics and Cominco Ltd. for financial support in the form of a graduate teaching assistantship and a graduate research assistantship,

Natural Sciences and Engineering Research Council of Canada for supporting the research work,

George Christie, Ken Marsh and the technicians in the Electronics Shop, especially Lars Holm and Bill Burris, for technical assistance and fruitful discussions.

Table of Contents

Chapter Page

1. INTRODUCTION 1

1.1 Liquid-Encapsulated Czochralski Semi-Insulating Gallium Arsenide (LEC SI GaAs) 1

1.1.1 Impurities in LEC SI GaAs 3

1.2 Photoluminescence Spectroscopy 8

1.2.1 Photoluminescence Emission Spectroscopy ...14

1.2.2 Transient Emission Spectroscopy 15

1.3 Fourier Transform Infra-Red (FTIR) Spectroscopy .16

1.3.1 Infra-Red Absorption: Electronic Transitions 18

1.3.2 Infra-Red Absorption: Point Defects in a Lattice 19

Bibliography 22

2. PHOTOLUMINESCENCE SPECTROSCOPY 28

2.1 Theory: Donor-Acceptor Pairs and Band-to-Acceptor Transitions 28

2.1.1 Radiative Recombination of Donor-Acceptor Pairs 28

2.1.1.1 Energy Distribution 28

2.1.1.2 Radiative Decay Rate 31

2.1.2 Conduction Band-to-Acceptor Recombination .33

2.2 Data Acquisition and Analytical Methods 34

2.2.1 Data Acquisition 34

2.2.1.1 Photoluminescence Emission Spectra 34

2.2.1.2 Transient Emission Spectra 38

2.2.2 Data Handling and Analysis: Transient Spectra 40

2.2.2.1 Treatment of Data 40

2.2.2.2 Least-Squares Curve Fitting (LSF) .42

Bibliography 45

3. A NEW METHOD OF ANALYSIS OF PHOTOLUMINESCENCE DECAY CURVES 47

3.1 Introduction 47

3.2 Theory and analysis 48

3.3 Experimental procedure and discussion 56

3.4 Conclusion 62

Bibliography 64

4. PHOTOLUMINESCENCE EMISSION SPECTROSCOPY OF LEC SI GaAs 65

4.1 Introduction 65

4.2 Experimental Procedure 65

4.3 Results 68

4.4 Discussion 78

4.5 Conclusion 86

Bibliography 88

5. TRANSIENT EMISSION SPECTROSCOPY OF CARBON IMPURITY IN LEC SI GaAs 90

5.1 Introduction 90

5.2 Experimental Procedure 91

5.3 Results 93

5.4 Discussions 104

5.4.1 Initial double exponential decay 108

5.4.2 Power-law decay 113

5.4.2.1 Existence of intermediate trapping states 113

5.4.2.2 Existence of a random distribution of D-A pairs 115

5.5 Conclusion 121

Bibliography 123

6. FOURIER TRANSFORM INFRA-RED (FTIR) SPECTROSCOPY OF UNDOPED LEC SI GaAs 125

6.1 Introduction 125

6.2 Theory: Fourier Transform Spectroscopy 125

6.3 Data Analysis 127

6.3.1 Concentration Determination 127

6.3.2 Computation of Optical Constants 129

6.4 Experimental Procedure 131

6.5 Results and Discussion 133

6.6 Conclusion 137

Bibliography 140

7. DISCUSSION AND CONCLUSION 142

Bibliography 146

APPENDIX A 147

APPENDIX B 158

VITA 173

List of Tables

Table		Page
3.1	Results obtained using two different methods of analysis	59
4.1	Concentration dependence of emission energy and D-A pair distance	74
5.1	Activation energies for samples with different carbon concentrations	97
5.2	Decay time constants of a sample with $N=1.08\times10^{15}cm^{-3}$	101
5.3	Activation energies, ΔE_a	102
5.4	Values of α_o and β in $p=\alpha_o+\beta T$ for $18\leq T\leq 30K$	105
6.1	Carbon concentrations measured at LVM absorption	136
6.2	Experimental and calculated α values	138

List of Figures

Figure		Page
1.1	Photoluminescence process in a direct-gap semiconductor	10
2.1	Donor-acceptor pair transition	30
2.2	Emission energies as a function of pair distance R	30
2.3	Block diagram for the data acquisition system	37
3.1	Theoretical curves of PTS for different activation energies	52
3.2	Theoretical curves of PTS for different delay times with close activation energies	53
3.3	Theoretical curves of PTS for different relative amplitudes	54
3.4	Theoretical curves of PTS for different delay times with large relative amplitudes	55
3.5	Experimental curves of PTS for Cu_2O	60
3.6	Graph of ln τ vs $10^3/T_m$ for 2 types of Cu_2O crystals	61
4.1	Photoluminescence system	66
4.2	A typical emission spectrum of undoped LEC SI GaAs	69
4.3	Luminescence intensity as a function of carbon concentration	70
4.4	Variation of emission energies as a function of carbon concentration	71
4.5	Comparison between experimental and theoretical values	72
4.6	Temperature dependence of luminescence emissions	75
4.7	Temperature dependence of luminescence at a higher resolution	76
4.8	Effect of annealing on the luminescence of D-A pairs	77

Figure		Page
4.9	Theoretical fit of the B-A band	85
5.1	Photoluminescence transient experiment	92
5.2	A typical decay curve at the ~1.49 eV emission at 4.1 K	94
5.3	Decay curves shown for three different temperatures	95
5.4	Temperature dependence of the exponential decay τ_b	98
5.5	Temperature dependence of the exponent p for different carbon concentration, N	99
5.6	Temperature dependence of decay time constant τ_a	103
5.7	Linear temperature dependence of exponent p in $18 \leq T \leq 30K$	106
5.8	Concentration dependence of β	107
5.9	Energy band diagram for photoluminescence	111
5.10	Schematic energy diagram with a set of traps	111
5.11	Decrease in recombination rate due to interaction between neighbouring states of similar kind	118
5.12	Non-radiative recombinations between neighbouring states	120
6.1	FTIR spectrometer	132
6.2	A typical transmission spectrum of LEC SI GaAs	134
A.1	TS1000 I/O interface and A-D converter	151
A.2	Peak detector	152
A.3	Monochromator driver	153
A.4	RS232 Serial interface	154
A.5	Data acquisition program	155
B.1	Non-linear least-squares program	159

1. INTRODUCTION

1.1 Liquid-Encapsulated Czochralski Semi-Insulating Gallium Arsenide (LEC SI GaAs)

Gallium arsenide (GaAs) is a direct band-gap III-V compound semiconductor. The potential uses of GaAs are in the making of high-speed devices which are especially useful in high-speed computers and communications. There are two main advantages of GaAs over silicon as material for high frequency devices. GaAs has a high mobility (electron mobility of GaAs at 300 K can attain a value of 8500 $cm^2V^{-1}s^{-1}$ compared to 1500 $cm^2V^{-1}s^{-1}$ for Si (Sze and Irvin, 1968)) and high drift velocity, $\sim 10^7$ cm s^{-1} at 300 K, which is at least twice the value for Si under the same field, hence devices made from GaAs can easily operate in the microwave frequency range where Si devices fail. The other advantage is that GaAs can be grown to be semi-insulating (SI) with resistivity $\rho > 10^8$ Ω cm, compared to Si (in the purest form) with $\rho \sim 10^3$ Ω cm. The semi-insulating property allows SI GaAs to be used as a substrate for GaAs devices where device isolation and low parasitic capacitance are important for full integration on a single chip. Besides the two principal advantages of GaAs over Si, GaAs devices can also withstand higher ionizing radiation intensity. Therefore GaAs is more suitable for space and military applications. Since GaAs is a direct gap semiconductor, it is also suitable for making optical devices such as lasers

and light emitting diodes (LED's) (Kressel and Butler, 1977). GaAs can also be used in the making of solar cells.

The potential uses of GaAs devices have created a demand for better quality semi-insulating GaAs material on which devices can be fabricated. The quality of the substrate material has a direct bearing on the reliability and performance of GaAs devices. A better understanding of the properties of such material is thus of importance to the production of SI GaAs with the required characteristics, such as high thermal stability and reproducible electrical properties.

Large crystals of semi-insulating GaAs can be manufactured by two principal methods (Kirkpatrick *et al.*, 1985; Mullin, 1975; Kaldis 1985): *liquid-encapsulated Czochralski* (LEC) and *Horizontal Bridgman* (HB). In the former method, the crystal is grown vertically by pulling it from a melt through a molten boric oxide (B_2O_3) encapsulant under high pressure, while in the latter method, the crystal is grown horizontally from the melt inside a sealed horizontal boat equipped with heaters that generate a temperature profile along the boat, or by pulling the boat through a gradual changing temperature gradient. The HB method imposes a size restriction on the wafer slices, hence the LEC method is preferred in the manufacturing of large circular wafers. Large circular wafers are preferred because fabrication of GaAs devices on such wafers can take full advantage of the existing processing technology which has

been developed for the silicon device industry.

1.1.1 Impurities in LEC SI GaAs

In the production of SI GaAs, impurities are often incorporated unintentionally. For example, carbon, which can originate from the graphite furnace transported in the form of a gaseous compound, such as CO, as well as being present in the starting material (arsenic), is a common impurity in GaAs. Silicon and copper are impurities that can originate from the quartz crucibles. Boron contamination comes from the B_2O_3 encapsulant or boron nitride (BN) crucibles. Other impurities such as O, Al, Mg, Fe and Ca are also present in minute quantities either in the starting materials or from the growth environment or both (Redden and Lent, 1986; Kirkpatrick *et al.*, 1984; Thomas *et al.*, 1984).

The presence of undesirable impurities reduces the resistivity of the material. Such unintentional doping is often compensated by intentional introduction of chromium into the material to produce the semi-insulating behavior. SI GaAs can be grown without any intentional doping and this type of material is most widely used. The resistivity of the GaAs material has been found to depend on the melt stoichiometry, with arsenic-rich melt favouring high resistivities (Holmes *et al.*, 1982a). The compensating level in the undoped material is a deep electron trap, designated as EL2, with an energy level located at E_c-0.75 eV (Martin *et al.*, 1977; Martin, 1980, 1981; Holmes *et al.*, 1982). The

EL2 deep donor level has been reported to be related to the antisite defect As_{Ga} (Wagner *et al.*, 1980; Elliott *et al.*, 1982; Lagowski *et al.*, 1982; Weber *et al.*, 1982). The exact nature of EL2 is still a controversial subject. This native defect has been widely studied by photoluminescence, where emission peaks at 0.68 eV (Yu *et al.*, 1982; Yu, 1984), 0.65 eV (Tajima, 1982), and 0.645 eV (Mircea-Roussel and Makram-Ebeid, 1981) have been reported, as well as by other optical and electrical methods (Brozel *et al.*, 1983; Shanabrook *et al.*, 1983; Martin and Makram-Ebeid, 1984). Unfortunately, due to the wavelength limitation of our present detector, this subject could not be investigated here.

The electrical performance of devices depends on the quality and stability of the semi-insulating GaAs substrate, which in turn depends strongly on the contamination and purity of the material. The presence of any impurity or defect in large amounts in the substrate material degrades device performances because the electron mobility is reduced by ionized impurities. Impurities have the tendency to cluster around dislocations and the propagation of decorated dislocations from the substrate into the device material is known to be the most common cause of device failure (Davey and Christou, 1981; Newman and Ritchie, 1981). During device processing (after ion implantation), the substrate must undergo an annealing cycle (800-900°C) to activate the implant and heal the lattice damage (Morgan and Eisen,

1985). It has been shown that high temperature annealing of GaAs causes the formation of a p-type conducting layer on the surface (Ta *et al.*, 1982). The cause of this has been widely studied and some reports have attributed this to the redistribution of impurities (Huber *et al.*, 1979; Oshima *et al.*, 1984) and creation of vacancies (Chiang and Pearson, 1975). Excessive and variable concentration of impurities especially Si, Cr, O and C in Cr-doped SI GaAs substrates, will cause non-uniformity in implant profiles.

The principal impurities in LEC GaAs are C, B and Si. The incorporation of carbon and boron impurities in undoped LEC SI GaAs seems to be dependent on the growth conditions, especially on the water content of the B_2O_3 encapsulant (Rumsby and Ware, 1981). Both the C (Hunter *et al.*, 1984) and B (Oliver *et al.*,1981) impurities have been shown to decrease in concentration with increasing water content in the B_2O_3 encapsulant. However, we have seen that some crystals grown with high water content B_2O_3 have high C concentration and that the C concentration increases with the size of the charge used in the growth[¤]. The dependence of the C concentration on the size of the charge indicates the possibility that the C concentration also depends on the amount present in the original starting material. We have also observed that high C content samples always contain high B concentration.

¤Teh, C.K., Tin, C.C. and Weichman, F.L., to be published in the May, 1987 issue of the Canadian Journal of Physics.

Boron is an isoelectronic impurity in GaAs, which gives rise to the LVM absorptions at 517 ($^{11}B_{Ga}$) and 540 cm^{-1} ($^{10}B_{Ga}$) (Thompson and Newman, 1972) for two different isotopes of B with natural abundance of 81% ^{11}B and 19% ^{10}B.

Due to the amphoteric behavior of silicon, it can be a substitutional impurity at either the Ga or As sites giving rise to either a shallow donor or acceptor respectively. The LVM absorptions are at 384 ($^{28}Si_{Ga}$) and 398 cm^{-1} ($^{28}Si_{As}$) (Thompson and Newman, 1972), and ionization energies of 5.85 and 35.2 meV (Watts, 1977) have been documented for the donor and acceptor levels respectively.

Carbon

The dominant shallow acceptor in undoped semi-insulating GaAs grown by the liquid-encapsulated Czochralski technique (LEC SI GaAs) from pyrolytic BN crucibles has been identified as carbon (Holmes *et al.*, 1982, 1982a; Ta *et al.*, 1982; Kirkpatrick *et al.*, 1984). The LVM absorption of C_{As} is at 582 cm^{-1} (Brozel *et al.*, 1978; Theis *et al.*, 1982).

Carbon in epitaxial GaAs has been studied extensively using photoluminescence spectroscopy and it has been accepted as a shallow acceptor level, C_{As}, with an ionization energy of ≈26 meV (Ashen *et al.*, 1975; Sze and Irvin, 1968). The luminescence lines of carbon are well known to be at 1.493 and 1.490 eV, which have been attributed to the conduction band-to-acceptor (B-A) transition (or sometimes referred to as free-to-bound

transition), and the donor-to-acceptor (D-A) transition respectively (Ozeki *et al.*, 1974; Ashen *et al.*, 1975; Jeong *et al.*, 1981; Stringfellow *et al.*, 1981).

The concentration of C impurity in undoped LEC SI GaAs plays an important role in the electrical properties of the material. The semi-insulating behavior in the undoped GaAs is due to the compensation mechanism of EL2 deep donors by carbon shallow acceptors (Holmes *et al.*, 1982a). However, the presence of a high concentration of C is undesirable. Obokata *et al.* (1986) have found that a high carbon content ($> 1.5 \times 10^{16}$ cm^{-3}) in the substrate degrades the thermal stability of the resistivity. The variation of the carbon concentration in the substrate material is also known to affect the threshold voltage for the ion-implanted layers used in FET's (field effect transistors). High carbon concentration was found to produce low threshold voltage (Chen *et al.*, 1984; Kirkpatrick *et al.*, 1985). Hence, the uniformity of the C concentration across a wafer and across a boule is crucial to the production of FET's. In view of the role of carbon in the compensation mechanism for providing the semi-insulating property, a complete removal of carbon is not recommended. Besides, it is almost impossible for the material to be completely free from carbon.

Therefore, the characterization of defects and impurities, and concentration determination, especially that of carbon, are important for the production of high quality

substrate material.

Photoluminescence (PL) and Fourier Transform Infra-Red (FTIR) spectroscopies have been used for the study of undoped LEC SI GaAs. Although FTIR alone can characterise the impurities (from the localized vibrational modes (LVM) absorption frequencies) and the impurity concentrations (from the absorption strengths), photoluminescence is still needed to study the recombination processes. From the analysis of the photoluminescence decay, detailed recombination mechanisms can be postulated. In addition, the types of centers that an impurity can form can be determined from the line-shape of the emission spectrum.

In this thesis we will concentrate on the carbon impurity in undoped LEC SI GaAs, studied by a combination of photoluminescence emission, photoluminescence transient and FTIR spectroscopies.

1.2 Photoluminescence Spectroscopy

When a semiconductor or insulator is irradiated with light of energy greater than its band-gap, electrons are excited from the valence band to the conduction band. Hence electron-hole pairs are created within the penetration depth of the exciting light. The recombination of these photo-excited carriers can occur via exciton recombinations and via free carrier recombinations in two different ways. That is, either by direct band-to-band transition or transition via some intermediary states in the forbidden

band which are produced by various impurities or imperfections. In some cases, these can result in the emission of optical radiation. This phenomenon of optical radiation (in excess of thermal radiation) is known as *photoluminescence*. The emitted radiation, which is often referred to as luminescence, is characteristic of the luminescent material. The term *luminescence* is also generally used for the process of light emission.

Photoluminescence spectroscopy has been developed into a very useful non-destructive contactless technique of defect characterization in semiconductors (Williams and Bebb, 1972). Due to the presence of impurities or defects in a semiconductor, localized electronic states are formed within the band-gap either as donors or acceptors according to the nature of the impurities or defects. The photoluminescence process in a semiconductor such as GaAs, can be explained according to figure 1.1. The creation of electron-hole pairs (figure 1.1 a) in the irradiated region, leads to an inhomogeneous distribution of excess carriers in a non-equilibrium system. Due to the mutual attraction between the electrons and the holes, these excess photo-excited carriers can exist as pairs or excitons. The electron-hole pairs will diffuse away from the illuminated surface until they are trapped at impurity or defect centers. In order to restore its homogeneous, equilibrium ground state, recombination takes place either through radiative or non-radiative processes. Radiative

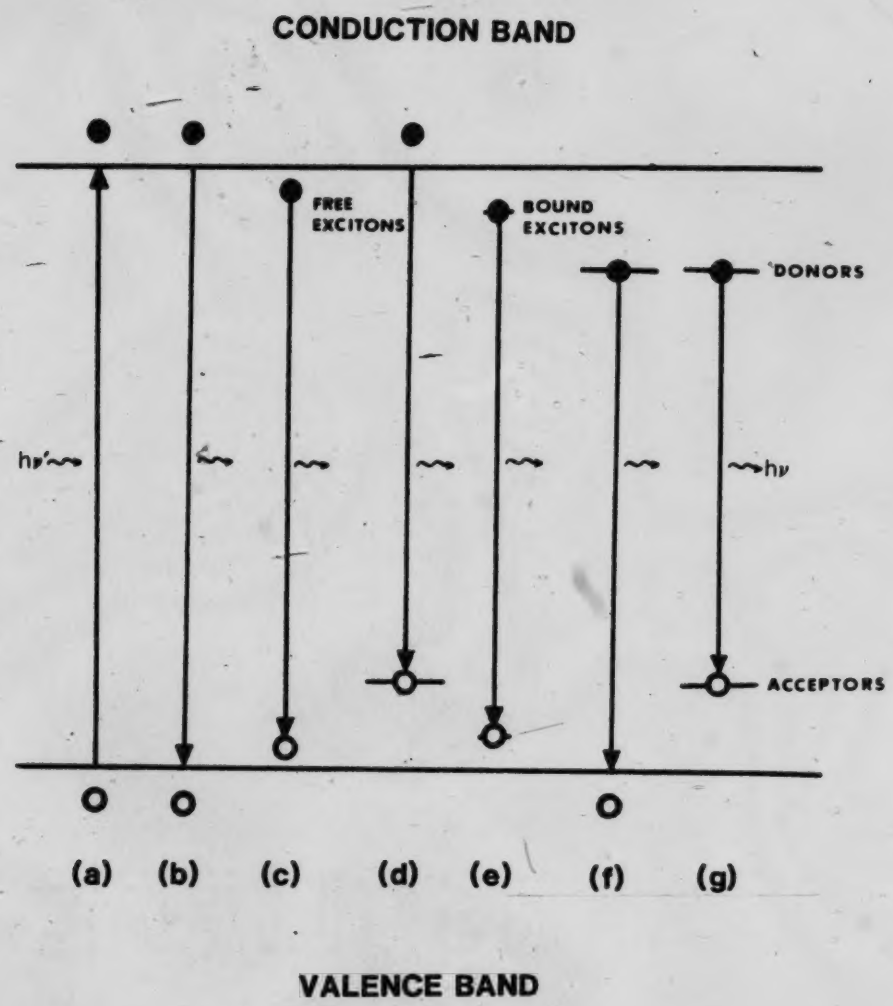

Figure 1.1 Photoluminescence process in a direct-gap semiconductor

recombination processes can result from transitions between the following different states within the band-gap:

a) band-to-band (B-B) recombination (figure 1.1 b),

b) free exciton (X) recombination (figure 1.1 c),

c) band-to-acceptor (B-A) recombination (figure 1.1 d),

d) bound exciton recombination (can be bound to donor or acceptor, i.e., D^0,X or A^0,X) (figure 1.1 e),

e) donor-to-band (D-B) recombination (figure 1.1 f), and

f) donor-to-acceptor (D-A) recombination (figure 1.1 g).

The emitted energy, which is the energy difference between the two states, is characteristic of the band-gap and of the nature of the impurities in the semiconductor. The recombination radiation must survive the probability of self-absorption and internal reflection at the surface in order to be detected as luminescence. Thus, the photoluminescence technique can provide information on the intrinsic and extrinsic semiconductor properties. This method is particularly suitable for shallow states which usually control the electrical properties. Certain deep states can also be studied provided that they form radiative centers. In all cases, photoluminescence measurements are usually carried out at low (cryogenic) temperatures where detailed spectroscopic information about electronic processes can be extracted.

Photoluminescence can be detected in two principal ways. One method is the most commonly used front surface photoluminescence where emission is collected from the same

side as the illuminated surface. The other method is by collecting the emission from the back surface and is known as transmission photoluminescence. The former is widely used as self-absorption can be avoided. Because most recombination processes occur within the attenuation length of the irradiated surface, the luminescence is mainly from the front surface, making the collection of luminescence easier.

The emission of luminescence can be studied by several techniques. The photon yields of an emission band can be measured as a function of *excitation* wavelength (or energy), hence termed *photoluminescence excitation spectroscopy*. *Photoluminescence emission spectroscopy*, on the other hand, is a study of the luminescence intensity as a function of *emission* wavelength when the luminescent material is irradiated by a monochromatic source of constant intensity. From these photoluminescence spectra, information on the radiative efficiency and the position of the energy level for the defect can be obtained, together with the identity of the defect, such as simple point defect or complex defect. For example, the type of center can be determined from the study of the line-shape of the emission peak. Simple centers can be fitted with a hydrogenic model. Peaks that deviate from the hydrogenic model could be complexes if they are broad and of low energy. Detailed analysis of the symmetry of the peak can also reveal the overlapping of more than one emission line due to the proximity of the emitted energies.

Another aspect of photoluminescence emission studies is the measurement of the time dependence of the photoluminescence emission following a pulsed excitation. Overlapping emissions with different decay times can be resolved by either *time-resolved spectroscopy* or *photoluminescence transient spectroscopy* (PTS)(Teh *et al.*, 1986). The former measures the emission spectra at a delayed time (variable) after the excitation pulse. There are various methods of data acquisition for time-resolved measurements which are used according to the time regime of interest (Hamilton *et al.*, 1978), and the most commonly used method is time-correlated single photon counting (O'Connor and Phillips, 1984). In the PTS method, which was based on the technique of deep level transient spectroscopy (DLTS) and photo-induced transient spectroscopy (PITS), the differential luminescence intensity is measured as a function of temperature at various instants of time following the extinction of the excitation pulse. The differential luminescence intensity can be obtained by direct subtraction done instrumentally with respect to the corresponding time-channels. This technique is applicable only if the decay times, τ, follow the Arrhenius relation: $\tau \propto \exp(E/kT)$, where E is the activation energy, k is the Boltzmann constant, and T is the temperature. The latter technique does not require a monochromator in the analysis of the signal once an initial calibration has been made. Details of the method are discussed in Chapter 3. The

identification of the defects or impurities is obtained from the peaks of the differential luminescence versus temperature plot together with the values of the activation energies.

1.2.1 Photoluminescence Emission Spectroscopy

The presence of C and Si in GaAs gives rise to shallow acceptor and donor states. At the lowest temperature, excess photo-excited carriers are often captured by these shallow states before recombination occurs. It is therefore common for radiative recombinations to occur predominantly as donor-acceptor (D-A) pair recombinations. Evidence for D-A pair radiative recombination in GaP has been widely presented (Hopfield *et al.*, 1963; Thomas *et al.*, 1964; Gershenzon, 1966; Dean *et al.*, 1968, 1970). In GaAs, because of the small donor and acceptor binding energies, emissions due to near D-A pairs will lie above the band-gap (Gershenzon, 1966a), thus only radiative recombinations due to distant D-A pairs separated by great distances have been observed (Dingle, 1969; Kamiya and Wagner, 1976).

The carriers in the shallow states often suffer thermal emission back into the band states when the temperature is raised, thereby increasing the probability of direct band-to-band recombination. In the case where the donor binding energies are very small (~6 meV in GaAs) compared to the acceptor binding energies, free-to-bound (F-B) transitions (from conduction band to acceptors) are easily

seen when D-A pair spectra are thermally quenched (Ashen, *et al.*, 1975; Bindermann *et al.*, 1978; Quisser, 1976). For example, in epitaxial layers of GaAs doped with Ge (Schairer and Graman, 1969), Mn (Schairer and Schmidt, 1974), Zn, Si, and C (Ashen *et al.*, 1975, Roth *et al.*, 1983), the F-B transitions have been observed to become prominent as temperature increases.

Since carbon in GaAs is known to give D-A emissions (Ozeki *et al.*, 1974) at low temperatures, we decided to study these D-A radiative recombinations in the photoluminescence emission spectroscopy of LEC SI GaAs.

1.2.2 Transient Emission Spectroscopy

The study of recombination processes in semiconductors is important because they determine the lifetimes of non-equilibrium charge carriers and thus control the parameters of semiconductor devices. A reduction in the lifetime of the charge carriers can improve the performance of high speed devices such as fast photodetectors (Lee, 1977), which are used in optical communications, and fast optoelectronic switches (Mourou and Knox, 1979). Leonberger and Moulton (1979) have shown that the lifetime of the photoexcited carriers can be reduced by introducing deep centers into the semiconductor materials.

The free carrier radiative recombination lifetimes for the band-to-band transition in both heavily doped and undoped crystalline GaAs have been studied extensively and

lifetimes ranging from picoseconds to microseconds have been observed (Nelson and Sobers, 1978; Weiner and Yu, 1984).

Radiative recombination processes involving Si in heavily doped expitaxial GaAs (Gobel and Graudszus, 1982) and impurity complexes in low-resistivity GaAs have also been investigated (Glinchuk et al., 1981). Donor-acceptor pair radiative lifetimes in both epitaxial and bulk GaAs involving C, Si, Zn, and Ge have also been studied (Kamiya and Wagner, 1976; Dingle and Rodgers, 1969; Dingle, 1969). However, most of the attention has been focused on the initial stage of the decay and most studies of decay time were conducted at temperatures $\leq$ 15 K.

To the best of our knowledge, no work has been reported on the temperature dependence of radiative recombination processes involving the carbon acceptor level, C_{As}, in LEC SI GaAs. Since photoluminescence decay is determined by the kinetics of the relaxation process, it is possible to derive important information, such as the nature of the center, as well as factors that govern the quenching of the photoluminescence signal, by studying the temperature dependence of the recombination processes.

1.3 Fourier Transform Infra-Red (FTIR) Spectroscopy

Optical absorption and photoluminescence are complementary techniques and their merits are comparable. In some cases, the impurity in a material gives very strong absorption and shows a weak luminescence signal or vice

versa.

Infra-red (IR) absorption spectra can be acquired using a conventional IR spectrometer which consists of a continuum source, a scanning monochromator and a detector. There are certain drawbacks with the conventional IR spectrometer, and most of the disadvantages are inherent in the monochromator. Because of the use of a dispersive element such as a prism or grating, the wavelength range is often limited. The measurements are usually very slow, as spectral information at different wavelengths is recorded individually, while the monochromator is scanned slowly through a wavelength region of interest. In addition, another disadvantage is in the restrictions in the size of the entrance and exit slits of the monochromator for high resolution spectra, which attenuate the radiation greatly before reaching the detector. Therefore, if a spectrum over a wide wavelength range with reasonable resolution is required, it is obvious that the scanning monochromator is an inefficient device.

A different widely used technique is based on the principle of the Michelson Interferometer, which involves the interference of two light beams with varying path difference. The spectrum is obtained by Fourier transformation (Fellgett, 1970) of the interferogram measured. Hence, the instrument is called the Fourier Transform Infra-Red (FTIR) spectrometer, sometimes known as an interferometer. The use of the FTIR Spectrometer has three basic advantages, known as i) Fellgett's advantage,

ii) Jacquinot's advantage and iii) Connes' advantage (Griffiths, 1975). The first basic advantage is that spectral information at all frequencies of a broad region of infra-red energy is collected simultaneously during the complete measurement, which accounts for the reduction in measurement time. Jacquinot's advantage is the accomplishment of a greater optical throughput compared to that obtained by a monochromator, which is limited by its slit size for achieving spectra of the same resolution, hence giving an improvement to the signal-to-noise ratio. By using the He-Ne laser interferometer to reference the position of the moving mirror, the frequency can be accurately determined, which accounts for the third basic advantage.

The use of minicomputers in data processing and controlling the FTIR spectrometers also adds very important advantages besides the optical advantages mentioned above. Spectra stored in digital form can be manipulated (e.g. adding or subtracting to remove interferences due to overlapping bands) and displayed with ease. Hence, maximum spectral information can be extracted from the measured spectra.

1.3.1 Infra-Red Absorption: Electronic Transitions

The characteristics of impurities in crystals can be detected from the absorption spectra. It is well known that in the near infra-red region, interband absorptions

resulting from electronic transitions involving deep-level defects can provide information on the content of the impurities. In addition, the band-gap of the material can also be obtained. In high resistivity GaAs, the absorption spectra near the fundamental edge and the mid-gap region have been reported by Sturge (1962). The impurity which has attracted widespread interest and which forms deep-level states in semi-insulating GaAs is chromium (Martin *et al.*, 1979; Martinez *et al*, 1981; Hennel *et al.*, 1981). Oxygen, which forms deep donor traps in GaAs, has also been investigated (Akkerman *et al.*, 1976). When both valence band-to-defect and defect-to-conduction band transitions occur, interpretation of the spectra is difficult because of the inability to distinguish these two processes. These absorption bands are often broad and featureless. They can be due to the overlap of several transitions from different defect levels but with similar transition energies. In addition, absorption resulting from transitions involving shallow levels either merges with the fundamental absorption edge or has absorption energies which are too small to be detected efficiently.

1.3.2 Infra-Red Absorption: Point Defects in a Lattice

It is known that the presence of point defects or substitutional impurities in a crystal will destroy the translational symmetry of the lattice. This disruption of the lattice symmetry will affect the normal modes of lattice

vibration. Depending on the mass of the substituent and the coupling between the substituted atom and its nearest neighbor, the modified modes can occur either at a higher or lower frequency than the maximum frequency of the perfect lattice vibration.

In a compound semiconductor such as GaAs, substitution of one of the host atoms by an impurity atom of a lighter atomic mass (such as carbon, silicon or boron) will cause the resonance modes of vibration (which are due to the localized vibrations of the impurity) to occur at frequencies higher than the maximum frequency of the lattice vibrations. This is true provided that the coupling force constants between the impurity atom and the host lattice are comparable in strength to the force constants between the pairs of host atoms (Newman, 1973; Barker and Sievers, 1975).

In certain materials (e.g. GaP) there exists a gap between the optic and acoustic bands in the lattice vibrational spectrum. The localized modes of the impurities that fall within the gap are known as gap modes. However, in the dispersion curves of GaAs, there is no such gap between the optic and acoustic bands because of the very similar masses of gallium and arsenic. Thus, no gap modes can exist in GaAs (Newman, 1973).

For heavier substitutional atoms or light atoms with weak coupling force constants, the resonance modes of vibrations usually fall within the optical band, and are

known as band modes. Impurities of heavier masses than the host atoms in GaAs have been less studied. A study of the resonant mode due to boron in GaAs has been reported by Angress *et al.* (1980).

The infra-red active localized vibrational modes (LVM) absorptions of impurities with lighter atomic masses such as C, Si, B, P, Al, Li, Mn, Mg, Cd, and Zn in GaAs have been studied extensively (Hayes, 1965; Lorimor and Spitzer, 1967; Thompson and Newman, 1972; Newman *et al.*, 1972; Leung *et al.*, 1972, 1974; Morrison *et al.*, 1974; Brozel and Newman, 1978; Brozel *et al.*, 1978; Theis *et al.*, 1982, 1983; Kleinert, 1983), with the first three elements attracting the most interest. The studies of IR LVM absorptions in ion-implanted species such as Al, P, Si, and C in GaAs (Skolnik *et al.*, 1970, 1971, 1972; Kreitman *et al.*, 1979) have also been reported.

Since the IR LVM absorption always results in sharp absorptions, the identification of such absorption lines serves as a very useful means of identifying impurities. It is also possible to obtain information on the substitutional sites. Furthermore, the concentration of impurities can be determined from the strength of the absorption line.

In addition to the qualitative and quantitative analyses, optical constants, n and k, can also be extracted from the infra-red spectra.

Bibliography

Akkerman, Z.L., Borisova, L.A., and Kravchenko, A.F. (1976). Sov. Phys. Semicond. 10, 590

Angress, J.F., and Gledhill, G.A. (1980). J. Phys. Chem. Solids. 41, 341

Ashen, D.J., Dean, P.J., Hurle, D.T.J., Mullin, J.B., and White, A.M. (1975). J. Phys. Chem. Solids 36, 1041

Barker, A.S., and Sievers, A.J. (1975). Rev. Mod. Phys. 47, Suppl. 2, S1

Bindemann, R., Schwabe, R., and Hansel, T. (1978). phys. stat. sol. (b) 87, 169

Brozel, M.R., Clegg, J.B., and Newman, R.C. (1978). J. Phys. D 11, 1331

Brozel, M.R., Grant, I., Ware, R.M., and Stirland, D.J. (1983). Appl. Phys. Lett. 42, 610

Brozel, M.R., and Newman, R.C. (1978). J. Phys. C 11, 3135

Chen, R.T., Holmes, D.E., and Asbeck, P.M. (1984). Appl. Phys. Lett. 45, 459

Chiang, S.Y., and Pearson, G.L. (1975). J. Appl. Phys. 46, 2986

Davey, J.E., and Christou, A. (1981). In *Reliability and Degradation, Semiconductor Devices and Circuits* (M.J. Howes and D.V. Morgan, eds.), p. 237 (John Wiley & Sons)

Dean, P.J., Faulkner, R.A., and Kimura, S. (1970). Phys. Rev. B2, 4062

Dean, P.J., Henry, C.H., and Frosch, C.J. (1968). Phys. Rev. 168, 812

Dingle, R. (1969). Phys. Rev. 184, 788

Dingle, R., and Rodgers, K.F. Jr. (1969). Appl. Phys. Lett. 14, 183

Elliott, K.R., Holmes, D.E., Chen, R.T., and Kirkpatrick, C.G. (1982). Appl. Phys. Lett. 40, 898

Fellgett, P. (1970). In *Aspen International Conference on Fourier Spectroscopy* (G.A. Vanasse, A.T. Stair and D.J.

Baker, eds.), p. 139

Gershenzon, M. (1966). In *Semiconductors and Semimetals* (R.K. Willardson and A.C. Beer, eds.), vol.2, p.289 (Academic Press, New York)

Gershenzon, M. (1966a). In *Semiconductors and Semimetals* (R.K. Willardson and A.C. Beer, eds.), vol.2, p.316 (Academic Press, New York)

Glinchuk, K.D., Lukat, K., and Rodionov, V.E. (1981). Sov. Phys. Semicond. 15, 772

Gobel, E.O., and Graudzus, W. (1982). Phys. Rev. Lett. 48, 1277

Griffiths, P.R. (1975). *Chemical Infrared Fourier Transform Spectroscopy* (Wiley-Interscience, New York)

Hamilton, T.D.S., Munro, I.H., and Walker, G. (1978). In *Luminescence Spectroscopy* (M.D. Lumb, ed.), p. 149 (Academic Press)

Hayes, W. (1965). Phys. Rev. A 138, 1227

Hennel, A.M., Szuszkiewicz, W., Balkanski, M., Martinez, G., and Clerjaud, B. (1981). Phys. Rev. B 23, 3933

Holmes, D.E., Chen, R.T., Elliott, K.R., Kirkpatrick, C.G., and Yu, P.W. (1982). IEEE Trans. Electron Devices 29, 1045

Holmes, D.E., Chen, R.T., Elliott, K.R., and Kirkpatrick, C.G. (1982a). Appl. Phys. Lett. 40, 46

Hopfield, J.J., Thomas, D.G., and Gershenzon, M. (1963). Phys. Rev. Lett. 10, 162

Huber, A.M., Linh, N.T., Valladon, M., Debrun, J.L., Martin, G.M., Mitonneau, A., and Mircea, A. (1979). J. Appl. Phys. 50, 4022

Hunter, A.T., Kimura, H., Baukus, J.P., Winston, H.V., and Marsh, O.J. (1984). Appl. Phys. Lett. 44, 74

Jeong, M., Shirafuji, J., and Inuishi, Y. (1981). Jpn. J. Appl. Phys. 20, 795

Kaldis, E. (ed.) (1985). *Crystal Growth of Electronic Materials* (North-Holland)

Kamiya, T., and Wagner, E. (1976). J. Appl. Phys. 47, 3219

Kirkpatrick, C.G., Chen, R.T., Holmes, D.E., Asbeck, P.M.,

Elliott, K.R., Fairman, R.D., and Oliver, J.R. (1984). In *Semiconductors and Semimetals* (R.K. Willardson and A.C. Beer, eds.), vol. 20, p. 159 (Academic Press, New York)

Kirkpatrick, C.G., Chen, R.T., Holmes, D.E., and Elliott, K.R. (1985). In *Gallium Arsenide Materials, Devices, and Circuits* (M.J. Howes and D.V. Morgan, eds.), p. 39 (John Wiley & Sons)

Kleinert, P. (1983). phys. stat. sol. (b) 119, K37

Kreitman, M.M., Farmer, J.W., Bajaj, K.K., and Litton, C.W. (1979). Solid State Commun. 32, 553

Kressel, H., and Butler, J.K. (1977). *Semiconductor Lasers and Heterojunction LEDs* (Academic Press, New York)

Lagowski, J., Gatos, H.C., Parsey, J.M., Wada, K., Kaminska, M., and Wolukiewiez, W. (1982). Appl. Phys. Lett. 40, 342

Lee, C.H. (1977). Appl. Phys. Lett. 30, 84

Leonberger, F.J., and Moulton, P.F. (1979). Appl. Phys. Lett. 35, 712

Leung, P.C., Fredrickson, J., Spitzer, W.G., Kahan, A., and Bouthillette, L. (1974). J. Appl. Phys. 45, 1009

Leung, P.C., Skolnik, L.H., Allred, W.P., and Spitzer, W.G.J. (1972). Appl. Phys. Lett. 43, 4096

Lorimor, O.G., and Spitzer, W.G. (1967). J. Appl. Phys. 38, 3008

Martin, G.M. (1980). In *Semi-Insulating III-V Materials* (G.J. Rees, ed.), p. 13 (Shiva, London)

Martin, G.M. (1981). Appl. Phys. Lett. 39, 747

Martin, G.M., and Makram-Ebeid, S. (1984). In *Deep Levels in Semiconductors* (S. Pantelides, ed.); Gordon and Breach.

Martin, G.M., Mitonneau, A., and Mircea, A. (1977). Electron. Lett. 13, 191

Martin, G.M., Verheijke, M.L., Jansen, J.A.J., and Poiblaud, G. (1979). J. Appl. Phys. 50, 467

Martinez, G., Hennel, A.M., Szuszkiewicz, W., Balkanski, M., and Clerjaud, B. (1981). Phys. Rev. B 23, 3920

Mircea-Roussel, A., and Makram-Ebeid, S. (1981). Appl. Phys.

Lett. 38, 1007

Morgan, D.V., and Eisen, F.H. (1985). In *Gallium Arsenide Materials, Devices, and Circuits* (M.J. Howes and D.V. Morgan, eds.), p. 161 (John Wiley & Sons)

Morrison, S.R., Newman, R.C., and Thompson, F. (1974). J. Phys. C 7, 633

Mourou, G. and Knox, W. (1979). Appl. Phys. Lett. 35, 492

Mullin, J.B. (1975). In *Crystal Growth and Characterization* (R. Ueda and J.B. Mullin, eds.), p. 61, 75 (North-Holland)

Nelson, R.J., and Sobers, R.G. (1978). J. Appl. Phys. 49, 6103

Newman, R.C. (1973). *Infrared Studies of Crystal Defects* (Taylor and Francis Ltd., London)

Newman, D.H., and Ritchie, S. (1981) In *Reliability and Degradation, Semiconductor Devices and Circuits* (M.J. Howes and D.V. Morgan, eds.), p. 301 (John Wiley & Sons)

Newman, R.C., Thompson, F., Hyliands, M., and Peart, R.F. (1972). Solid State Commun. 10, 505

Obokata, T., Okada, H., Katsumata, T., and Fukuda, T. (1986). Jpn. J. Appl. Phys. 25, L179

O'Connor, D.V., and Phillips, D. (1984). *Time-correlated Single Photon Counting* (Academic Press)

Oliver, J.R., Fairman, R.D., and Chen, R.T. (1981). Electron. Lett. 17, 839

Oshima, M., Watanabe, K., and Miyazawa, S. (1984). J. Electrochem. Soc. 131, 130

Ozeki, M., Nakai, K., Dazai, K., and Ryuzan, O. (1974). Jpn. J. Appl. Phys. 13, 1121

Quisser, H.J. (1976). Appl. Phys. 10, 275

Redden, R.F., and Lent, B. (1986). Private Communication

Roth, A.P., Charbonneau, S., and Goodchild, R.G. (1983). J. Appl. Phys. 54, 5350

Rumsby, D.H., and Ware, R.M. (1981). Inst. Phys. Conf. Ser. No. 63, p. 573

Schairer, W., and Graman, W. (1969). J. Phys. Chem. Solids

30, 2225

Schairer, W., and Schmidt, M. (1974). Phys. Rev. B10, 2501

Shanabrook, B.V., Klein, P.B., Swiggard, E.M., and Bishop, S.G. (1983). J. Appl. Phys. 54, 336

Skolnik, L.H., Spitzer, W.G., and Kahan, A. (1970). Bull. Am. Phys. Soc. 15, 1614

Skolnik, L.H., Spitzer, W.G., Kahan, A., and Hunsperger, R.G. (1971). J. Appl. Phys. 42, 5223

Skolnik, L.H., Spitzer, W.G., Kahan, A., Euler, F., and Hunsperger, R.G. (1972). J. Appl. Phys. 43, 2146

Stringfellow, G.B., Koschel, W., Briones, F., Gladstone, J., and Patterson, G. (1981). Appl. Phys. Lett. 39, 581

Sturge, M.D. (1962). Phys. Rev. 127, 768

Sze, S.M., and Irvin, J.C. (1968). Solid State Electron. 11, 599

Ta, L.B., Hobgood, A.M., Rohatgi, A., and Thomas, R.N. (1982). J. Appl. Phys. 53, 5771

Tajima, M. (1982). Jpn. J. Appl. Phys. 21, L227

Teh, C.K., Tin, C.C., and Weichman, F.L. (1986). J. Luminescence 35, 17

Theis, W.M., Bajaj, K.K., Litton, C.W., and Spitzer, W.G. (1982). Appl. Phys. Lett. 41, 70

Theis, W.M., Bajaj, K.K., Litton, C.W., and Spitzer, W.G. (1983). Physica 117B and 118B, 116

Thomas, D.G., Gershenzon, M., and Trumbore, F.A., (1964). Phys. Rev. 133, A269

Thomas, R.N., Hobgood, H.M., Eldridge, G.W., Barrett, D.L., Braggins, T.T., Ta, L.B., and Wang, S.K. (1984). In *Semiconductors and Semimetals* (R.K. Willardson and A.C. Beer, eds.), vol. 20, p. 1 (Academic Press, New York)

Thompson, F., and Newman, R.C. (1972). J. Phys. C 5, 1999

Wagner, R.J., Krebs, J.J., Stauss, G.H., and White, A.M. (1980). Solid State Commun. 36, 15

Watts, R.K. (1977). *Point Defects in Crystals*, chap. 8, p. 206 (John Wiley & Sons)

Weber, E.R., Ennen, H., Kaufmann, U., Windschief, J., Schneider, J., and Wasinki, T. (1982). Appl. Phys. Lett. 53, 6140

Weiner, J.S., and Yu, P.Y. (1984). J. Appl. Phys. 55, 3889

Williams, E.W., and Bebb, H.B. (1972). In *Semiconductors and semimetals* (R.K. Willardson and A.C. Beer, eds.), vol. 8, p. 321 (Academic Press, New York)

Yu, P.W. (1984). Appl. Phys. Lett. 44, 330

Yu, P.W., Holmes, D.E., and Chen, R.T. (1982). Inst. Phys. Conc. Ser. No. 63, p. 209

2. PHOTOLUMINESCENCE SPECTROSCOPY

2.1 Theory: Donor-Acceptor Pairs and Band-to-Acceptor Transitions

2.1.1 Radiative Recombination of Donor-Acceptor Pairs

During the growth of crystals, unintentionally incorporated impurities will be ionized at the elevated temperature and can diffuse freely in the melt. If the Coulomb attraction energy between the oppositely charged impurities (donor and acceptor ions) is greater than the thermal motion, associated donor-acceptor (D-A) pairs are usually formed. This associated pair formation is usually enhanced by slow cooling of the crystal. However, if the cooling from high temperature is rapid, impurities will be "frozen" at random sites. Even for a random distribution of impurities, there will be a finite number of donors and acceptors which are close enough to form distant D-A pairs. The number of distant D-A pairs will be dependent on the concentrations of the impurities.

2.1.1.1 Energy Distribution

Consider a semiconductor containing both donors and acceptors separated by a donor-acceptor (D-A) pair distance R as shown in figure 2.1. Due to Coulomb interaction, the donor and acceptor binding energies $E_D + E_A$ are reduced by the Coulomb interaction term, $-\frac{e^2}{\kappa R}$. Hence the emitted recombination radiation is

modified and for distant D-A pairs, the emitted energy is approximately given by (Hopfield *et al.*, 1963; Dean, 1969):

$$h\nu(R) = E_g - (E_D + E_A - \frac{e^2}{\kappa R}) , \qquad (2.1)$$

where E_g is the band-gap energy, e is the electronic charge, and $\kappa = 4\pi\epsilon\epsilon_0$ (where ϵ is the static dielectric constant).

The Coulomb interaction term increases for decreasing pair distance, thus increasing the energy of the emission as shown in figure 2.2, and the lowest possible energy is obtained for pairs at infinite distance apart where the interaction term approaches zero, i.e.,

$$h\nu(\infty) = E_g - (E_D + E_A) . \qquad (2.2)$$

Since the impurities usually occupy substitutional sites, the R values are discrete. Hence, a spectrum of discrete lines is expected for distant D-A pairs separated by small R distance. These discrete emission lines have been observed in GaP (Hopfield *et al.*, 1963; Thomas *et al.*, 1964). When the distant D-A pair separation increases, the line separation decreases and the lines usually merge together to form a broad band. At the same time the recombination lifetimes increase with separation.

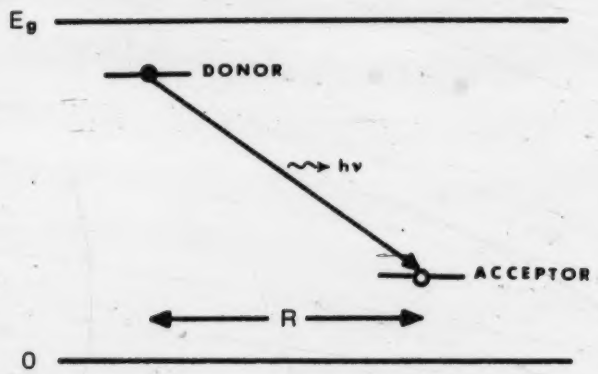

Figure 2.1 Donor-acceptor pair transition

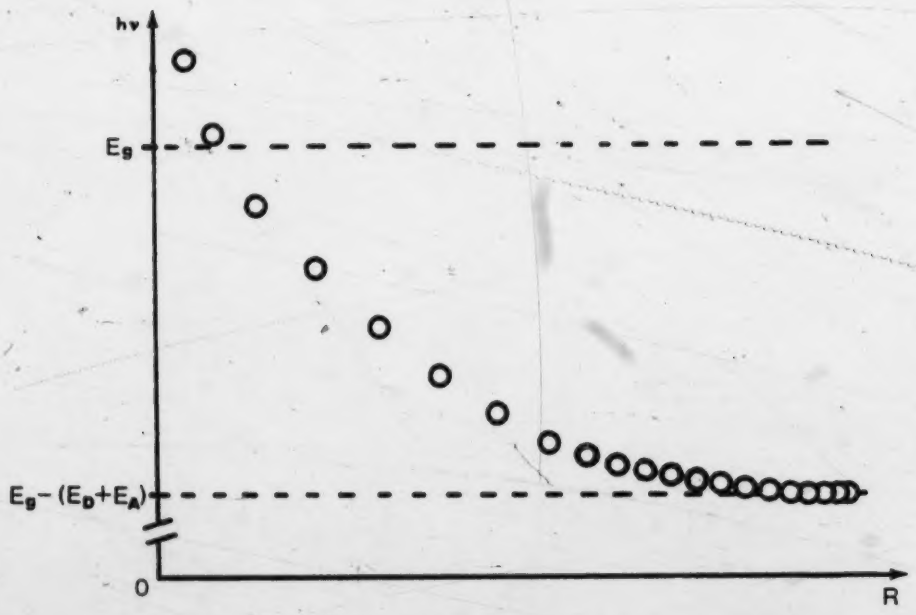

Figure 2.2 Emission energies as a function of pair distance R

The intensity of the emission is expected to be proportional to the number of isolated D-A pairs, N(R). Therefore the emission intensity should increase with decreasing R distances. However, the number of pairings is usually reduced when R decreases (Pankove, 1971). Hence, the emission intensity will go through a maximum as R changes.

In GaAs, due to the small binding energies $E_D + E_A$, and as a result of the Coulomb interaction, the discrete lines for close D-A pairs would fall above the band-gap. Thus D-A pairs that are separated by large distances will contribute to the emission spectrum.

2.1.1.2 Radiative Decay Rate

The decay rate of an isolated D-A pair can be expressed as a function of its separation distance R.

For a weakly bound electron at the donor, it can be shown that the recombination rate will have the form (Thomas *et al*, 1965):

$$R(R) = R_{max} \cdot \exp(-\frac{2R}{a_o}) \quad , \qquad (2.3)$$

where R_{max} is a constant

and a_o is the Bohr radius of the donor.

If N_D and N_A are the concentrations of donors and acceptors respectively in a sample where a random distribution of donors and acceptors exists, then the D-A emission is governed by the lesser of these two quantities. For instance, if either one of the donor or

acceptor is in excess, e.g. $N_D > N_A$, and no redistribution of holes or electrons takes place, then the D-A emission is determined by the rate of change of the concentration of neutral acceptor. Thomas *et al.*, (1965) have shown quantitatively that, the higher the concentration of the carrier, the shorter will be the decay time. At high doping levels, the compensation process has the effect of reducing the decay rate. At low concentrations, i.e. N_D, $N_A \sim 10^{15}$ cm^{-3}, the decay time is only weakly affected by compensation.

For a fixed concentration of carriers, irrespective of whether the sample is exactly compensated or partially compensated, the deviation between the decay times is negligible at the early stage of the decay process. However, at a later stage of the decay, the deviation is more significant, and in the case with exact compensation, the decay rate becomes more complex.

For material which is exactly or almost exactly compensated ($N_D \sim N_A$), the calculation of the decay times is complicated by the fact that each donor to acceptor transition is dependent on the number of vacant hole states, which decreases with time. Thomas *et al.* (1965) have shown quantitatively that at sufficiently long times, the intensity varies as t^{-2}, for heavily doped samples, and follows t^{-1} for lightly doped samples ($\sim 10^{15}$ cm^{-3}). They have also found that the decay rate is temperature independent at low temperatures (< 20 K).

2.1.2 Conduction Band-to-Acceptor Recombination

If the acceptor center is hydrogenic, and the semiconductor has a simple valence band, Eagles (1960) has shown that for a direct transition of electrons from the acceptors (with density N_A) to the conduction band, the absorption coefficient is given by

$$\alpha(\omega) = N_A \frac{128\pi e^2\hbar^2}{ncm^2\omega E_A} \frac{m_1}{m_o} |I_o|^2 \frac{\sqrt{z}}{(1+z)^4} , \qquad (2.4)$$

where

$$z = \frac{m_1}{m_o} \frac{(\hbar\omega - E_g + E_A)}{E_A} . \qquad (2.5)$$

m_1 : effective mass of electron in the conduction band,

m_o : effective mass of holes in the valence band,

E_A : binding energy of acceptor,

E_g : band gap energy,

m : free-electron mass,

and n : refractive index of the material.

By neglecting any shift in the energy levels due to interaction of the electrons at the impurity levels with the lattice, the emission spectrum due to spontaneous radiative recombination between conduction band and the acceptor levels is related to the absorption spectrum according to:

$$L(\omega) = A\omega^2 \frac{\sqrt{z}}{(1+z)^4} \cdot f_o , \qquad (2.6)$$

where A is frequency independent, and f_o is the probability of the upper states in the conduction band with energy $(\hbar\omega - E_g + E_A)$ being occupied by electrons. This probability is normally $\sim\exp(-y)$, where $y = (\hbar\omega - E_g + E_A)/(kT)$ (where k :

Boltzmann's constant and T is the temperature).

Eagles found that by evaluating equation (2.6), the line shape of the spectrum due to free-to-bound transition is approximately proportional to the function

$$g(y) \equiv \sqrt{y} \cdot \exp(-y) \ , \qquad (2.7)$$

with y as expressed above. The maximum intensity occurs at the energy

$$\hbar\omega^{max} = E_g - E_A + \frac{1}{2}kT \ . \qquad (2.8)$$

2.2 Data Acquisition and Analytical Methods

2.2.1 Data Acquisition

2.2.1.1 Photoluminescence Emission Spectra

Three of the most commonly used signal recovery techniques are: lock-in amplification, signal averaging and photon counting (Hamilton, 1977).

Among these techniques,the photon counting technique gives the highest signal-to-noise ratio (SNR) (Jones *et al.*, 1971; Poultney, 1972). However, this technique is efficient only for continuous signals or pulses with high repetition rate. Photon counting is normally unsuitable when a low repetition rate (< 100 Hz) excitation source is used. For our low repetition rate laser (< 10 Hz), it would require more than 10 hrs to scan from a wavelength of 810–1000 nm at 1 nm

intervals with standard photon counting circuits. Due to the short excitation pulse (~ 800 ps) the number of photons captured for each pulse is very low, thus 2000 or more trigger pulses are needed for each point in order to recover the signal from the noise.

The lock-in amplification method is used when continuous signals can be modulated by a mechanical chopper. When the ratio of the "off/on" periods is large, the lock-in method becomes inefficient (Abernethy, 1973). It is least applicable when the excitation pulses are narrow and of low repetition rate.

The signal averaging method is capable of recovering both chopped CW signals as well as pulsed signals from noise. If one chooses to digitize the signal in order to obtain the magnitude as well as the shape of the pulse, then the minimum sampling frequency must be at least twice the frequency of the waveform according to the Nyquist sampling theorem (Fogarty *et al.*, 1982). Thus, for narrow pulses with pulse duration of ~10 ns, a high sampling frequency of ~200 MHz is required, and the cost of the electronics is usually very high.

In the following experiments, due to the availability of a pulsed excitation source of low repetition rate (< 10 Hz) with narrow pulses (~800 ps), the above-mentioned signal recovery methods are unsuitable. In order to acquire data at a minimum cost,

a data acquisition system that can function efficiently has been developed. With it both fast and slow components of the emission can be digitized and transferred to a storage device.

The data acquisition system basically consists of a peak detector, an 8-bit analogue-to-digital converter (ADC), a monochromator drive unit, a parallel to serial interface (RS232), and an input/output (I/O) interface, all controlled by a Timex/Sinclair 1000 (TS1000) microcomputer, and operating, in this case, in conjunction with an Osborne 1 microcomputer. The block diagram is shown in figure 2.3. Detailed description of both the hardware and software of the data acquisition system is discussed in Appendix A.

Briefly, the data acquisition sequence involves amplifying the output current from the photomultiplier, followed by holding the maximum signal level for a considerable length of time to allow for analogue-to-digital conversion by the ADC. Typical 8-bit conversion time is less than 20 μs. At the end of the conversion, the datum is read by the TS1000 microcomputer. Data can be accumulated for a preset number of laser triggers for a particular wavelength setting, on completion of which, the data are sent serially at a rate of 1200 baud through the RS232 interface to an Osborne 1 microcomputer for storage. After the end of data transmission, the whole sequence

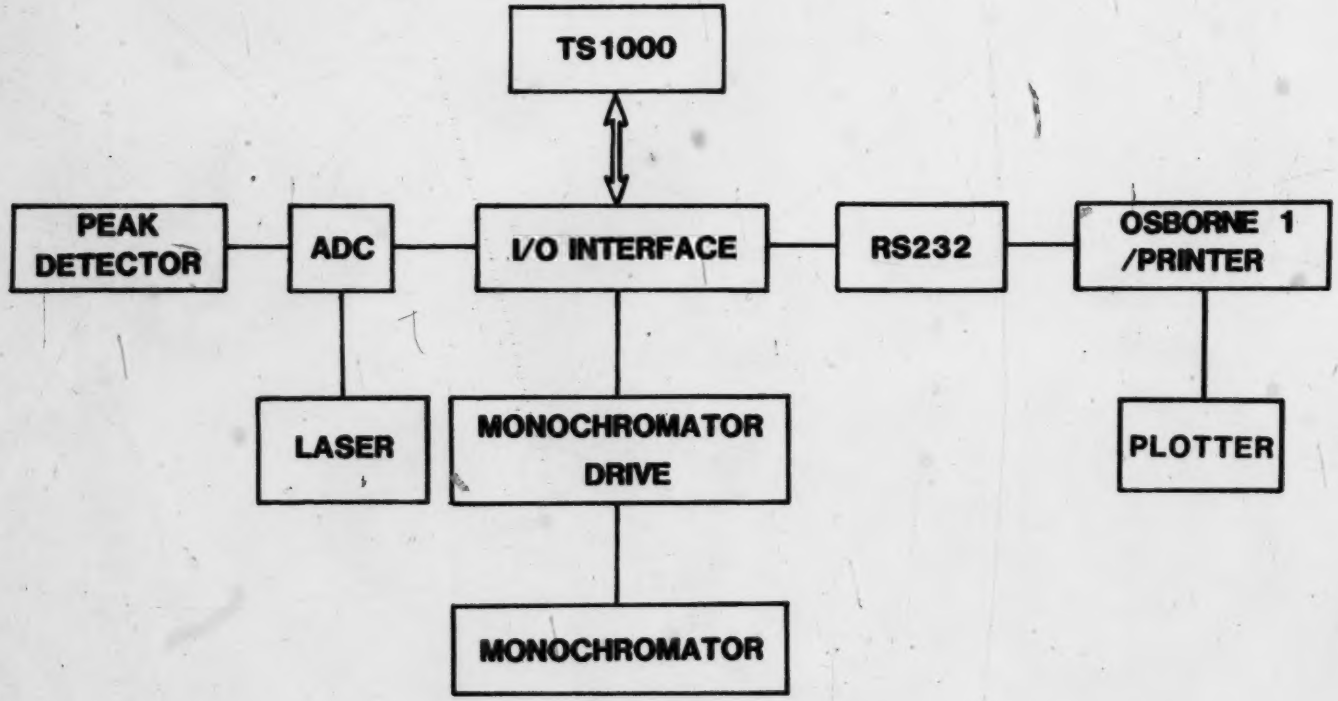

Figure 2.3 BLOCK DIAGRAM FOR THE DATA ACQUISITION SYSTEM

is repeated at a new wavelength setting selected by the TS1000 microcomputer, until the final wavelength (preset by the operator) is reached. The interval between adjacent wavelength settings is presetable to values which are multiples of $\frac{1}{72}$ nm. This system enables the whole emission spectrum to be collected automatically.

2.2.1.2 Transient Emission Spectra

In the measurements of photoluminescence decay, it is without doubt that the most sensitive technique is *photon counting. Time-correlated single photon counting* employing the time-to-amplitude conversion technique is a common practice in acquiring luminescence decay curves (O'Connor and Phillips, 1984). In the time-to-amplitude conversion technique, part of the excitation laser pulse is used to start the clock, which is then stopped by the arrival of the first single photon pulse. The time is then converted to an amplitude and stored in the channel number corresponding to the amplitude. This technique is based on the principle that *the probability distribution for single photon emission after an excitation pulse is similar to the probability of the emission of photons as a function of time after the excitation pulse has ceased* (Hartig *et al.*, 1976). This method is efficient only if the excitation pulse rate is high (e.g. in the MHz range), because for every laser pulse, only the first single photon emitted is registered.

If an excitation laser with a repetition rate of less than 10 Hz is used, as in our case, the measurement time involved in acquiring a transient spectrum would be impractically long. Thus, a fast photon counter (Lawton *et al.*, 1976) is employed to capture as many photons as possible, as a function of time after the extinction of the excitation pulse.

When a laser trigger (part of the excitation pulse reflected by a beam splitter) is received, the time channels in the counter will open sequentially and any pulse (discriminated from noise), resulting from either a single or multiple photons, arriving within the time channel will be registered as one event in the specified time channel. The photoluminescence decay curve is then accumulated for a preset number of trigger pulses. The number of triggers selected or the number of maximum counts required will be dependent on the number of components expected, either of single or multiple components, and their corresponding ratios, so that the later components can be uncovered from the background noise (Kalantar, 1983). Maximum counts of 10^6 to $> 10^7$ have been used in the measurement of decay lifetimes (Cooper *et al.*, 1965; Isenberg *et al.*, 1973; Grinvald, 1976).

The decay curves are then analyzed using the following methods.

2.2.2 Data Handling and Analysis: Transient Spectra

2.2.2.1 Treatment of Data

In the time dependence of the emission of photons resulting from an excitation pulse, if a true average number of photons, η, is detected during a time interval Δt, then the probability that n photons are emitted in that time interval is given by the Poisson distribution (Mandel and Wolf, 1965):

$$P(n) = \frac{\exp(-\eta)}{n!} \cdot \eta^n \quad . \tag{2.9}$$

In the photon counting experiment, one or more photons arriving in a given time channel are counted as one. Since the width of the time channel is not infinitesimally small, distortion in the measured decay curve will result at high count rate due to the limited capacity. Therefore, a correction must be applied to the measured curves.

The probability, P, is modified for zero and one photon as follows (Lawton *et al.*, 1976):

$$P(0) = \exp(-\eta) \quad , \tag{2.10}$$

$$P(1) = 1 - \exp(-\eta) \quad . \tag{2.11}$$

The observed total number of counts, N_i, in channel i, during the time interval Δt after a repeated M number of excitation pulses is then given by:

$$N_i = M[1 - \exp(-\eta)] \quad . \tag{2.12}$$

Hence, the true number of counts, C_i, at the end of M number of laser pulses can be calculated from the observed number of counts, by inverting equation (2.12), and leads to the following relation:

$$C_i = - M \cdot \ln\left(1 - \frac{N_i}{M}\right) . \qquad (2.13)$$

The recorded number of counts in each channel for a decay curve measured is then corrected using equation (2.13).

If the signal at the peak of the luminescence is kept low, (either by lowering the excitation intensity using neutral density filters in the beam path or by reducing the slit-size of the monochromator) such that the total number of counts observed at the maximum is less than 1% of the number of trigger pulses, then no correction is necessary. However, if a low repetition rate excitation laser (~10 Hz) is used, it would require more than 27 hrs (assuming that every laser pulse is accepted) to obtain 10^4 counts at the maximum of the decay curve. It is thus obvious that limiting the rate to < 1% is not a practical solution. Hence, correction must be introduced, and care must be taken to avoid saturation at the peak intensity. Due to the low repetition rate of the excitation source, for practical reasons, a correction factor of ~20% was tolerated by allowing the observed counts at the maximum to be ~40%

of the total number of trigger pulses.

Since the duration of the laser pulse is short (~800 ps) compared to the smallest time channel (10 ns) available, and the decay times measured are fairly long (usually several hundreds of nanoseconds), deconvolution of the data to remove the excitation pulse profile is not necessary. The corrected (for distortion) decay curve is represented in a histogram (not a continuous distribution) where the number of counts in each channel is an integrated decay over a time width, Δt, instead of the decay signal at an instantaneous time, t_i. O'Connor and Phillips (1984) have proven that the integrated intensity is proportional to the decay function and that it is reasonable to use the observed histogram in the deconvolution procedure to determine the decay law of the sample.

2.2.2.2 Least-Squares Curve Fitting (LSF)

The most popular method employed in analyzing a decay curve is by *reiterative least-squares curve fitting technique* (Irvin and Livingston, 1974).

In the least-squares technique, the main aim is to minimize the value of χ^2, which is the weighted sum of the squares of the difference between the measured data, $y(t_i)$, and the fitting function, $f(t_i)$. The equation for χ^2 is given by (O'Connor and Phillips, 1984):

$$\chi^2 = \sum_{i=1}^{n} W_i[y(t_i) - f(t_i)]^2 , \qquad (2.14)$$

where m is the total number of data points measured, and W_i is the weighting factor for the i^{th} point, which is the reciprocal of the expected value. Irvin and Livingston (1974) have equated this value to the reciprocal of the sum of the fitting function and the background. Assuming that the background = 0, then

$$\chi^2 = \sum_{i=1}^{m} \left\{ \frac{[y(t_i) - f(t_i)]^2}{f(t_i)} \right\} . \qquad (2.15)$$

The fitting functions are linearized by assuming a Taylor series expansion (Bevington, 1969) to first order in the fitting parameters a_j (j=1,p) with parameter increments α_j: (for simplicity, $f(t_i)$ is written as f_i)

$$f_i(a+\alpha) \simeq f_i(a) + \sum_{j=1}^{p} \frac{\partial f_i}{\partial a_j} \cdot \alpha_j . \qquad (2.16)$$

The condition for a minimum is:

$$\frac{\partial \chi^2}{\partial \alpha_j} = 0 , \qquad (2.17)$$

which leads to equations of the form:

$$\sum_{j=1}^{p} \alpha_j \cdot B_{jk} = A_k , \quad k=1,p \qquad (2.18)$$

where $B_{jk} = \sum_{i=1}^{m} \frac{\partial f_i}{\partial a_j} \cdot \frac{\partial f_i}{\partial a_k} \cdot \frac{1}{f_i}$, (2.19)

and

$$A_k = \sum_{i=1}^{m} \frac{\partial f_i}{\partial a_k} \left(\frac{y_i - f_i}{f_i} \right) . \qquad (2.20)$$

Equation 2.18 can also be written in the matrix form

$$\alpha \cdot B = A , \qquad (2.21)$$

and the parameter increment, α, is calculated by inverting the matrix B, i.e.,

$$\alpha = A \cdot B^{-1} \ . \qquad (2.22)$$

For computation, initial estimated values for all the parameters, a_k, are supplied. The fitting function, f_i, is calculated and followed by calculation of the value of χ^2. The partial derivatives are determined and the matrix B is set up and inverted. The increments of parameters, α_k, are calculated from the inverted matrix B, and a new fitting function, f_i, is then calculated using new parameters:

$$a_k = a_k^o + \alpha_k \ , \qquad (2.23)$$

followed by the determination of new value for χ^2.

The procedure of calculating the value α is repeated until the value calculated for χ^2 converges to a minimum.

A computer programme written in Fortran and modified from that of Irvin and Livingston (1974) is listed in Appendix B.

An alternative method for solving single or multiple component exponential decay curves has recently been proposed (Teh *et al.*, 1986) to simplify the data analysis process. Details of this method are discussed in the next chapter.

Bibliography

Abernethy, J.D.W. (1973). Physics Bulletin, 24, 591

Bevington, P.B. (1969). *Data Reduction and Error Analysis for the Physical Sciences* (MacGraw-Gill, New York)

Cooper, J.A., Hollander, J.M., and Rasmussen, J.O. (1965). Phys. Rev. Lett. 15, 680

Dean, P.J. (1969). In *Applied Solid State Science* (R. Wolfe, and C.J. Kriessman, eds.), vol. 1, p. 1 (Academic Press, New York)

Eagles, D.M. (1960). J. Phys. Chem. Solids 16, 76

Fogarty, M.P., Ho, C.N., and Warner, I.M. (1982). In *Optical Radiation Measurements* (K.D. Mielenz, ed.), vol. 3, p. 249 (Academic Press)

Grinvald, A. (1976). Anal. Biochem. 75, 260

Hamilton, T.D.S. (1977). *Handbook of Linear Integrated Electronics for Research* (McGraw-Hill, London)

Hartig, P.R., Sauer, K., Lo, C.C., and Leskovar, B. (1976). Rev. Sci. Instrum. 47, 1122

Hopfield, J.J., Thomas, D.G., and Gershenzon, M. (1963). Phys. Rev. Lett. 10, 162

Irvin, D.J.G., and Livingston, A.E. (1974). Computer Physics Commun. 7, 95

Isenberg, I., Dyson, R.D., and Hanson, R. (1973). Biophys. J. 13, 1090

Jones, R., Oliver, C.J., and Pike, E.R. (1971). Appl. Optics 10, 1673

Kalantar, A.H. (1983). Computer Physics Commun. 28, 315

Lawton, M., Bolden, R.C., and Shaw, M.J. (1976). J. Phys. E 9, 686

Mandel, L., and Wolf, E. (1965). Rev. Mod. Phys. 37, 231

O'Connor, D.V., and Phillips, D.(1984). *Time-correlated Single Photon Counting*, p. 171 (Academic Press)

Pankove, J.I. (1971). *Optical Processes in Semiconductors*,

chap. 6, p. 143 (Prentice Hall)

Poultney, S.K. (1972). In *Advances in Electronics and Electron Physics* (L. Marton, ed.), vol. 31, p. 39 (Academic Press, New York)

Teh, C.K., Tin, C.C., and Weichman, F.L. (1986). J. Luminescence 35, 17

Thomas, D.G., Gershenzon, M., and Trumbore, F.A. (1964). Phys. Rev. 133, A269

Thomas, D.G., Hopfield, J.J., and Augustyniak, W.M. (1965). Phys. Rev. 140, A202

3. A NEW METHOD OF ANALYSIS OF PHOTOLUMINESCENCE DECAY CURVES

3.1 Introduction

The analysis of the temperature dependence of the decay time constant of a luminescent signal can be employed to study the luminescent activation energies of defect levels and also the binding energies of excitons in semiconductors. The common method used in extracting the decay time constant from the luminescent signal decay data is either a linear least-squares method for a single-component decay curve or an iterative non-linear least-squares method for multiple-component decay curve. The iterative non-linear least-squares method requires more computer time and is also inefficient in resolving time constants of nearly equal magnitude.

For a luminescence decay that follows the Arrhenius relation: $\tau \propto \exp(E/kT)$, where τ is the decay time constant, E is the activation energy, k is the Boltzmann constant and T is the temperature, we present here an alternative method of extracting the parameter associated with the luminescence decay signal, i.e., the activation energy of the defect levels. This method, which we shall call Photoluminescence Transient Spectroscopy (PTS), involves the study of the temperature dependence of the differential luminescent intensity and it enables the extraction of the decay time

---

This chapter has been published. Teh, C.K., Tin, C.C. and Weichman, F.L. (1986). Journal of Luminescence 35, 17-23.

constant to be done instrumentally. The method is basically the same as that employed in DLTS (deep-level transient spectroscopy)(Lang, 1974) and PITS (photo-induced transient spectroscopy)(Hurtes *et al.*, 1978; Yoshie and Kamihara, 1983a,b).

The advantage of this method is that the plot of the differential luminescent intensity as a function of temperature can be used as a signature for defects and impurities in a sample, enhancing further the usefulness of photoluminescence spectroscopy.

The method has been tested using luminescence decay data for Cu_2O crystals and was found to be both effective and efficient without any major alteration to our experimental equipment.

3.2 Theory and analysis

A luminescence decay signal can originate from either a single- or multiple-component process. In the following analysis, we will discuss the case where the luminescence decay signal is a superposition of two exponential components with decay time constants τ_m and τ_n. If $L(t_1)$ is the intensity of the transient luminescence measured after a time delay t_1 from the moment of maximum intensity and $L(t_2)$ is the intensity after a time delay t_2 from the moment of maximum intensity , then the difference in the intensities is given by

$$\Delta L(T) = L(t_1) - L(t_2)$$
$$= M \{\exp(-t_1/\tau_m) - \exp(-t_2/\tau_m)\}$$
$$+ N \{\exp(-t_1/\tau_n) - \exp(-t_2/\tau_n)\} , \qquad (3.1)$$

where M and N are the maximum values of the two components at t=0.

The time constant τ_i (where i=m,n) is related to the trapping parameters according to the equation:

$$\tau_i(T) = \tau_{oi} \exp(E_i/kT) , \qquad (3.2)$$

where τ_{oi} is the time constant at infinite temperature.

It follows from equations (3.1) and (3.2) that plotting $\Delta L(T)$ against temperature should give a peak whenever the decay time constant τ_i matches the time gate $(t_2 - t_1)$. The decay time constant can be obtained from the position of the peak as shown below. At the position of the peak,

$$\partial \Delta L/\partial T = (\partial \Delta L/\partial \tau_i)(\partial \tau_i/\partial T) = 0 . \qquad (3.3)$$

Differentiating equation (3.1) with respect to their corresponding τ_i parameters and equating to zero, we obtain

$$1/\tau_i = \ln r/(t_2 - t_1) , \qquad (3.4)$$

where $r = t_2/t_1$.

Therefore, at the temperature T_m (i is omitted for simplicity) corresponding to a peak, the decay time constant is given by equation (3.4).

The activation energy of the defect level can easily be obtained by running spectra with different values of t_1 and t_2 to obtain different values of τ and T_m. The trapping activation energy can then be obtained from the graph of ln τ against $1/T_m$ (see equation(3.2)). It is advisable to keep the ratio $r = t_2/t_1$ a constant. A small value of r gives a more accurate result but the spectra tend to have a poor signal-to-noise ratio. A large value of r will give a better signal-to-noise ratio but too large a value will produce an erroneous result (Yoshie and Kamihara, 1983b).

If a single time gate method is employed, several temperature scans, each with a different time gate, must be carried out in order to obtain several spectra to evaluate the activation energy according to equation (3.2). However, if the measurement is carried out in a multichannel mode, then only a single temperature scan is necessary. A multichannel mode can be realized in many ways. The photon counting method is suitable, particularly for low efficiency luminescence, because it determines the intensities at various instants of time following the extinction of the excitation pulse. Other data acquisition systems such as the multichannel analyzer, digital sampling oscilloscopes or signal averager can also render the results suitable for analysis by using the present method.

In a multichannel mode, the signal is digitized and stored in a computer for later analysis. The differential luminescent intensities are then calculated for different

values of t_1 using the computer. By varying the parameters t_1 and the ratio r in the computer program, a series of curves can be obtained. The optimum range of t_1 values which give the best peak resolution and the ratio r which gives the best signal-to-noise ratio are then selected for evaluating E.

We have done a series of calculations using artificially generated data to determine the resolution obtainable with the method described. In all the following calculations an arbitrary value of r=2 was used. In the case where the two amplitudes M and N are equal, the peaks cannot be resolved when the difference in the two activation energies $\Delta E < 0.03$ eV for $E_m = 0.20$ eV and $E_n = 0.23$ eV, as shown in figure 3.1. For simplicity, only the curves corresponding to $t_1 = 5$ μs are shown in figure 3.1. The peaks can be resolved by taking a longer delay time t_1. Figure 3.2 shows that when t_1 is longer than 20 μs, the two peaks begin to separate out. The resolution of the peaks is also affected by the M:N ratio. If the two activation energies are fairly close, e.g., $E_m = 0.20$ eV and $E_n = 0.25$ eV, figure 3.3 shows that when $t_1 = 2$ μs and M:N = 10:1, the peak associated with M dominates and the peak associated with N begins to flatten out. However, the peaks are still resolvable when the delay time t_1 is longer than 4 μs (figure 3.4).

When two peaks are closely merged together, it may still be possible to differentiate the peaks by numerical

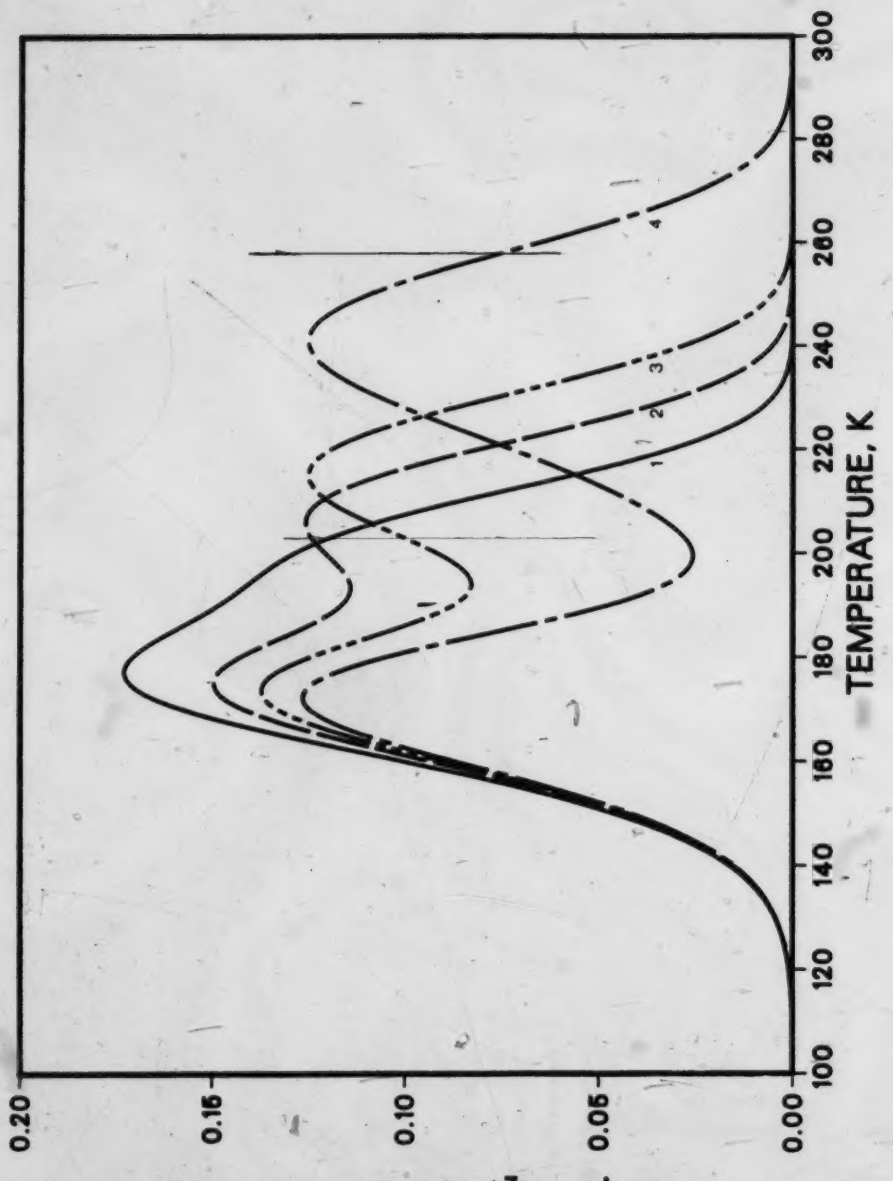

Figure 3.1 Theoretical curves of PTS for different activation energies.

$M/N=1$, $t_1=5\ \mu s$, $t_2/t_1=2$, $\tau_{0m}=\tau_{0n}=10^{-11}$ s, $E_m=0.20$ eV
(1)$E_n=0.23$ eV, (2)$E_n=0.24$ eV, (3)$E_n=0.25$ eV, (4)$E_n=0.28$ eV

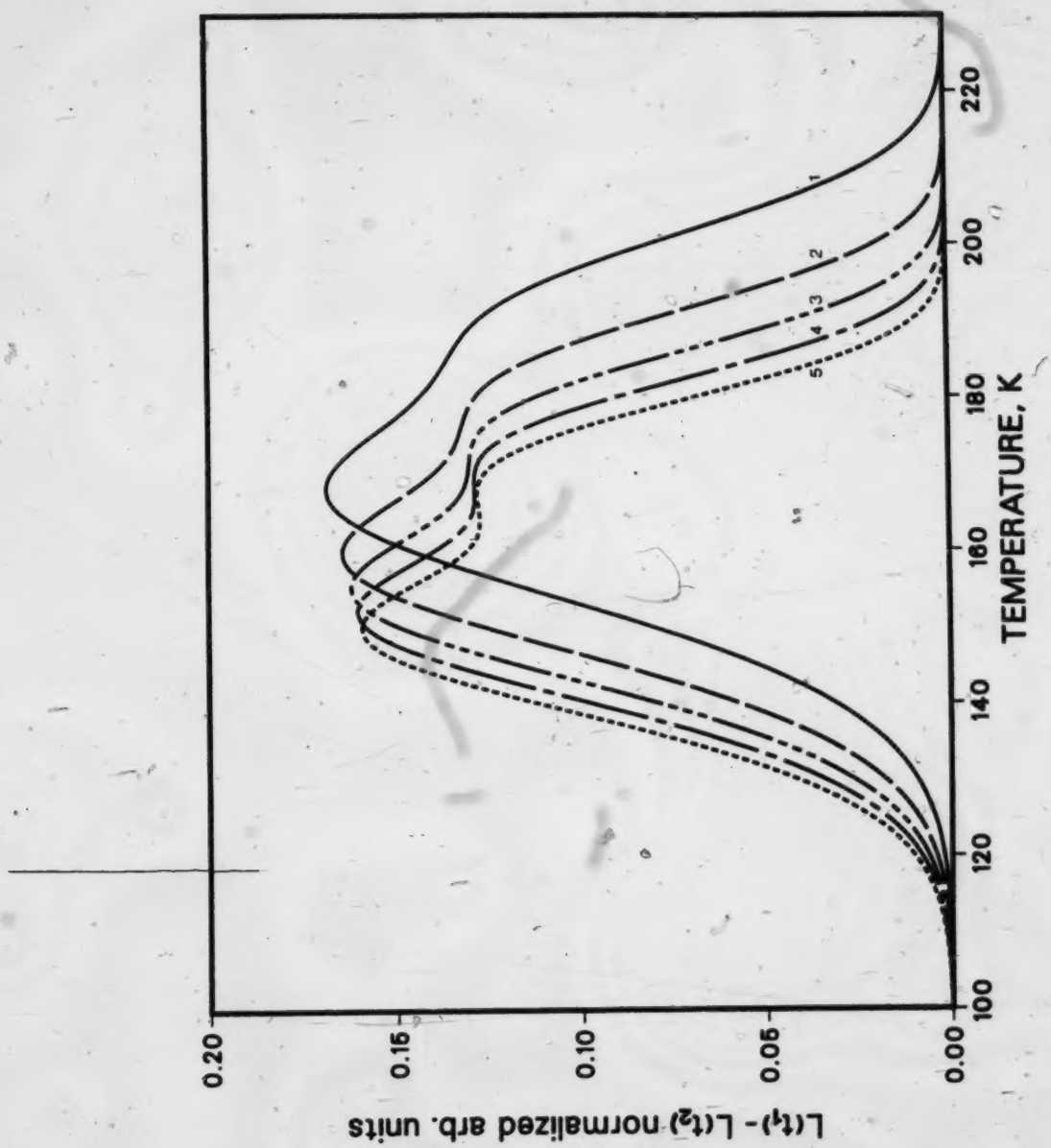

Figure 3.2 Theoretical curves of PTS for different delay times with close activation energies.

M/N=1, $t_2/t_1=2$, $\tau_{0m}=\tau_{0n}=10^{-11}$s, $E_m=0.20$ eV, $E_n=0.213$ eV
(1)$t_1=10$ μs, (2)$t_1=20$ μs, (3)$t_1=30$ μs, (4)$t_1=40$ μs,
(5)$t_1=50$ μs

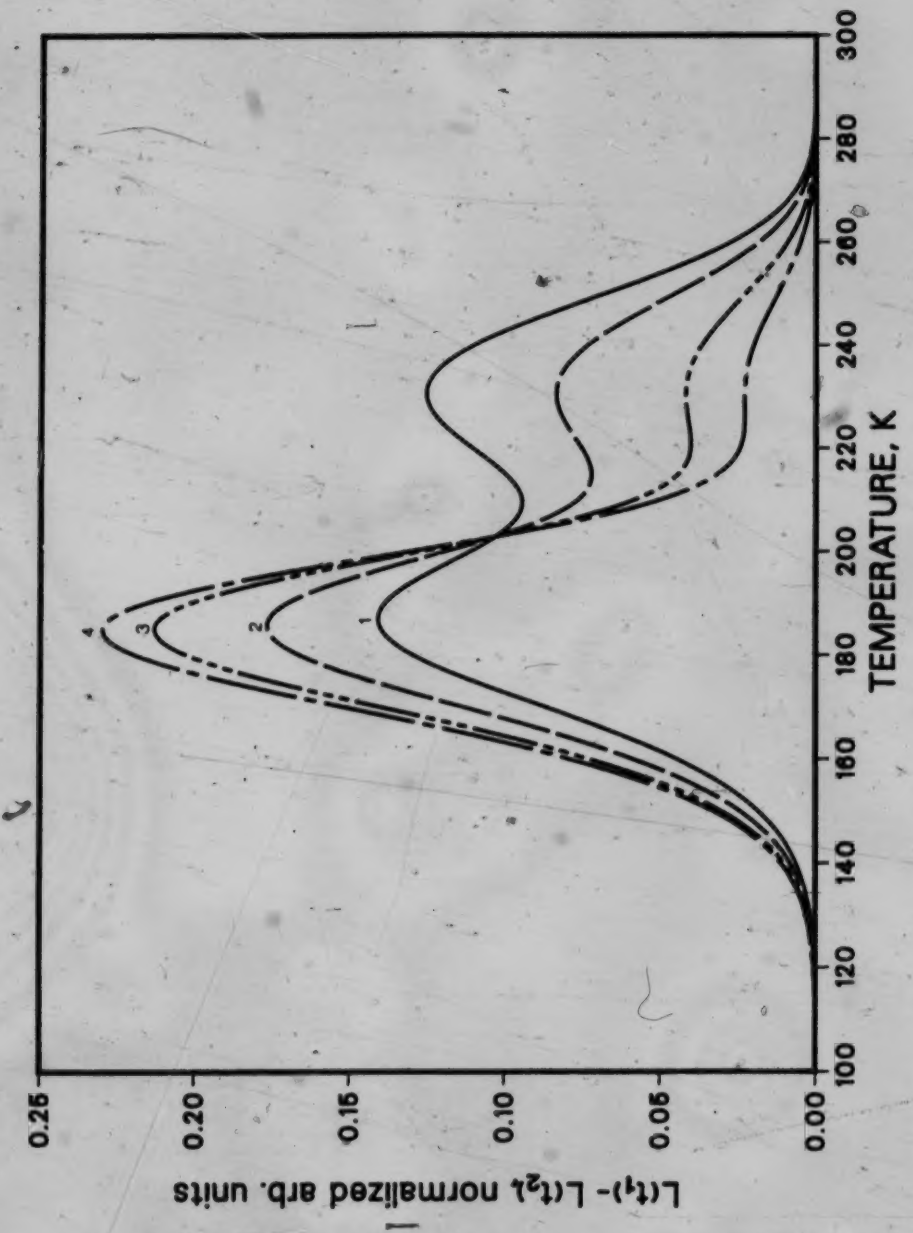

Figure 3.3 Theoretical curves of PTS for different relative amplitudes.

t_1=2 μs, t_2/t_1=2, E_m=0.20 eV, E_n=0.25 eV, $\tau_{0m}=\tau_{0n}=10^{-11}$ s, (1)M/N=1, (2)M/N=2, (3)M/N=5, (4)M/N=10

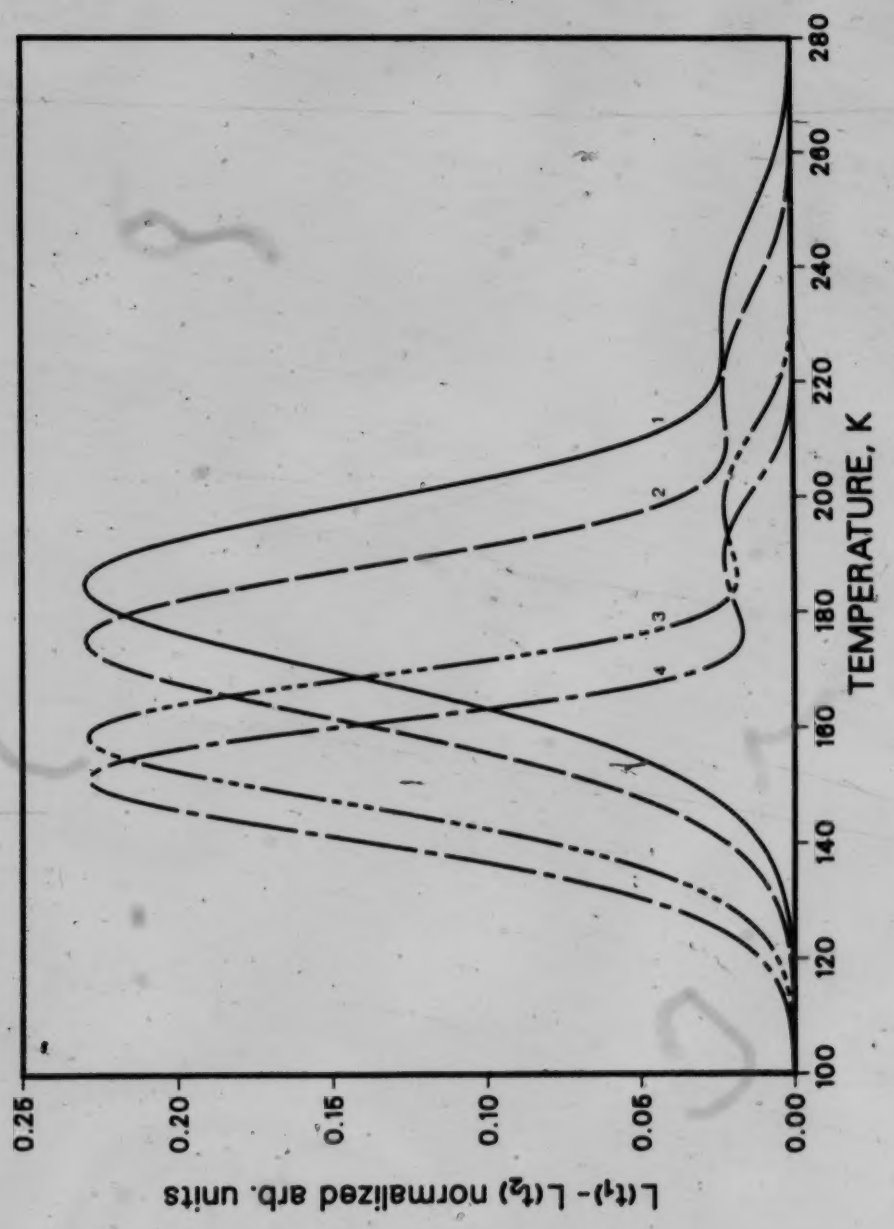

Figure 3.4 Theoretical curves of PTS for different delay times with large relative amplitudes.

M/N=10, $t_2/t_1=2$, $E_m=0.20$ eV, $E_n=0.25$ eV, $\tau_{0m}=\tau_{0n}=10^{-11}$ s,
(1)$t_1=2$ μs, (2)$t_1=4$ μs, (3)$t_1=16$ μs, (4)$t_1=32$ μs

curve fitting of the lineshape using equation (3.1).

3.3 Experimental procedure and discussion

Cuprous oxide is suitable for testing this method of analysis because it has three known, well-defined luminescence peaks (Teh and Weichman, 1983) which have different decay time constants, and is also readily available.

The sample is mounted at the heat sink of a *Cryotran* continuousflow optical cryostat (model CT-310) which can be cooled by either liquid helium or nitrogen. The temperature is monitored through a silicon diode sensor (accuracy ±0.5 K) by a digital temperature controller (model DRC-80C Digital Cryogenic Thermometer/Controller manufactured by Lake Shore Cryotronics Inc.) with temperature stability of ±0.1 K.

The excitation source used is a tunable dye-laser (PRA LN102) pumped by a nitrogen laser (PRA LN1000) with pulse duration of 800 ps (operating at 10 Hz). An excitation wavelength of 510 nm is obtained by using Coumarin 500 dye. The excitation intensity is attenuated by a neutral density filter and maintained at a fixed level of $\simeq 10^{14}$ photons/pulse. A pair of discriminators is used to monitor the laser intensity. A trigger pulse to the photon counter is only generated when the laser intensity is within a preset window. (The laser light is focused to a spot of ≃2 mm diameter on the sample.)

The luminescent signal is focussed directly into a S-1 response photomultiplier (RCA 7102) without the use of a monochromator. Filter and iris are employed to prevent detection of the exciting light and saturation of the photomultiplier, respectively. The signal is collected by a fast photon counter capable of $10-10^3$ ns resolution (which is controlled by an internal 100 MHz crystal oscillator) and the data are processed by a microcomputer (Osborne 1). The photon counter has 256 channels which is provided by 2 interleaving ECL MC10147 (1x128) memory chips.

Data was collected for a temperature range of 4-260 K at 5 degree intervals. For 80-260 K, two transient spectra were collected at each temperature with channel time-window set at 10 ns and 1 μs, so that all the luminescent signals could be resolved. It was necessary to run the experiment with 2 different time-windows of two orders of magnitude difference because two of the luminescent lines of Cu_2O have decay constants differing by more than 2 orders of magnitude. (The third line at 720 nm was found to have decay time constant less than the smallest time-window available with our system in the temperature range studied, hence it could not be resolved). For 4-80 K, only the minimum time-window of 10 ns was used.

Each luminescence decay spectrum was analyzed by setting the ratio $t_2/t_1 = 5$. When the differential luminescent intensity $\Delta L(T) = L(t_1) - L(t_2)$ was plotted against temperature for different values of t_1, a series of

curves was obtained. The peaks can be seen shifting towards lower temperatures as t_1 increases (figure 3.5). It was found that the decay time constant for the 930 nm luminescent line did not follow the simple exponential decay. Only one peak corresponding to the 820 nm luminescent line was obtained.

Noting the temperature T_m corresponding to each peak for different delay time t_1 and evaluating the value of τ according to equation (3.4), a plot of ln τ vs $1/T_m$ was then obtained as shown in figure 3.6. The activation energy, E, and τ_o values were then evaluated from the slope and y-intercept of the linear graph respectively.

The value of E compares favourably with that obtained using the least-squares method (table 3.1). The experiment was repeated using a differently prepared Cu_2O crystal containing the same centre, and the results are shown in table 3.1 (see also figure 3.6).

From the results, it can be seen that the same kind of centre in different types of Cu_2O crystal gives the same activation energy as expected (within experimental errors). This shows that the curves of $\Delta L(T)$ as a function of temperature, for a fixed time gate, can be used to characterize defect levels if a calibration of the activation energies together with the position of the peaks on the $\Delta L(T)$ vs T plot, is first obtained using a monochromator. The plot of $\Delta L(T)$ vs T with a fixed time gate can also be used to compare different samples because a

Table 3.1 Results obtained using two different methods of analysis.

Sample	Activation energy, E (eV)		τ_o (s)	
	PTS†	LSF‡	PTS	LSF
Cu_2O (type B)	0.27±0.01	0.29±0.03	4×10^{-11}	1×10^{-11}
Cu_2O (type C)	0.28±0.02		2×10^{-11}	

† Photoluminescence Transient Spectroscopy

‡ Least-squares method

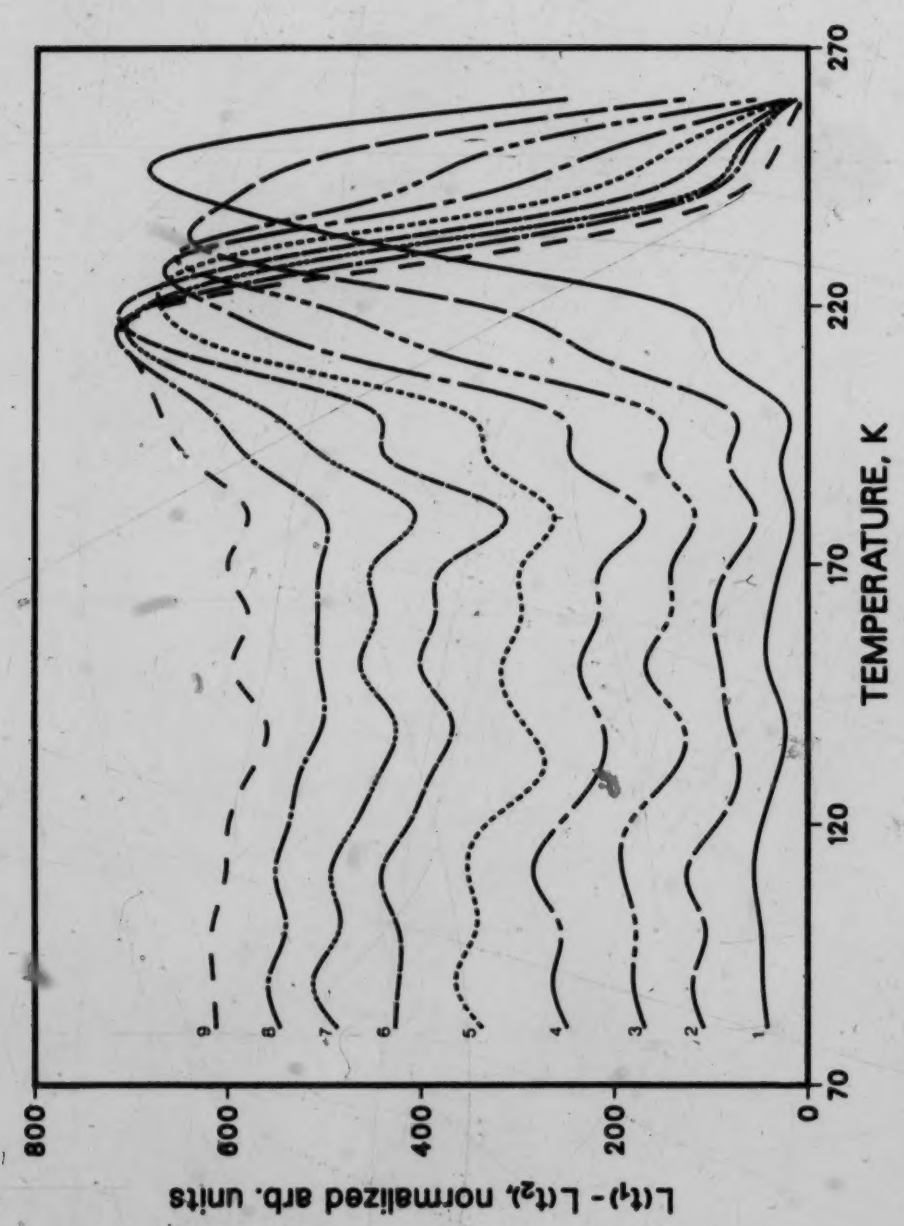

Figure 3.5 Experimental curves of PTS for Cu_2O.

t_2/t_1=5, (1)t_1=6 μs, (2)t_1=11 μs, (3)t_1=16 μs, (4)t_1=21 μs, (5)t_1=26 μs, (6)t_1=31 μs, (7)t_1=36 μs, (8)t_1=41 μs, (9)t_1=46 μs

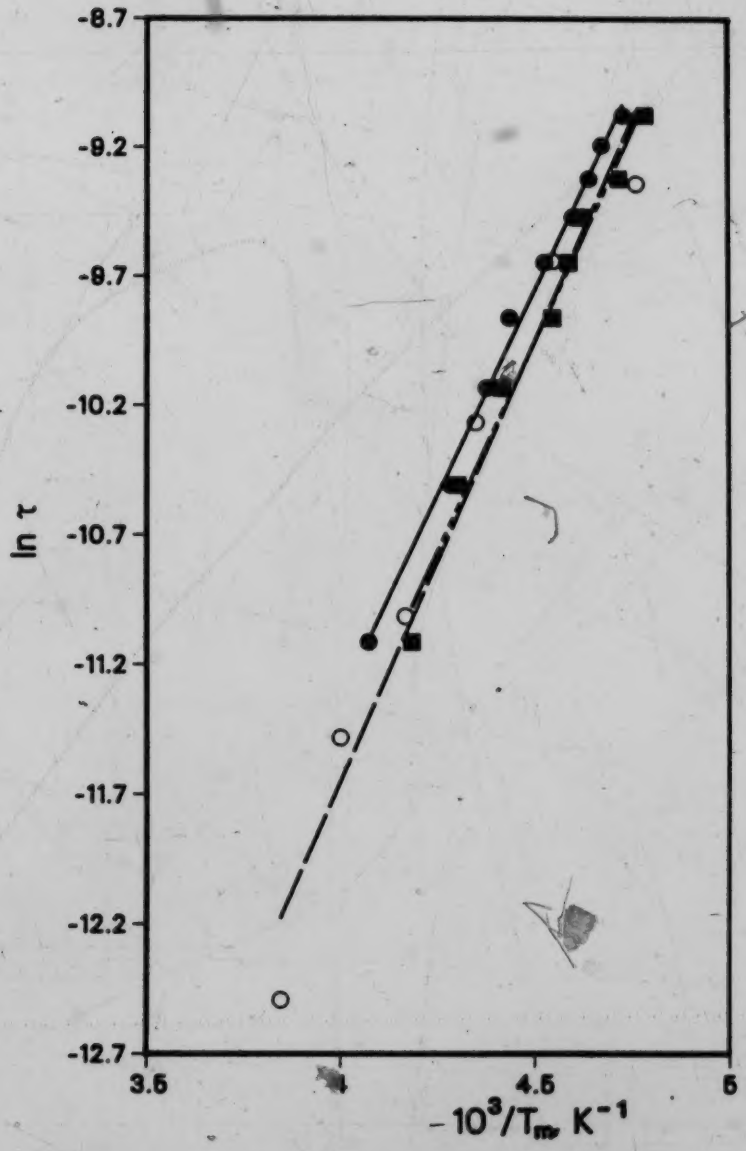

Figure 3.6 Graph of ln τ vs $10^3/T_m$ for 2 types of Cu_2O crystals.

(•,o) type B, and (■) type C. (•,■) are calculated by PTS; (o) type B sample fitted by least-squares method.

defect centre with a particular activation energy will always produce a peak at the same temperature for a particular value of the time gate.

The same method has also been applied successfully in the study of luminescence in semi-insulating GaAs, the results of which will be discussed in chapter 5.

This method of analysis has several advantages:

(i) easy to use (no need to write complicated programs),

(ii) all the defects or impurities can be detected in just one thermal scan if all the time constants are in the right range,

(iii) independent of the background count,

(iv) relative defect concentration can be noted from the height of the peaks, and

(v) since the use of the monochromator can be excluded, very small luminescent intensity can be detected, enabling very low concentration of impurities or defects to be detected.

In our experiments, data collection speed was limited by the low pulse repetition rate of the nitrogen laser. This limitation is financial rather than fundamental.

3.4 Conclusion

We have discussed a new method of analysis of the photoluminescence decay curves. This method works well with luminescence data obtained from Cu_2O crystals. The results

obtained agree with those obtained using non-linear least-squares method. Good agreement between results from different samples of Cu_2O shows that the proposed method can serve as a useful alternative method in characterizing impurities by photoluminescence thereby enhancing the capabilities of photoluminescence spectroscopy.

Bibliography

Hurtes, Ch., Boulou, M., Mitonneau, A., and Bois, D. (1978). Appl. Phys. Lett. 32, 821

Lang, D.V. (1974). J. Appl. Phys. 45, 3023

Teh, C.K., and Weichman, F.L. (1983). Can. J. Phys. 61, 1423

Yoshie, O., and Kamihara, M. (1983a). Jpn. J. Appl. Phys. 22, 621

Yoshie, O., and Kamihara, M. (1983b). Jpn. J. Appl. Phys. 22, 629

4. PHOTOLUMINESCENCE EMISSION SPECTROSCOPY OF LEC SI GaAs

4.1 Introduction

The photoluminescence emission spectra related to the donor-acceptor (D-A) pairs radiative recombinations for samples of LEC SI GaAs with different concentrations have been studied. The range of the average D-A pair distances R has been investigated and R is found to be proportional to the cube root of the reciprocal of the carbon concentration (shallow acceptor). It has been found that the most probable radiative recombination occurs for $200 < R < 1300$ Å.

The detailed line-shape of the emission, which consists of both the D-A and the B-A (band-to-acceptor) emissions has been studied as a funtion of temperature. A competing process between the D-A and B-A transitions is observed when the temperature changes.

The effect of annealing on the D-A emission has also been discussed.

4.2 Experimental Procedure

The experimental set-up used for obtaining a photoluminescence spectrum is shown in figure 4.1. Only front surface luminescence was studied. The equipment used for the excitation and the sample holder were the same as those described in §3.3. An excitation wavelength of 510 nm was used in most cases except for the studying of the annealed samples where a wavelength of 620 nm was obtained from the

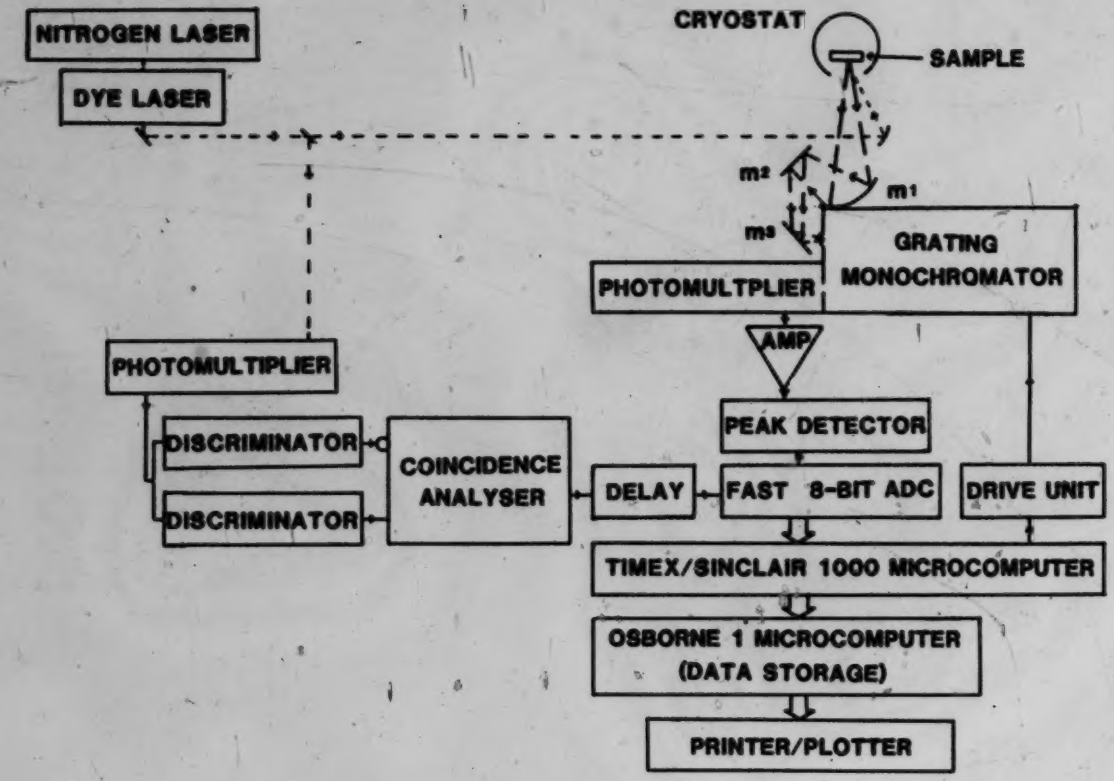

Figure 4.1 PHOTOLUMINESCENCE SYSTEM

dye Rhodamine 6G.

The emission wavelength was resolved by a 0.45 m Czerny-Turner grating (590 lines mm^{-1}) monochromator with reciprocal linear dispersion of 3.5 nm mm^{-1}, (Pacific Precision Instruments model MP-1018B) which was equipped with a remote control. The width of the slits was set such that the spectral resolution was 0.8 meV at 1.5 eV. A resolution of 0.4 meV was used in the study of the line-shape as a function of temperature. A cylindrical mirror (m_1 in figure 4.1) was used to focus the emission onto the entrance slit of the monochromator through two plane mirrors m_2 and m_3. The luminescence signal was detected by an S-1 response photomultiplier placed at the exit slit of the monochromator. The signal was then processed by the data acquisition system described in §2.2.1.

Sample preparation

For all the annealed samples, the damaged surfaces were (i) ground off on a 600 grit silicon carbide paper, (ii) followed by chemo-mechanical polishing on a lint-free tissue (LABX 170) using freshly prepared 2% Br_2 in methanol (electronic grade) and then rinsed in methanol, and (iii) finally etched in a freshly prepared solution of 5 H_2SO_4:1 H_2O_2:1 H_2O, then rinsed in deionized water followed by methanol. Subsequent depth profiling was done by using the same etchant as in step (iii), on one side of the crystal, while the opposite side was protected by a coating

of lacquer.

For the unannealed samples, steps (ii) and (iii) were followed prior to measurements.

4.3 Results

Several samples of LEC SI GaAs with different carbon concentrations† have been investigated using the photoluminescence emission spectrometer in the energy range of 1.24–1.53 eV, at a temperature range of 4.1–28 K. Figure 4.2 shows a typical emission spectrum (normalized) of undoped LEC SI GaAs at 4.1 K. Four main peaks can be resolved clearly at 1.5120±0.0008 eV, 1.4916, 1.4554, and 1.4192 eV, with decreasing intensity from ~1.49 eV towards lower energies.

The intensity of the ~1.49 eV emission peak is plotted as a function of carbon concentration as shown in figure 4.3. Figure 4.4 shows the concentration dependence of the peak energies for different carbon concentrations (for clarity only 6 curves are shown). Figure 4.5 is obtained from the peak energies of figure 4.4 and compared with the expected energies calculated from the concentration of carbon. The peak shifts towards lower energies as the concentration of carbon decreases. However, when the concentration is too low ($<10^{14}$ cm^{-3}), another peak at 1.493±0.001 eV becomes prominent (curve 1 in figure 4.4). The values of R (donor-acceptor pair distance) can be

---

† The concentrations were determined from the IR LVM absorption at 582.5 cm^{-1} which is discussed in Chapter 6.

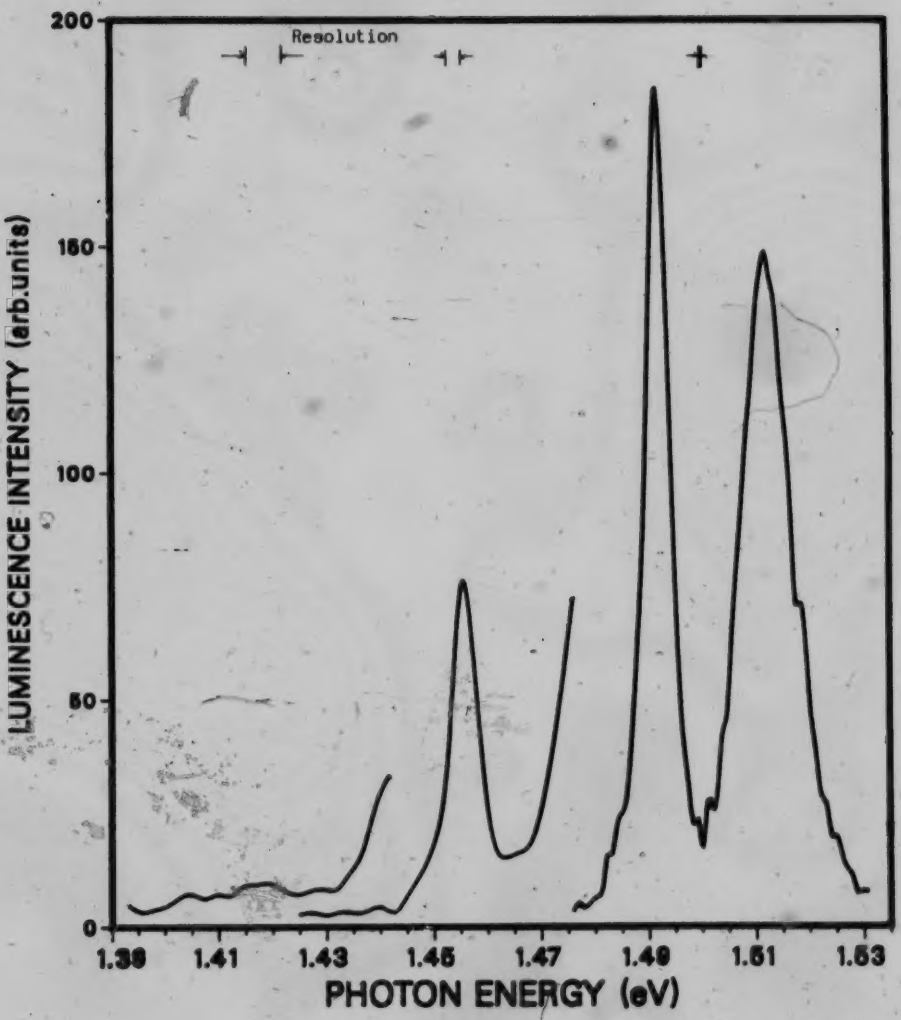

Figure 4.2 A typical emission spectrum of undoped LEC SI GaAs

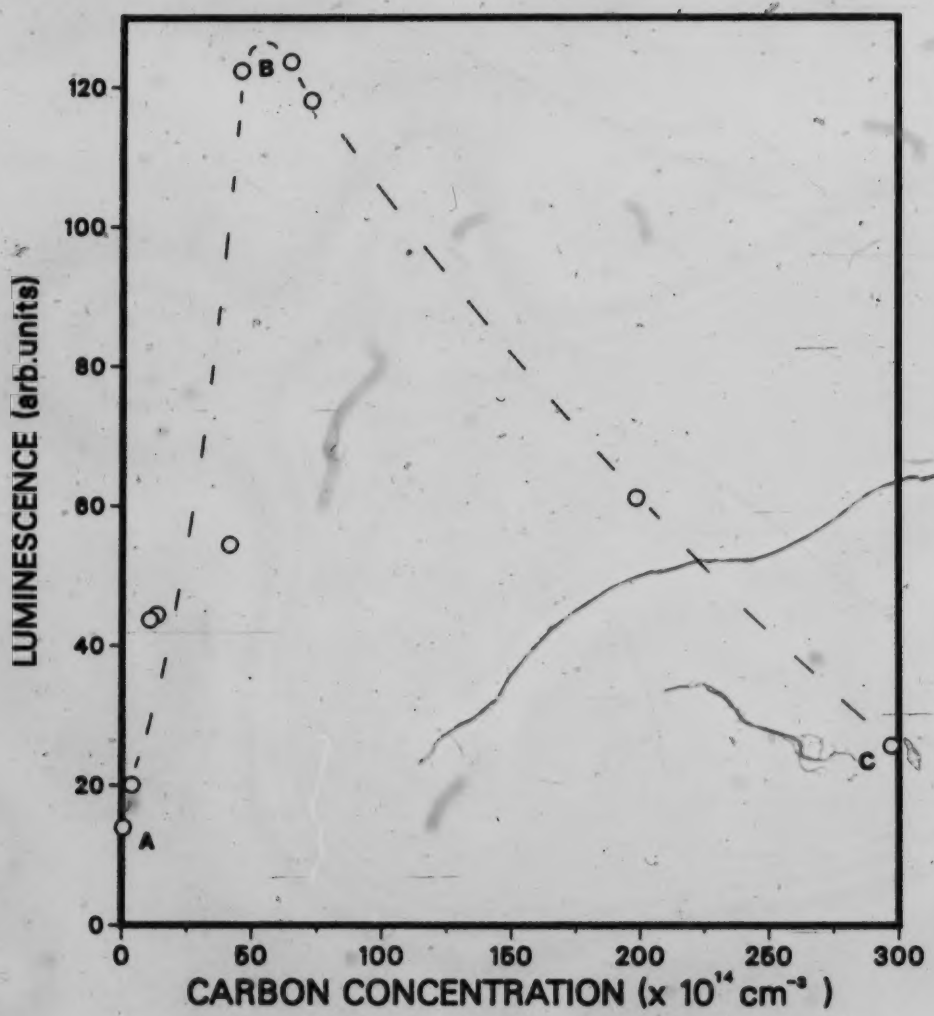

Figure 4.3 Luminescence intensity as a function of carbon concentration

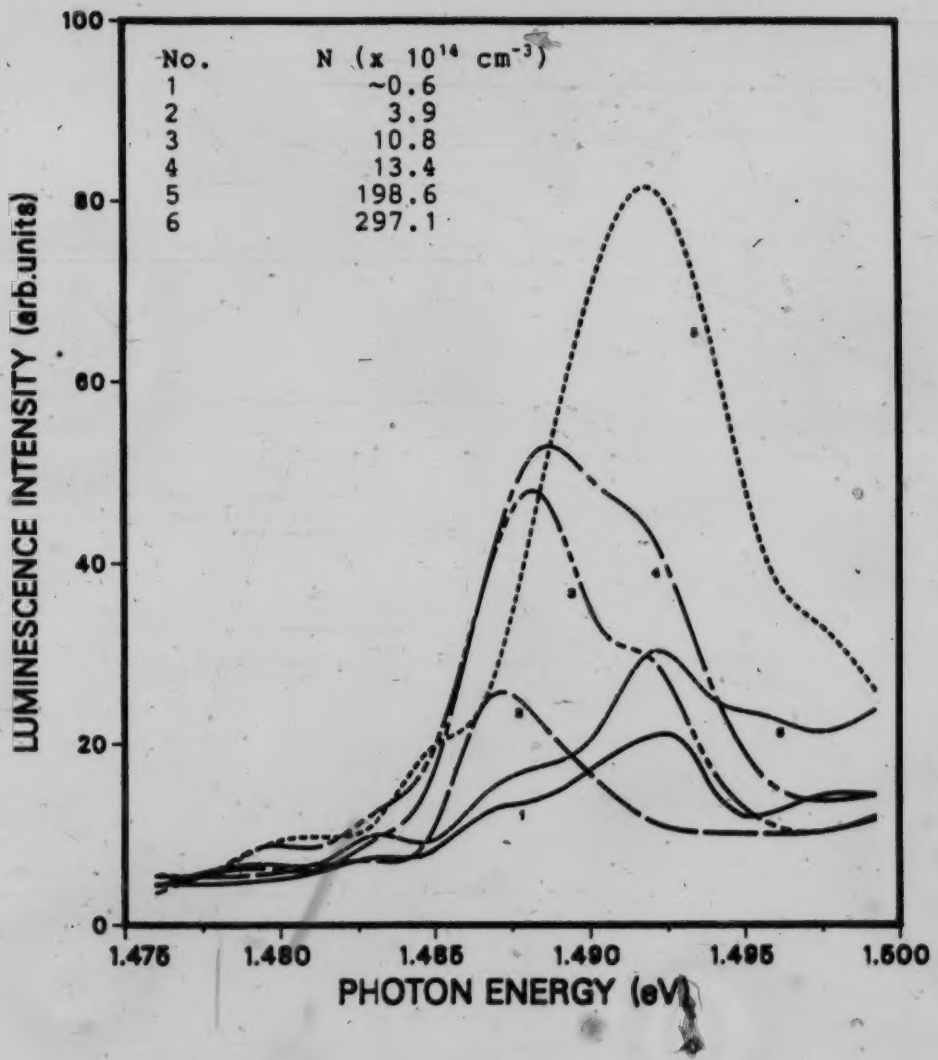

Figure 4.4 Variation of emission energies as a function of carbon concentration

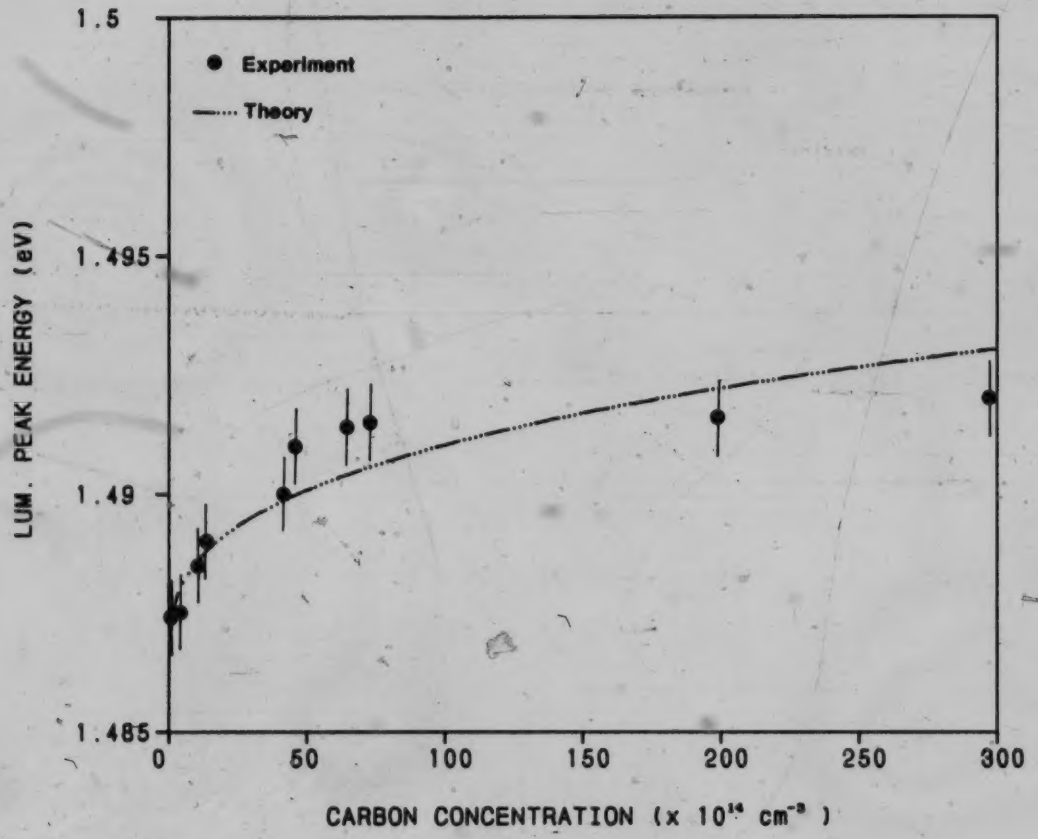

Figure 4.5 Comparison between experimental and theoretical values

calculated from the peak energies according to equation (2.1), using the relative static dielectric constant ϵ=12.5 (Hambleton *et al.*, 1961). The results are shown for different carbon concentrations in table 4.1, together with the theoretical values.

The temperature dependence of the ~1.49 eV emission peak is shown in figure 4.6. The intensity dropped considerably for temperatures above 20 K (from 18→26 K, the intensity is reduced by 75%), and became almost undetectable above 30 K with the present system. The position of the peak shifts towards higher energies when the temperature is raised. The emission peak is at 1.4930 eV when the temperature is at 26 K (figure 4.6). Detailed analysis of the line-shape shows that the emission band consists of two overlapping peaks. Figure 4.7 shows the spectra at different temperatures at a higher resolution. As the temperature is increased from 4.1 to 11 K, the peak begins to split into two peaks at 1.4930 and 1.4916 eV with the dominating peak at the lower energy. When the temperature is increased to 18 K, the higher energy peak is increased while the lower energy peak is decreased. From 18–28 K, the intensity of both peaks is greatly reduced with the higher energy peak becoming dominant.

Figure 4.8 shows the emission spectra for samples annealed at 450, 550 and 850°C. The annealing times for 450 and 550°C were 12 hrs and for 850°C were 24 hrs. Curve 1 for the original unannealed sample is included for comparison.

Table 4.1 Concentration dependence of emission energy and D-A pair distance.

Carbon Conc. ($\times 10^{15}$ cm^{-3})	Theoretical Value R_m (Å)	$h\nu$ (eV)	Experimental Value $h\nu$ (eV) ±0.0008	R (Å)
29.71	175	1.4930	1.4920	207
19.86	200	1.4922	1.4916	224
7.26	280	1.4906	1.4915	228
6.45	291	1.4904	1.4914	233
4.55	327	1.4900	1.4910	253
4.15	337	1.4899	1.4900	324
1.34	492	1.4888	1.4890	451
1.08	528	1.4886	1.4885	561
0.39	742	1.4880	1.4875	1093
~0.06	1384	1.4873	1.4874	1293

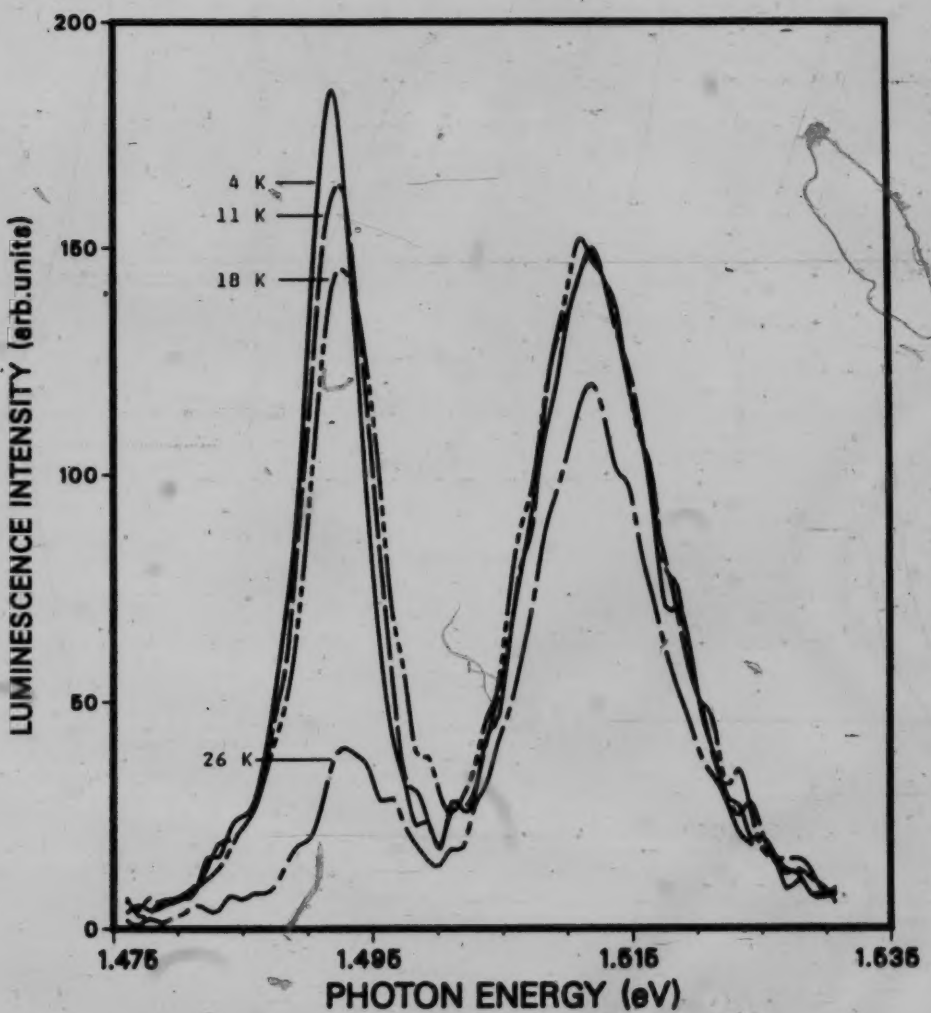

Figure 4.6 Temperature dependence of luminescence emissions

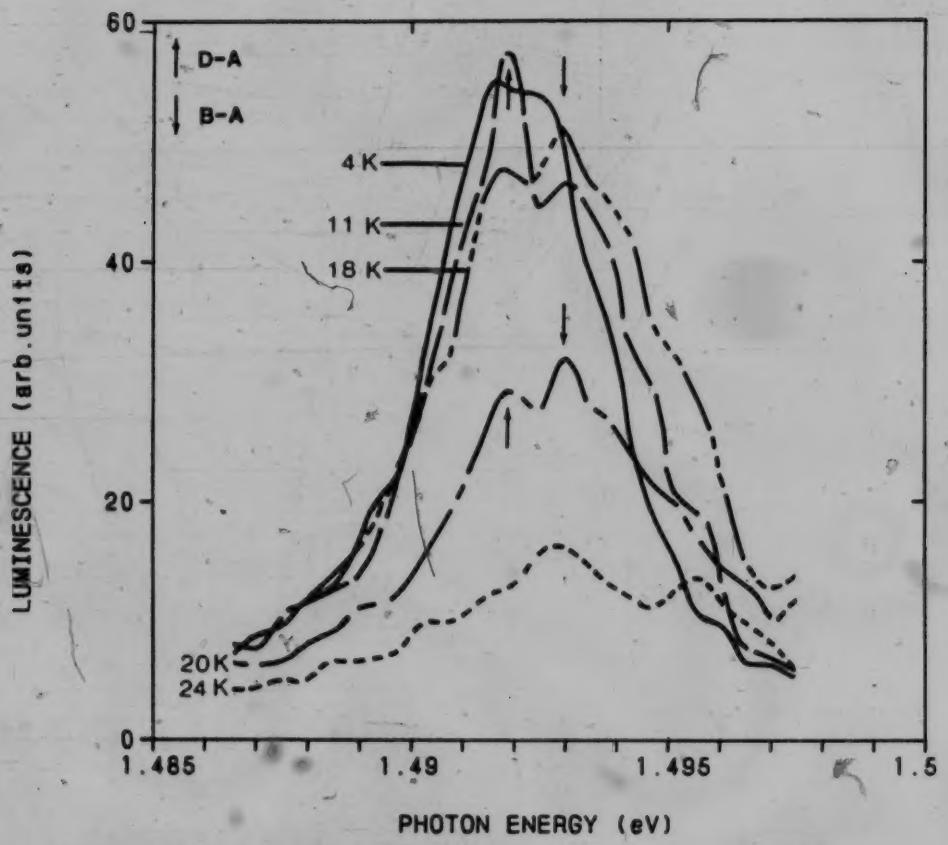

Figure 4.7 Temperature dependence of luminescence at a higher resolution

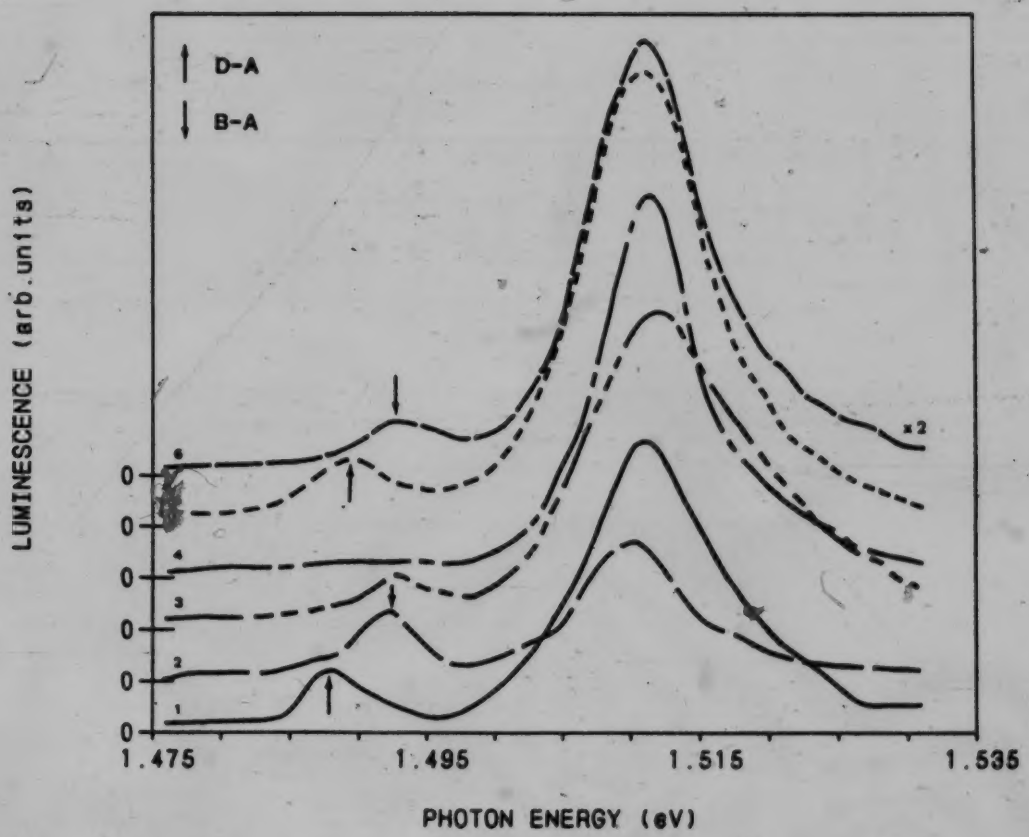

Figure 4.8 Effect of annealing on the luminescence of D-A pairs

Curves 2, 3 and 4 show the spectra measured near the surface of the samples which were annealed at 450, 550 and 850°C respectively. The position of the emission peak shifts from 1.489 to 1.493 eV as shown by curves 2 and 3. Curve 4 shows that the ~1.49 eV peak is reduced. Curves 5 and 6 show the emissions near the center of two different samples taken from the same wafer and annealed at 850°C for 24 hrs.

4.4 Discussion

The position of the 1.512 eV peak agrees with that observed by Leite and DiGiovanni (1967), which they proposed to be involved with a bound exciton. Other investigators (Bogardus and Bebb, 1968; Shah *et at*, 1969; Hill, 1970; White *et at*, 1972; Heim and Hiesinger, 1974; Stringfellow *et al.*, 1981; Roth *et al.*, 1983a; Heiblum *et al.*, 1983) have also reported that such emission is due to an exciton bound to a neutral acceptor (A^0,X), either zinc or carbon. Although the full width at half maximum (FWHM) of the peak is too broad (≃10 meV) for a bound exciton line, this could be due to the fact that it consists of a fine structure of multiple exciton lines (Roth *et al.*, 1983) that were not resolved by our low resolution monochromator. Therefore, since the samples measured contain carbon, this 1.512 eV emission could be the same line reported for the exciton bound to carbon impurity. A small hump at ~1.518 eV is observed that could be due to the free exciton at its excited state (n=2) (Heiblum *et al.*, 1983).

The luminescence peak at ~1.49 eV has been attributed to recombination between distant donor-acceptor (D-A) pairs related to the carbon acceptor level C_{As} (Ozeki *et al.*, 1974; Stringfellow *et al.*, 1981). The two low energy peaks, which are separated by 36.2 and 72.4 meV from the carbon line are due to the LO phonon replica and 2LO phonon replica of the zero phonon carbon peak (Nathan and Burns, 1963). The LO phonon energy ($E_{no\text{-}phonon}-E_{LO}$) of 36.2 meV is in excellent agreement with documented data (Watts, 1977).

The intensity of the D-A pair recombination peak usually increases with increasing carbon concentration as shown in the AB region of figure 4.3. However, this is not always true, especially when the carbon concentration is very high. In the case where the carbon content is $> 6 \times 10^{15}$ cm^{-3}, the luminescence begins to quench as shown by the BC region of figure 4.3. This shows that the intensity of the D-A pair recombination does not depend on the concentration alone but also on other factors such as D-A pair distances, and the presence of surface states that usually act as non-radiative centers. This is shown by the observation of a higher efficiency of the emission at a greater depth from the surface (when a longer excitation wavelength with same intensity is used). Generally, the intensity of the emission is proportional to the number of D-A pairs if the sample is free of surface states.

The broad emission peak of the D-A transition shows the presence of a range of donor-acceptor pair distances R. The

emitted energy is dependent on $\frac{1}{R}$ as predicted by equation (2.1). The variation of the peak energies for different carbon concentrations indicates that the average distance R is different for different carbon concentrations. When the carbon concentration is increased, the decrease in R distance contributes to a higher emission energy as a result of an increase in the Coulomb interaction energy. This is shown by the increasing emission energy with concentration.

The energy $E_A + E_D$ is usually very small in GaAs. When the R value decreases below a certain limit, the Coulomb interaction term would cause the donor and acceptor levels to be located outside the energy gap (figure 2.2). There would be a competing process between transitions due to those D-A states (which are localised in the intrinsic bands) and the band states. Since the intrinsic bands have a higher density of states, the probability of recombination is higher for the band-to-band (B-B) transition, thus resulting in the predominance of B-B transitions. Hence, distant D-A pairs separated by small R values are not observed (Gershenzon, 1966; Pankove, 1971; Watts, 1977) and only distant D-A pairs with large R distances will contribute to the emission spectrum.

The weak emission at 1.492±0.001 eV for the highest carbon content measured is due to a small number of distant D-A pairs. When the carbon concentration decreases slightly, a slightly more distant D-A pair is present which contributes to a higher intensity as shown by curve 5 of

figure 4.4.

For very low carbon concentration (< 10^{14} cm^{-3}), the D-A pairs are too far apart resulting in a reduced probability of recombination. Hence only a few 'not so' distant pairs contribute to the D-A transition, indicated by a weak hump at ~ 1.487 eV, and the conduction band-to-acceptor (B-A) transition at 1.493±0.001 eV is seen (curve 1, figure 4.4).

The theoretical R values denoted by R_m shown in table 4.1 are calculated using the equation $R_m = \sqrt[3]{(\frac{1}{2\pi N})}$ obtained by Williams (1968) from the maximum of the distribution function for ion pairs which interact coulombically. The expected emission energies are then calculated using equation (2.1). It can be seen that the first two values of the expected R distances for concentrations ≥ 2 x 10^{16} cm^{-3} are smaller than the experimental values. Since only distant D-A pairs with large R distances will contribute to the emission spectrum, this could explain why the intensity of the D-A emission is reduced. This supports the argument made earlier.

For the emission energies between 1.4910 and 1.4915 eV, the slightly higher energies measured could be due to the influence of the B-A peak, which will be discussed in the later part of this section. The rest of the measured energies are in agreement with the theoretical values within experimental errors as shown by the broken line in figure 4.5.

This result shows that the most probable D-A transition occurs only at R values within a certain range that is found to be from ~210 to ~1300 Å (table 4.1).

For the samples annealed at 850°C, there is a reduction in the intensity of the carbon peak near the surface (curve 4, figure 4.8). This could be due to the creation of arsenic vacancy, V_{As}, on the surface (Chiang and Pearson, 1975), which leads to the formation of complexes between C_{As} and V_{As}.

For samples annealed at 450 and 550°C (curves 2 and 3 respectively in figure 4.8) the carbon peak is still visible. This could probably be due to the fact that the annealing time and temperature have not reached the equilibrium condition for vacancy creation. The shift of the emission peak energy from the D-A (1.489±0.001 eV) to the B-A (1.493 eV) emissions, shows that annealing destroys the shallow donors. This seems logical as annealing causes p-type conversion that is due to the presence of excess uncompensated acceptors.

The two samples (curves 5 and 6 in figure 4.8) that were annealed under the same conditions give different results upon etching into the middle of the crystals. The discrepancy could be due to the non-uniformity of the wafer, and the two samples could be of different quality. It can be seen that the relative luminescence intensity of curves 5 and 6 is higher for number 5. This shows that it has a higher efficiency and that the sample could be of better

quality and also thermally stable as shown by the reappearance of the D-A emissions upon etching.

The initial observation of the shift of the D-A peak towards higher energies at increasing temperature is in agreement with Leite and DiGiovanni (1967). This is consistent with the behavior of the D-A pair recombination process. Leite and DiGiovanni have discussed that the peak shifts towards higher energies because of an increase in the Coulomb energy (see equation (2.1)), which in turn is caused by recombination at a closer distance R at higher temperatures. However, careful examination of the line-shape of the carbon emission peak proves the co-existence of B-A and D-A transitions with the B-A transition dominating at higher temperatures.

The mechanism involved can be explained as follows: consider the existence of a set of closely spaced excited levels, I, related to a donor center with ground level, E_D, lying close to the band edge within an energy region kT_D, where T_D is the Debye temperature. A photo-excited free carrier in the conduction band can be trapped by the donor level by making a series of successive one-phonon transitions via these excited levels. The one-phonon transition is of a higher probability compared to the cascading of many-phonons in a single step (Bonch-Bruevich and Landsberg, 1968). At low temperatures, where $kT < I < kT_D$, these levels will play a dominating role in the electron capturing process, thus contributing to the

predominance of the D-A transition. At elevated temperatures, some of the excited levels may have I < kT. In all probability, the electrons will suffer thermal emission back into the band states, thereby increasing the probability of the B-A transition. There is also a slight increase in the (A^0,X) line, shown by a small increase in intensity of the 1.512 eV band from 4.1-18 K (figure 4.6), while the D-A emission is quenched. For some levels with I > kT, capture of an electron is still possible. When the temperature is increased further, the radiative emissions are quenched by other non-radiative processes. This observation of the D-A transition at low temperatures and B-A transition dominating at high temperatures is in agreement with observations reported by others for epitaxial layers of GaAs doped with C, Si, Ge, Zn, Mn, and Mg (Skromme and Stillman, 1984; Roth *et al.*, 1983; Ashen *et al.*, 1975; Schairer and Schmidt, 1974; Schairer and Graman, 1969).

Theoretical calculation of the band shape of the B-A band using Eagles' (1960) equation (equation (2.7)) shows a good fit between theory and experiment (figure 4.9). Using a least-squares curve fitting method, a value for the acceptor ionization energy of 27 meV is obtained, which is in close agreement with reported value of 26.7 meV for C_{As} level (Watts, 1977).

We have also observed a peak at ~1.496 eV which becomes prominent at 24 K (figure 4.7). A similar emission line has also been observed by Rao *et al.* (1985) and at ~1.495 eV by

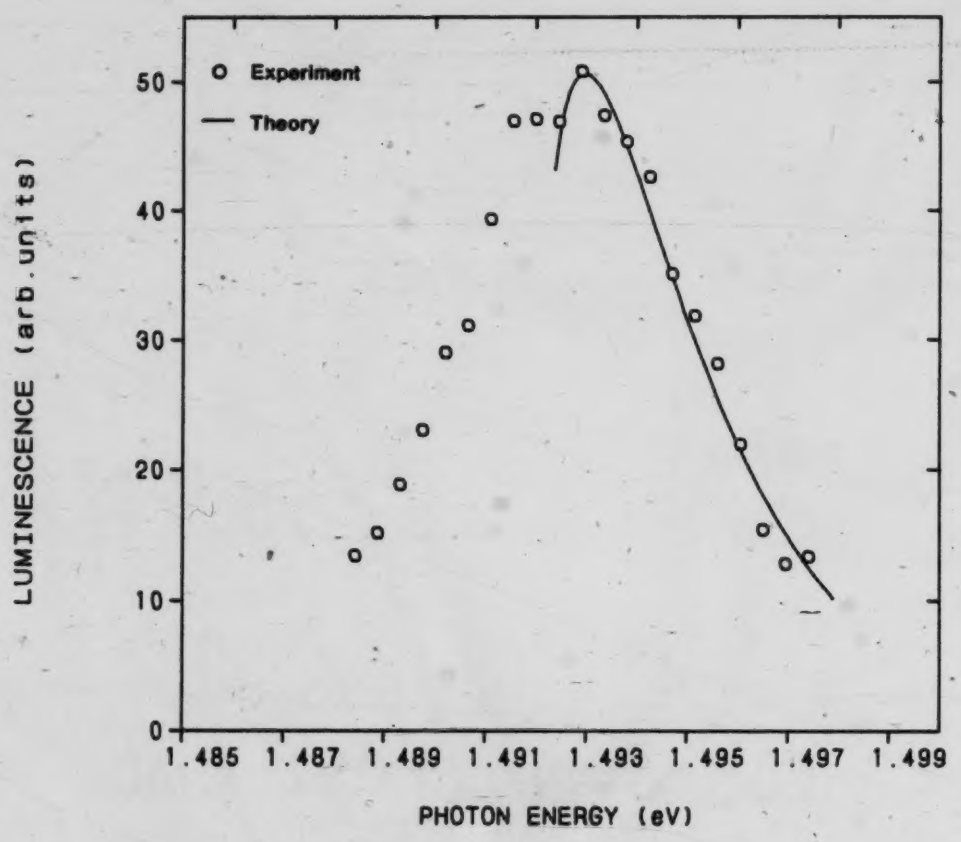

Figure 4.9 Theoretical fit of the B-A band

Contour *et al.* (1983). It has been referred to as an unidentified F-B peak related to a level shallower than the carbon acceptor by about 3 meV.

We have only seen this emission at high resolution and it becomes more prominent when the temperature rises above 20 K. At low temperature, only a weak hump is observed. The presence of this emission has been observed on three other samples even after repeated measurements. We are convinced, therefore, that this emission is genuine and not an artefact. However, at this stage we do not have any conclusive information on the origin of this peak.

4.5 Conclusion

From the above results, we conclude that there exists a range of D-A pair distances R with an average R value varying inversely with the cube root of the carbon concentrations. The results also show that the most probable D-A transition only occurs at R values within a certain range which is found to be from ~210 to ~1300 Å.

The quenching of the donor-acceptor pairs radiative recombination is caused by the change in the occupancy of the donor level with temperature.

The annealing of the samples at high temperatures destroys the shallow donors, which could be a possible cause for the p-type conversion. Judging from the higher efficiency of the luminescence, and the unaffected interior of sample 5 even after annealing at 850°C for 24 hours, we

can conclude that the crystal is thermally stable.

We have also observed the presence of an unidentified level at ~1.496 eV. More detailed studies need to be made to discover the identity of this emission line at ~1.496 eV.

Bibliography

Ashen, D.J., Dean, P.J., Hurle, D.T.J., Mullin, J.B., and White, A.M. (1975). J. Phys. Chem. Solids 36, 1041

Bogardus, E.H., and Bebb, H.B. (1968). Phys. Rev. 176, 993

Bonch-Bruevich, V.L., and Landsberg, E.G. (1968). phys. stat. sol. 29, 9

Chiang, S.Y., and Pearson, G.L. (1975). J. Appl. Phys. 46, 2986

Contour, J.P., Neu, G., Leroux, M., Chaix, C., Levesque, B., and Etienne, P. (1983). J. Vac. Sci. Technol. B1, 811

Eagles, D.M. (1960). J. Phys. Chem. Solids 16, 76

Gershenzon, M. (1966). In *Semiconductors and Semimetals* (R.K. Willardson and A.C. Beer, eds.), vol. 2, p. 289, 316 (Academic Press, New York)

Hambleton, K.G., Hilsum, C., and Holeman, B.R. (1961). Proc. Phys. Soc. 77, 1147

Heiblum, M., Mendlz, E.E., and Osterling, L. (1983). J. Appl. Phys. 54, 6982

Heim, U., and Hiesinger, P. (1974). phys. stat. solidi B66, 461

Hill, D.E. (1970). Phys. Rev. B1, 1863

Leite, R.C.C., and DiGiovanni (1967). Phys. Rev. 153, 841

Nathan, M.I., and Burns, G. (1963). Phys. Rev. 129, 125

Ozeki, M., Nakai, K., Dazai, K., and Ryuzan, O. (1974). Jpn. J. Appl. Phys. 13, 1121

Pankove, J.I. (1971). *Optical Processes in Semiconductors*, chap. 6, p. 143 (Prentice Hall)

Rao, E.V.K., Alexandre, F., Masson, J.M., Allovon, M., and Goldstein, L. (1985). J. Appl. Phys. 57, 503

Roth, A.P., Charbonneau, S., and Goodchild, R.G. (1983). J. Appl. Phys. 54, 5350

Roth, A.P., Goodchild, R.G., Charbonneau, S., and Williams, D.F. (1983a). J. Appl. Phys. 54, 3427

Schairer, W., and Graman, W. (1969). J. Phys. Chem. Solids 30, 2225

Schairer, W., and Schmidt, M. (1974). Phys. Rev. B10, 2501

Shah, J., Leite, R.C.C., and Nahory, R.E. (1969). Phys. Rev. 184, 811

Skromme, B.J., and Stillman, G.E. (1984). Phys. Rev. B29, 1982

Stringfellow, G.B., Koschel, W., Briones, E., Gladstone, J., and Patterson, G. (1981). Appl. Phys. Lett. 39, 581

Watts, R.K. (1977). *Point Defects in Crystals*, p. 206 (John Wiley & Sons)

White, A.M., Dean, P.J., Taylor, L.L., Clarke, R.C., Ashen, D.J., and Mullin, J.B. (1972). J. Phys. C 5, 1727

Williams, R. (1968). phys. stat. solidi 25, 493

5. TRANSIENT EMISSION SPECTROSCOPY OF CARBON IMPURITY IN LEC SI GaAs

5.1 Introduction

It has already been reported by Dingle (1969) and Kamiya and Wagner (1976) that the decay of the D-A pair photoluminescence signal consists of an exponential decay at the initial stage followed by a non-exponential decay. Dingle (1969) has observed that at 4.2 K, the photoluminescence signal decays as t^{-p} ($p=1.3$) after a long delay from the instant of termination of the excitation pulse.

From our studies of the temperature dependence of this power law for samples of LEC SI GaAs with carbon concentration ranging from $\sim 10^{14}$ to $\sim 10^{16}$ cm^{-3}, we have found that in the temperature range of $18 < T < 32$ K, the exponent p is linearly dependent on temperature according to the expression: $p(T) = -1 + \beta T$, where β is proportional to the concentration of acceptors, C_{As}. We believe that there has been no previous report on such an observation in GaAs.

There exist in the literature (Jonscher and de Polignac, 1984) various proposals to explain the power-law behavior of the recombination processes especially in amorphous materials. We will discuss the possible mechanisms to explain the power-law behavior of our results and the

---

The indented sections of this chapter are parts of a paper which has been accepted for publication. Teh, C.K., Tin, C.C. and Weichman, F.L., to be published in the May, 1987 issue of the Canadian Journal of Physics.

quenching of the photoluminescence decay signals at increasing temperature.

5.2 Experimental Procedure

Photoluminescence decay curves were measured at low temperatures using the time resolved photon counting technique. The experimental set-up is shown in figure 5.1. The set-up is similar to that shown in figure 4.1 except for the data acquisition system. An excitation wavelength of 510 nm was used in these studies.

The data acquisition system consists of a fast pulse amplifier (150 MHz), delay line, and a fast photon counter (FPC), which is the same as that described in §3.3.

When a trigger pulse (part of the excitation pulse) is received, each channel will open sequentially for a time period selected by the front panel switches. Any photon detected at a particular time period will be stored in the corresponding channel. The whole decay curve is accumulated for a preset number of laser triggers. The threshold level at the input is set at -40 mV, such that only input signal ≥ a single photon level is registered.

The signal was collected centrally at and near the carbon peak (~1.49 eV obtained from the emission spectrum) for different temperatures from 4.1 to 34 K at 1 degree intervals. Each decay curve was accumulated for 2 x 10^4 laser trigger pulses. The decay curves were first corrected using the Poisson distribution and then plotted using a

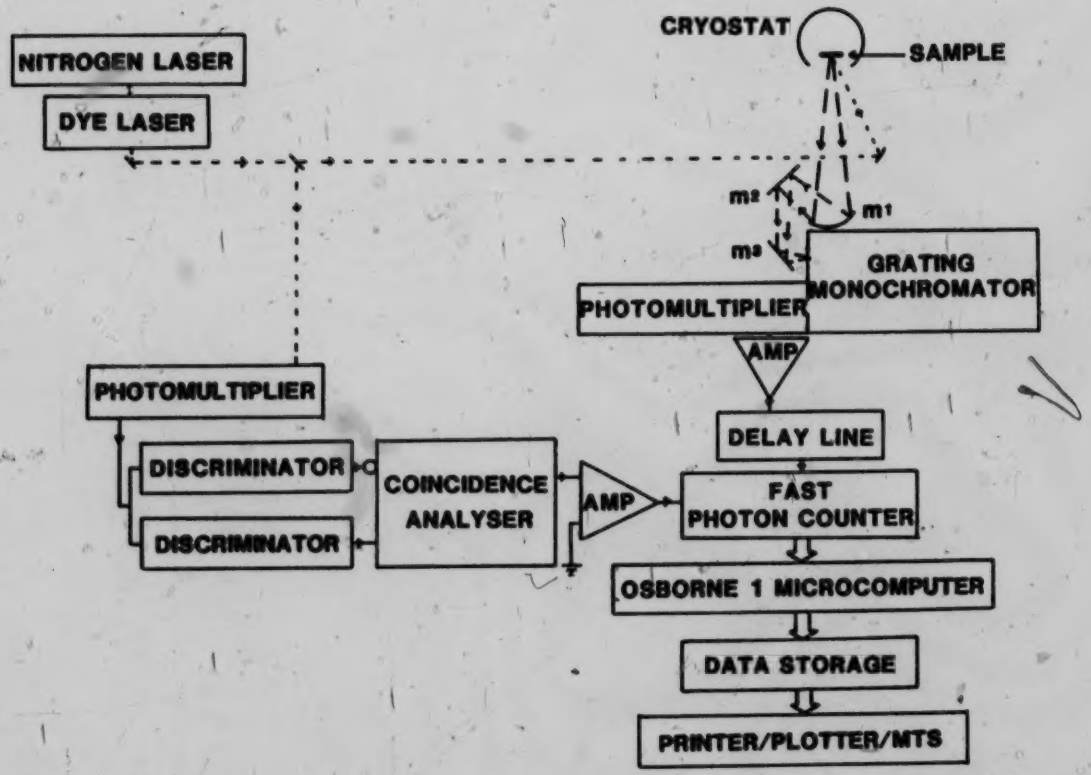

Figure 5.1 PHOTOLUMINESCENCE TRANSIENT EXPERIMENT

log-log scale to determine the region where the power-law (Dingle, 1969) is obeyed. The non-linear portion of the log-log plot was then fitted using a least-squares curve-fitting (LSF) method to find the decay time constants. The complete computer program for LSF analysis is given in Appendix B. We have also applied our newly developed technique of analysis (as discussed in Chapter 3) to analyse the initial stage of the decay.

The whole decay curve was also fitted by LSF method according to the equation:

$$y = A \exp(-t/\tau_a) + B \exp(-t/\tau_b) + C\, t^{-p(T)} \quad . \qquad (5.1)$$

The exponent p was also fitted using linear LSF method to yield a temperature dependent relationship.

5.3 Results

A typical photoluminescence decay curve measured centrally at the D-A emission peak (~1.49 eV) at 4.1 K is shown in figure 5.2. Figure 5.3 shows the luminescence decay at different temperatures. All the curves were normalised with respect to their maximum intensities.

Detailed analysis of the transient signal shows that the decay is exponential in the initial part of the transient, similar to that seen by Dingle (1969) and Kamiya and Wagner (1976). For this initial portion, the signal can be fitted by the least-squares method and a double exponential was

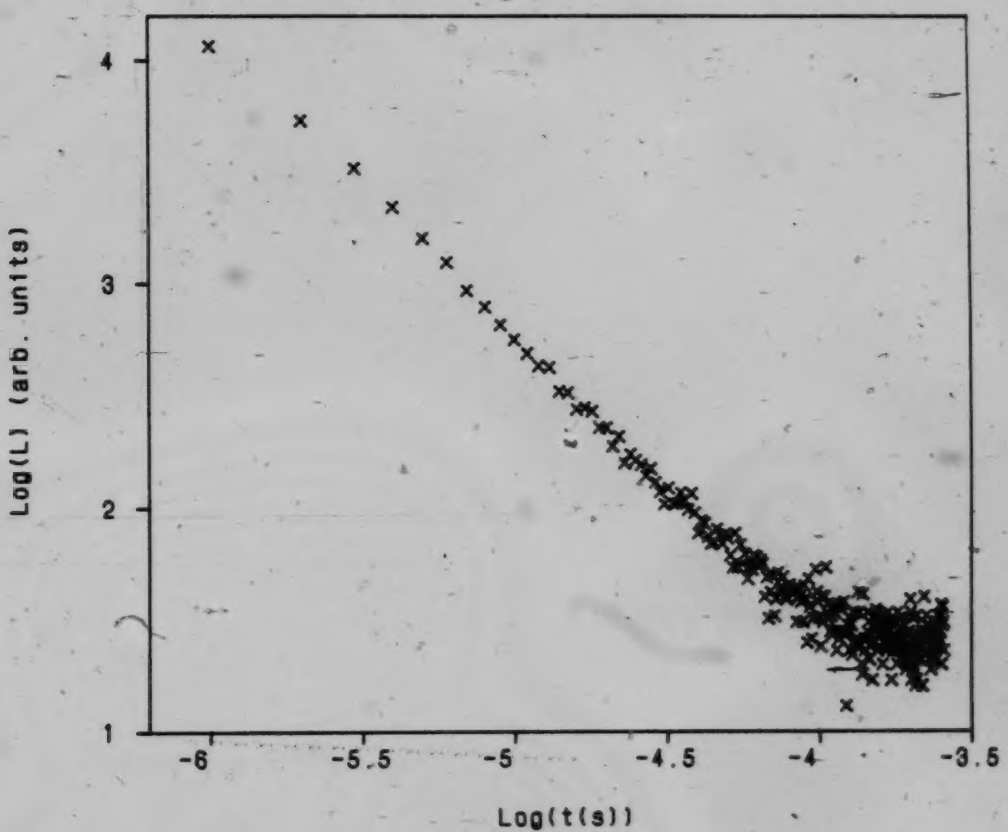

Figure 5.2 A typical decay curve at the ~1.49 eV emission at 4.1 K

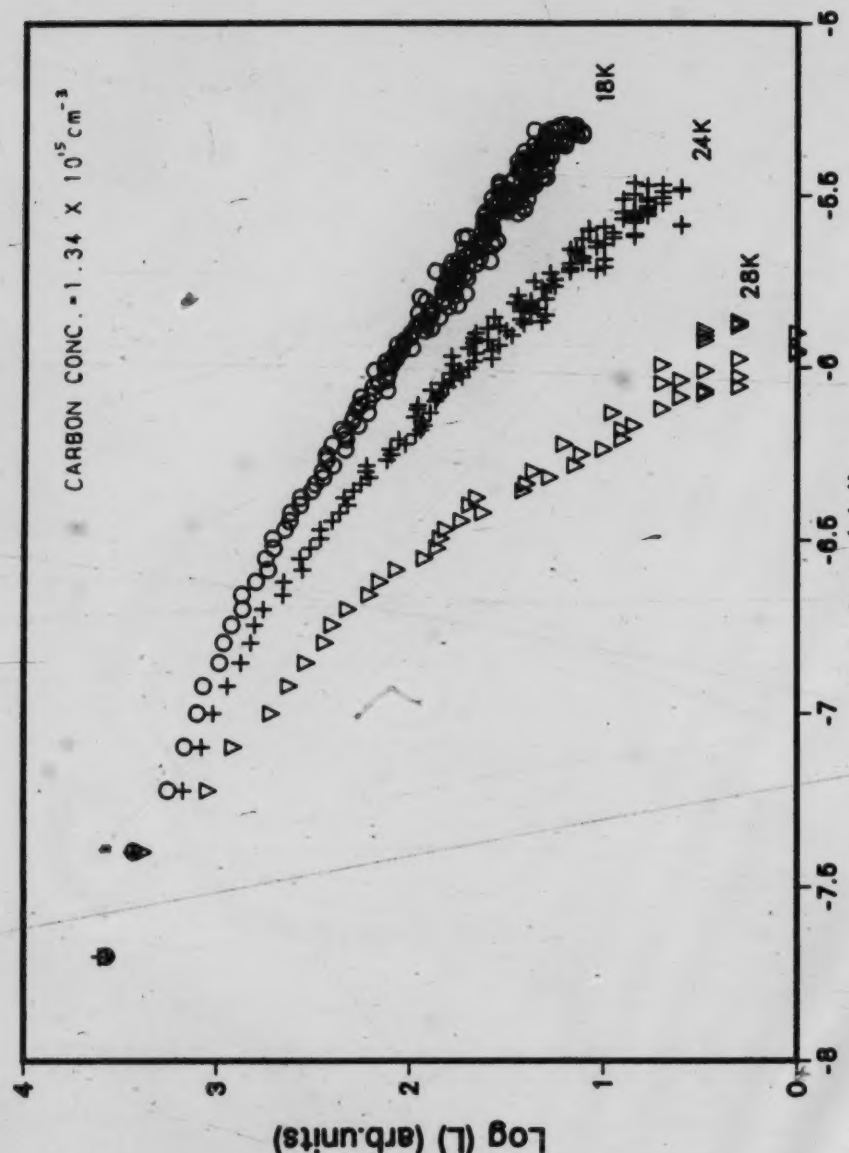

Figure 5.3 Decay curves shown for three different temperatures

obtained. The fast component, which vanishes within 100 ns, has been attributed by Dingle (1969) to the transition at the band-gap while the slower component is due to the donor-acceptor emission (Dingle, 1969). The decay time constant was temperature independent below 18 K; however, it was found that from 25 to 32 K, the decay constant follows the Arrhenius relation $\tau = \tau_0 \exp(\Delta E/kT)$ as shown in figure 5.4 and gives an activation energy ΔE of 15 ± 1 meV. The exponential part of the data was also analyzed using PTS (Teh et al., 1986) to confirm the validity of our newly developed technique of analysis. The results agree with the former analysis of 15 ± 1 meV. This value was consistently obtained for all the samples studied, which have carbon concentrations varying from $\sim 10^{14}$ to $\sim 10^{16}$ cm^{-3}. (See table 5.1).

From the log-log plot of the signal, it was found that following the exponential behavior, the decay obeys the power law of t^{-p}. ($p = 1.4$ at 4.1 K which agrees with Dingle's result (Dingle, 1969)). It was observed that this exponent p varies as a function of temperature and increases to ≈3.5 in the temperature range between 18 and 30 K. The change in p as a function of temperature seems to depend on the carbon concentration, as shown in figure 5.5.

Table 5.1 Activation energies for samples with different carbon concentrations.

Carbon Concentration ($\times 10^{14}$ cm^{-3})	Activation Energy ΔE (meV) PTS†	LSF‡
~0.6	14.9 ± 1.0	14.6 ± 0.9
3.9	14.7 ± 1.0	15.0 ± 0.6
10.8	16.0 ± 1.0	14.5 ± 0.7
13.4	14.7 ± 1.0	15.9 ± 0.8
45.5	15.0 ± 2.0	15.0 ± 2.0

† Photoluminescence Transient Spectroscopy

‡ Least-squares method

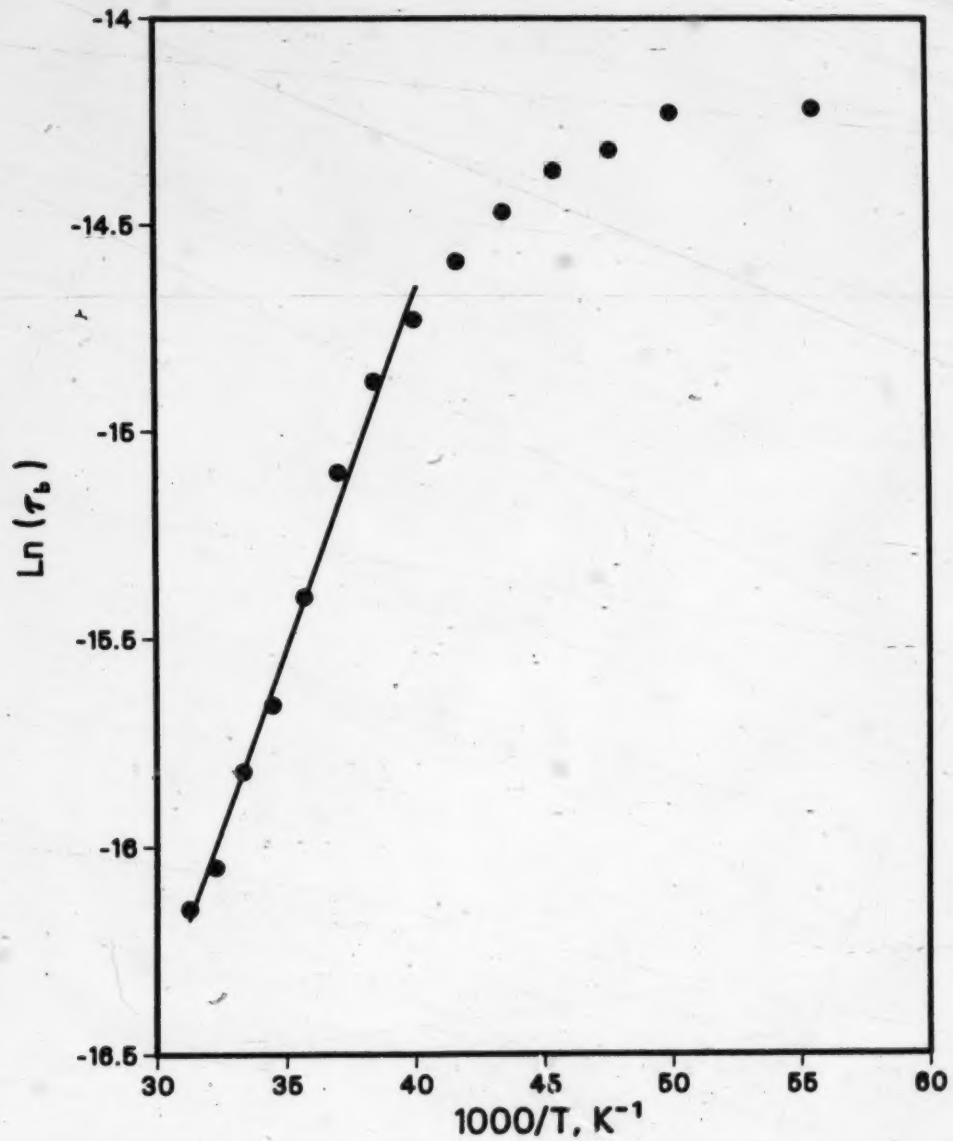

Figure 5.4 Temperature dependence of the exponential decay τ_b

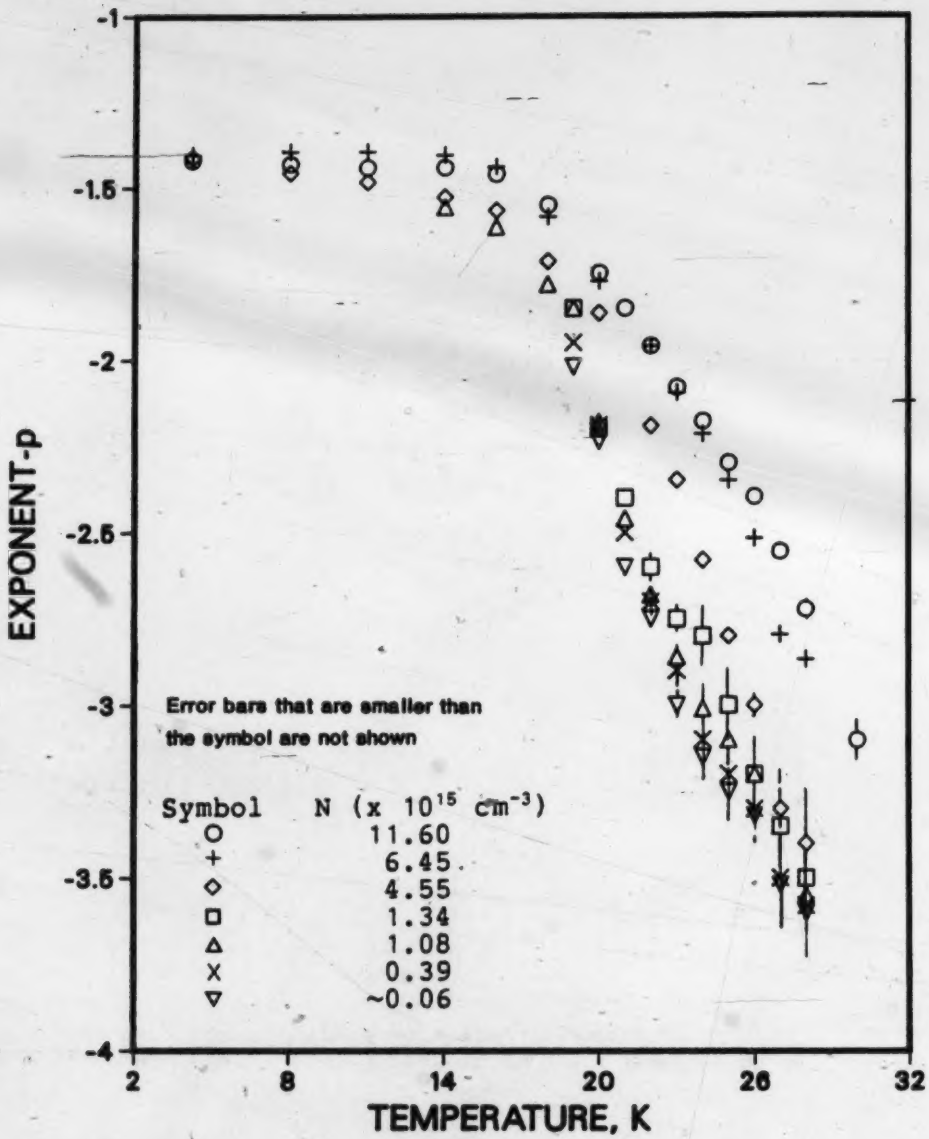

Figure 5.5 Temperature dependence of the exponent p for different carbon concentrations, N

At the initial part of the decay ($t < 1\ \mu s$), the double exponential decay can be written as follows:

$$L_s(t) = A \exp(-t/\tau_a) + B \exp(-t/\tau_b) , \qquad (5.2)$$

with decay time constants τ_a varying from ~85-20 ns and τ_b varying from ~700-70 ns for various samples in the temperature range 4.1 - 34 K. Results obtained from LSF analysis are shown for a typical sample in table 5.2. In the same temperature range, the fast decay time constant, τ_a, was also found to follow the Arrhenius relation (figure 5.6):

$$\tau_a = \tau_{ao} \exp (\Delta E_a/kT) , \qquad (5.3)$$

where $1/\tau_{ao}$ is the maximum recombination frequency, ΔE_a is the activation energy, k is the Boltzmann constant and T is the temperature. The activation energy ΔE_a was found to be 5.7 ±0.7 meV. Table 5.3 shows the value of ΔE_a for different carbon contents. At temperature around 34 K, only the fast component A of the exponential decay remained.

Due to the low resolution in the time window of the FPC, the number of data points which described the fast component was insufficient to allow for PTS analysis.

At a later stage of the decay ($t > 1\ \mu s$), the exponent, p, was found to be linearly temperature dependent in the temperature range $18 \leq T \leq 30$ K (where the decay time constants start to decrease (figure 5.4)). This is shown by the linear least-squares fit of the data points in figure

Table 5.2 Decay time constants for a sample with $N = 1.08 \times 10^{15}$ cm^{-3}.

Temperature (K)	τ_a (ns)	τ_b (ns)
19	85.3	677
20	81.5	647
21	75.2	588
22	73.3	547
23	67.2	470
24	67.2	446
25	64.1	384
26	59.2	333
27	53.1	259
28	48.5	211
29	43.4	155
30	39.7	131
31	37.1	112
32	32.3	106
33	31.8	-
34	28.0	-

$T \leq 18$ K : no significant change in values

Table 5.3 Activation energies, ΔE_a

N (x 10^{15} cm^{-3})	ΔE_a (meV)
4.55	4.8 ± 0.7
1.34	6.0 ± 0.4
1.08	6.6 ± 0.2
0.39	5.5 ± 0.3
~0.06	5.4 ± 0.3

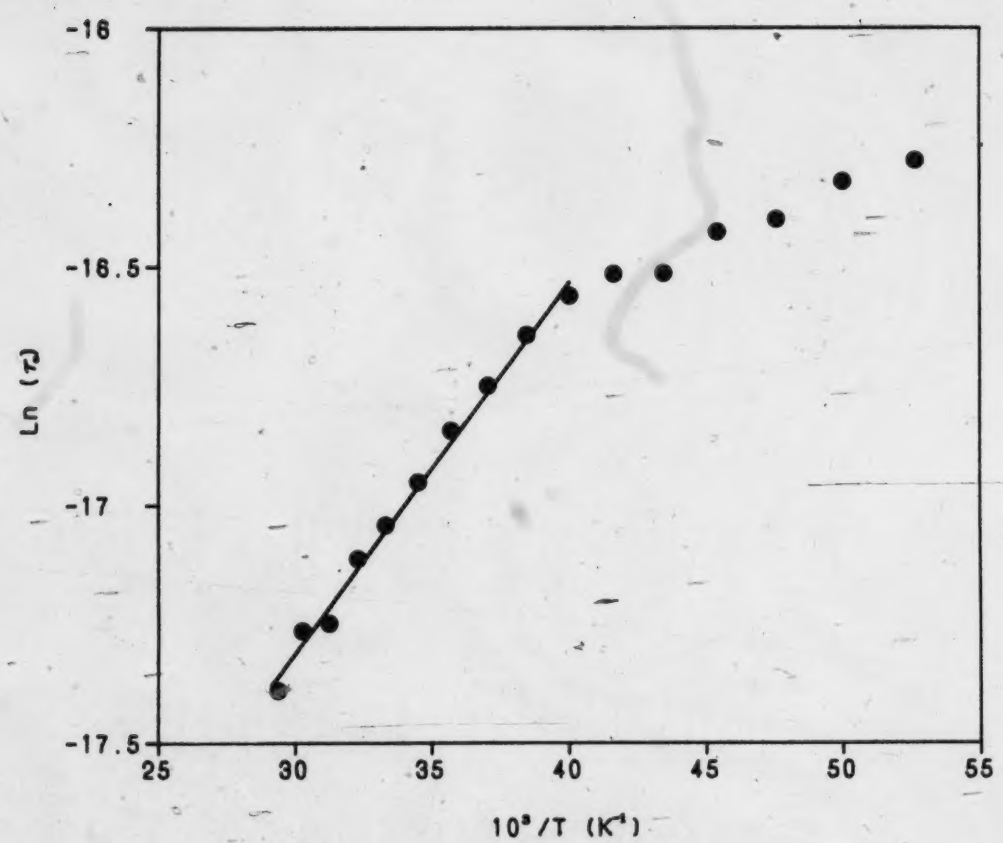

Figure 5.6 Temperature dependence of decay time constant τ_o

5.7 according to the expression:

$$p = \alpha_o + \beta T \ , \qquad (5.4)$$

with $\alpha_o = -1$, and β, the temperature dependent coefficient, being dependent on the carbon concentration, as shown in table 5.4, and figure 5.8. However, for very low carbon concentrations ($< 10^{15}$ cm^{-3}), the variation in β was negligible.

From the least-squares curve fitting analysis of the entire decay curve measured at 4.1 K, it was found that the different decay mechanisms that were responsible for the double exponential and power-law behaviors did not coexist over the entire time range. In fact the power-law mechanism occurs only ~ 1 μs after the excitation has ceased and is always preceded by the exponential decay.

Similar analysis on the luminescence curves measured on both sides of the ~1.49 eV peak shows that the decay rate is faster on the higher energy side, with smaller activation energy and larger p value, and the reverse is true on the lower energy side.

5.4 Discussions

Since the results show that the photoluminescence decay obeys two different laws at difference stages, we will discuss the different components in turn.

Table 5.4 Values of α_o and β in $p = \alpha_o + \beta T$ for $18 \leq T \leq 30$ K.

N (x 10^{15} cm^{-3})	α_o	β
11.60	-0.9 ± 0.1	0.129 ± 0.006
6.45	-1.2 ± 0.2	0.144 ± 0.009
4.55	-1.2 ± 0.1	0.159 ± 0.006
1.34	-1.1 ± 0.2	0.165 ± 0.009
1.08	-1.1 ± 0.2	0.166 ± 0.009
0.39	-1.1 ± 0.2	0.172 ± 0.009
~0.06	-1.2 ± 0.2	0.176 ± 0.009

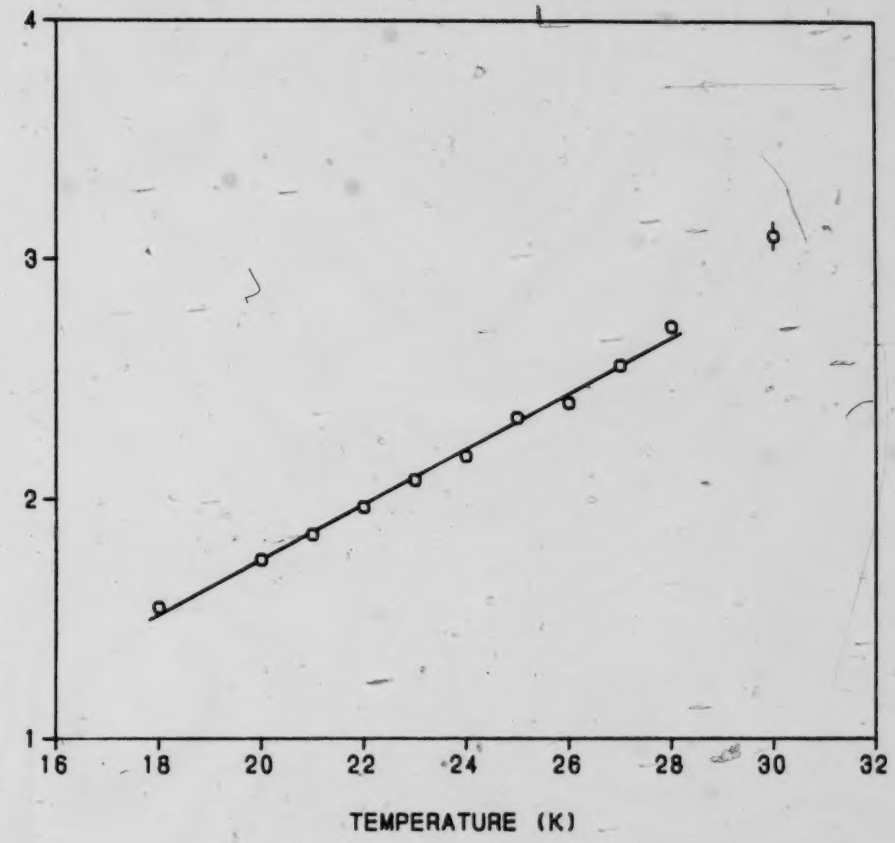

Figure 5.7 Linear temperature dependence of exponent p in $18 \leq T \leq 30K$

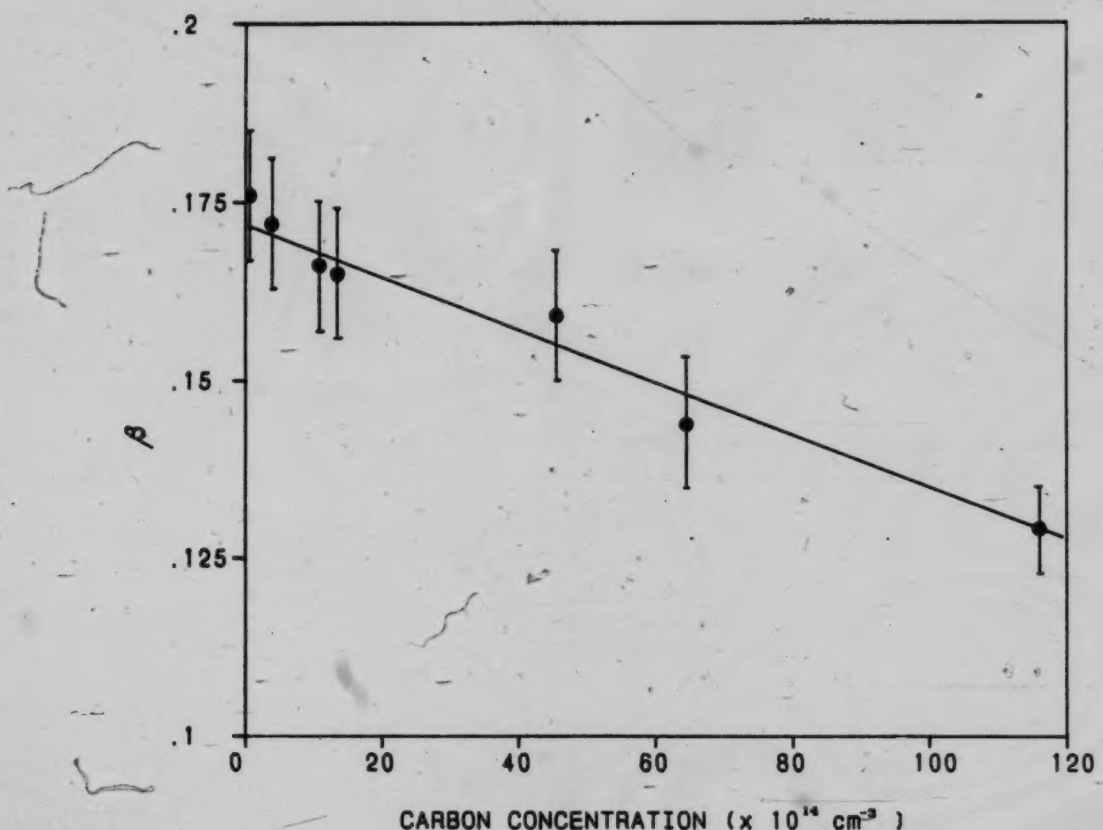

Figure 5.8 Concentration dependence of β

5.4.1 Initial double exponential decay

In our preliminary analysis of the initial double exponential decay, we have attributed the fast component to band-gap recombination, in accordance with Dingle's proposal (Dingle, 1969), and the slow component was attributed to D-A pairs recombination related to the C_{As} acceptor level (Kamiya and Wagner, 1976). We have observed that the decay time constant, τ, due to the bound exciton recombination at 1.512 eV is < 10 ns, which is beyond the measuring capability of our FPC. Weiner and Yu (1984) have reported that the free carrier lifetime for band-to-band transition is 1.2 ns for undoped SI GaAs. Since the decay time constant, τ_a, is ~80 ns, it is not possible, therefore, for the fast component to be related to the band-gap or bound exciton recombination. The decay time constant for band-to-acceptor transition has been reported by Ulbrich (1974) for epitaxial GaAs to be 80 ns. In Chapter 4, we have mentioned that there is an overlap of two radiative processes involving the D-A pairs recombination and B-A transitions. The values of τ_a that we observed are close to that reported by Ulbrich (1974) for B-A transition. We, therefore, propose that the fast component A is due to the B-A recombination. In addition, the emission spectra in Chapter 4 show that the B-A transition becomes prominent as temperature increases. The decay measurements also show that the A:B ratio increases with temperature until ~34 K when only the A component remains. For annealed samples, where no

discernible D-A transition was recorded, neither the B component nor the power-law decay was detected. For the sample with the highest carbon content (~3 x 10^{16} cm^{-3}), only a fast decay was observed. Dingle (1969) has also shown that highly-doped crystals have very fast decay times (τ < 15 ns), which convinced him that when the doping level is increased to a point where the donor levels become degenerate with the conduction band, recombination will then be mainly of the free-to-bound type of transition.

From the above observations, we propose that the A component is due to the B-A transition instead of the band-gap transition as reported by Dingle (1969).

The two decay time constants, τ_a and τ_b, follow the Arrhenius relationship in the same temperature range (25-32 K) as shown in figures 5.4 and 5.6. They should therefore be related to the same center, C_{As}.

A relaxation process involving discrete centers usually results in an exponential decay. This recombination process is more probable for electrons escaping from hydrogenic shallow levels than from deep levels. The B component of the double exponential decay could be due to transitions between distant D-A pairs with small R values because the probability of small R (D-A spatial distance) recombination is higher. During the early stage of the decay, close D-A pairs will recombine as simple discrete pairs (Dingle, 1969). For temperatures < 18 K, the recombination process will involve only a simple transition between the D-A

levels, giving rise to the temperature-independent exponential decay.

We will now explain the origin of the activation energy ΔE = 15 meV.

The activation energy obtained from our results is significantly different from that of the binding energy of the carbon acceptor level of 26 meV obtained by others (Ozeki et al., 1974; Ashen et al., 1975; Kamiya and Wagner, 1976). The mechanism involved in our photoluminescence study could be due to trapping levels in the intermediate transition stage as shown in the schematic energy band diagram in figure 5.9. The broken line denotes the trapping level *T*, the donor and acceptor levels are labeled as *D* and *A* respectively. The double arrows show prompt radiative transition and the broken arrows show traps emptying into their neighboring states. If the transition from levels *T* to *A* is not completely forbidden (single arrow in figure 5.9 a), then this transition will be a temperature independent exponential decay. However, the transition from *T* to *A* via *D* will follow a temperature dependent exponential decay with an activation energy of ΔE. This activation energy ΔE is required to raise the electron out of the trap *T* to the radiative stage *D* (Leverenz, 1950). The value of 15 meV, which we found from our analysis, is the

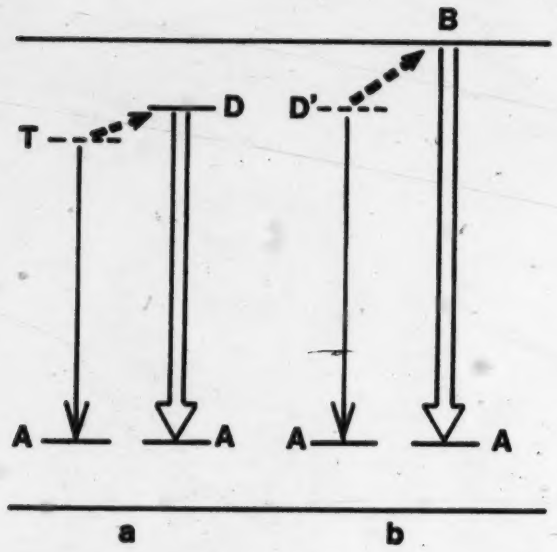

Figure 5.9 Energy band diagram for photoluminescence.

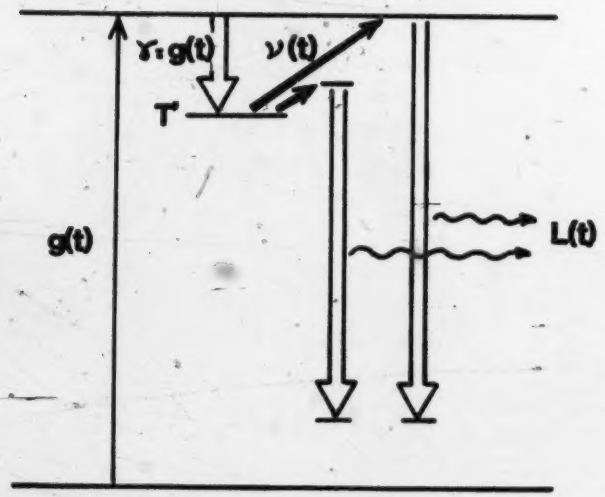

Figure 5.10 Schematic energy diagram with a set of traps.

activation energy ΔE.

Using the same argument as above, the B-A transition (figure 5.9 b) for temperatures > 18 K can also involve some intermediate states D', where an activation energy of ΔE_a = 5.7 meV is required to raise the electron out of the trap.

Decay curves measured at two different emission energies on both sides of the D-A emission peak give slightly different activation energies. At the higher energy side of the emission peak where the decay rate is faster, the activation energies ΔE_a < 5.7 meV and ΔE_b < 15 meV. At the lower energy side of the emission peak, the decay rate is slower and ΔE_a > 5.7 meV and ΔE_b > 15 meV.

It is known that most impurities like Se, S, Si substituted at gallium sites have energies ~6 meV (Watts, 1977). Fourier transform infrared measurements‡ show the presence of a weak local vibrational mode absorption at 384 cm^{-1}, attributed to Si_{Ga}, in all the samples studied. This weak absorption shows that silicon impurity is present in a low concentration of ~10^{15} cm^{-3}, which could account for the presence of donors involved in the D-A recombination. Even though carbon has an amphoteric nature, which when substituted at the gallium site would provide a donor level, we do not have conclusive evidence of the presence of C_{Ga}.

The presence of a trapping level at ~5.7 meV from the conduction band could be related to the Si_{Ga} donor levels. The level with an activation energy of ~15 meV below the

---

‡This is discussed in Chapter 6.

donor level could be related to the EL2 level as will be discussed below.

5.4.2 Power-law decay

The broad band observed in the D-A emission peak (figure 4.4) is due to a distribution of distant D-A pairs with different R values. The presence of such a distribution could affect the kinetics of the recombination processes and may be responsible for the power-law behavior. Several possible mechanisms exist to explain this power-law behavior and we will discuss each of these mechanisms in turn.

5.4.2.1 Existence of intermediate trapping states

If a continuum of trapping levels exists at T (figure 5.9), then each of these traps will contribute to the radiative transition from levels D to A. The power-law response will occur if the trap concentration varies exponentially with depth (Leverenz, 1950). This accounts for the power-law decay that occurs after the initial exponential decay. The rate of detrapping from the traps seems to be temperature dependent between 18 and 30 K (as reflected on the temperature variation of the exponent, p). For temperatures above 32 K the signal is too small to be detectable with our present equipment. The traps seem to empty faster when the concentration of carbon is low

and vice versa. This could be due to a retrapping process that depends on the concentration of the traps, which we assume to be proportional to the carbon content.

A variation of the above mechanism has been proposed by Jonscher and de Polignac (1984). According to their proposal, the power-law decay is due to the presence of either one or two sets of deep traps. Assuming that a single set of traps exists in our case, as denoted by T' in figure 5.10, then the rate of luminescence decay is determined by the rate of the detrapping process from the traps.

The detrapping process is usually thermally assisted. Kurita et al., (1979) suggested that the luminescence decay time is determined by the rate of thermal detrapping.

The probability, p, of releasing electrons from traps at energy levels denoted by E_T is (Levshin et al., 1964; Mott, 1978):

$$p = p_o \exp(-E_T/kT) \quad . \qquad (5.5)$$

Since the decay time is governed by the detrapping rate, a shallower set of traps will give a faster decay. For a set of deeper traps, the decay rate will be small due to the reduced probability, p, of freeing electrons from the traps.

Walukiewicz et al., (1983) have reported a set of new trapping levels at 20-30 meV below the conduction band. From their observation of the correlation between the concentrations of these new levels and those of the major traps, EL2, they concluded that the two levels are related. They have also shown that the depths of these shallow trapping states increase with concentration.

It is known that the presence of carbon in LEC SI GaAs is compensated by the EL2 levels to give the semi-insulating property (Holmes et al., 1982a). Since the samples in our studies are semi-insulating, we can assume, therefore, that the samples with more carbon will have more EL2, which in turn means that there will be more shallow trapping levels of the type reported by Walukiewicz et al., (1983). The increase in carbon concentration will then lead to *deeper* traps.

If these shallow traps are indeed involved in the recombination process as previously described, then samples with high carbon contents will have slower rates of decay because the detrapping process now involves *deeper* traps. This could explain the smaller p values for samples with high carbon concentrations.

5.4.2.2 Existence of a random distribution of D-A pairs

A hopping mechanism has been widely discussed in systems involving a random distribution of defects such as in amorphous materials. This mechanism has also been proposed for crystalline GaP (Thomas et al., 1965) and

GaAs (Dingle, 1969).

Thomas et al., (1965) have shown theoretically that radiative recombinations involving a random distribution of donors and acceptors throughout a crystal with exact or nearly exact compensation results in power-law decay. The power-law decay usually occurs after a certain time from the termination of the excitation pulse. The reason for this is that after a certain time when the photo-excited electrons have been partially de-excited, it will be easier for these electrons to move through the crystal, from one impurity to another, until they are at a critical distance R_c from a neutral acceptor where recombination can occur. The lifetime in this case will be dependent on the rate of hopping, which is strongly temperature dependent (Thomas et al., 1965; Dingle, 1969).

At low temperatures, once the electron is trapped, it remains trapped until the temperature is high enough to release it. Thus, below 18 K the decay rate remains unchanged until the electron can be thermally excited out of its trap, thereby increasing the hopping rate. The increasing hopping rate explains the increase in recombination rate as temperature is increased beyond 18 K. The energy difference between hopping sites must be within the value of kT for the hopping mechanism to be possible.

For a sample with a low concentration of impurities, the centers will be further separated, in both energy and linear distance, than those in a sample with a higher concentration.

Since SI GaAs is a compensated crystal, we can assume that the number of donor traps is proportional to the carbon concentration. For a sample with a high carbon content, the close proximity of the impurity sites encourages the electron to linger longer among the sites (figure 5.11 a), hence resulting in a slower decay and a smaller exponent, p. When the concentration of impurities is very low (10^{14} - 10^{15} cm^{-3}), the hopping mechanism is limited, causing little change to the value of β.

We will now discuss the observed quenching of the photoluminescence signal. We will also propose another possible mechanism related to non-radiative processes that affects the exponent p for different carbon concentrations at temperatures > 20 K.

During the hopping of electrons between impurity sites, those electrons with excess thermal energy can also be recaptured by the conduction band which contributes to the quenching of the D-A pairs radiation with an increase in B-A transition. At higher temperatures, the carriers will have enough energy to diffuse away and then be recaptured at a non-radiative center (Street, 1981), which explains the reduction in

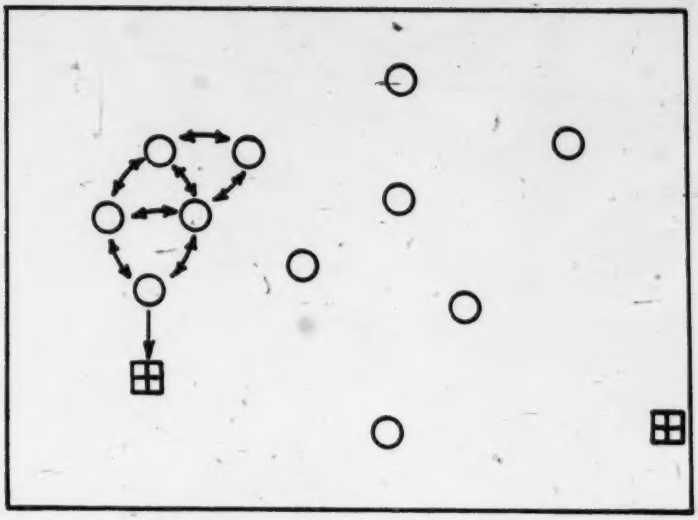

(a) High carbon concentration
o electrons ; ⊞ holes
Recombination between electron and hole is delayed.

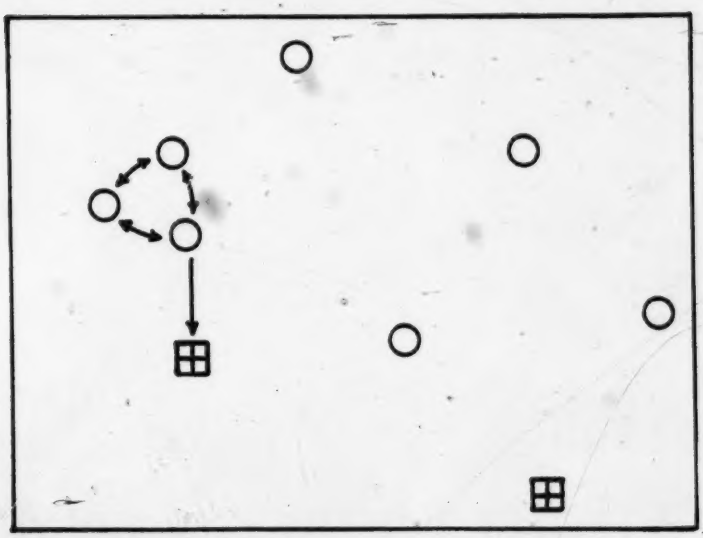

(b) Low carbon concentration
o electrons ; ⊞ holes
Recombination rate is faster as more sites are separated by energy difference >kT, which limit the hopping mechanism.

Figure 5.11 Decrease in recombination rate due to interaction between neighboring states of similar kind.

luminescence intensity at increasing temperatures.

The increase in the probability of non-radiative recombination with temperature will change the rate of radiative recombination and thus changes the temperature dependence of the exponent p.

In order to explain the difference in the change of p as a function of temperature for different carbon concentrations, it is necessary to use the hopping rate expression (Thomas *et al.*, 1965):

$$R = R_{max} \exp(-\frac{2R}{a_o}) ,$$

where a_o is the Bohr radius of the donor. It is obvious that the hopping rate increases for small R (D-A separation) distances. If this hopping mechanism involves non-radiative centers, then at elevated temperatures, the probability of radiative recombination is reduced for D-A pairs with small R values as they are being depleted by non-radiative processes. The contribution for radiative recombination must be from D-A pairs with large separations R. As the density of defects is increased, as in high carbon content samples, the fraction of pairs that recombine radiatively decreases (see figure 5.12). As the concentration of distant D-A pairs with large R distances is higher in low carbon samples, the decay rate is faster. This fast recombination rate is shown by a higher value of the exponent, p, which leads to a greater change in p as a

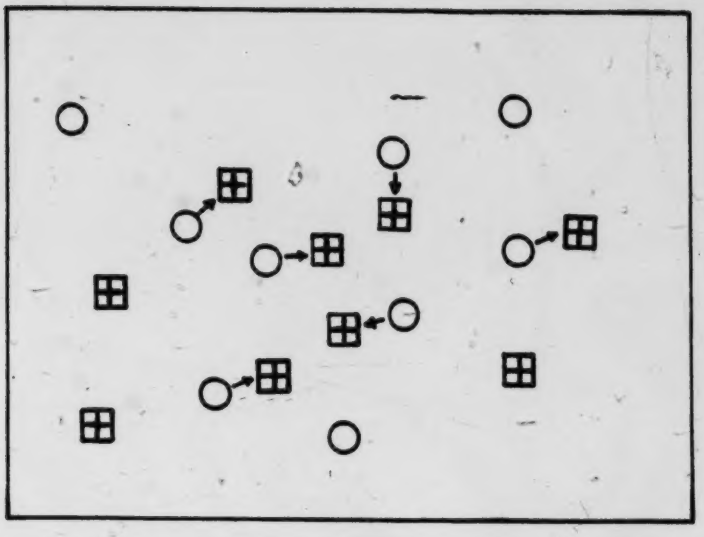

(a) In high carbon content sample, the fraction of distant pairs that recombine radiatively decreases.

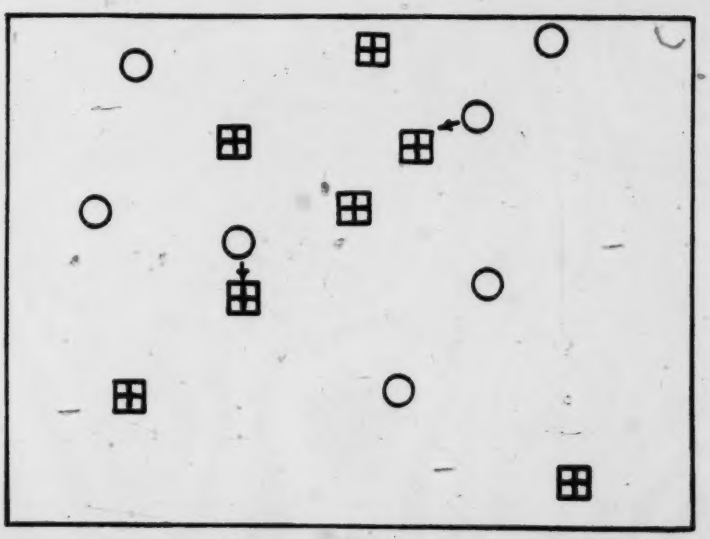

(b) In low carbon content sample, the concentration of distant pairs is higher, hence the decay rate is faster.

Figure 5.12 Non-radiative recombinations between neighboring states

function of temperature. In the case of crystals with only a few distant pairs, recombination will occur at a slower rate.

For carbon concentrations varying from ~10^{16} to 10^{15} cm^{-3}, the increase in β is ~20%. The change in p, and consequently β, is negligible for carbon concentrations varying from 10^{15} - 10^{14} cm^{-3}. This shows that there is a certain limit in the number of distant D-A pairs with large R distances that contribute to the radiative decay.

Tunnelling processes have also been proposed to explain the power-law behavior of the luminescence decay in amorphous materials. However, we believe that these processes do not apply in our case because the single-crystalline materials used in our studies have low densities of defects. Furthermore, tunnelling is a low temperature process and loses its significance at high temperatures (Hong et al., 1981).

5.5 Conclusion

We have shown from the photoluminescence studies that the time response of the emission at ~1.49 eV, due to C_{As}, actually obeys a double exponential and a power-law behavior. The activation energies obtained from the temperature dependence of the double exponential of the photoluminescence transients were about 5.7 and 15 meV. The power-law behavior follows the relation t^{-p} where p ranges

from 1.4 to ≃3.5.

In the temperature range $18 \leq T \leq 30$ K, the exponent p follows the equation: $p(T) = -1 + \beta T$ where β is proportional to the concentration of C_{As}.

To explain the power-law results, we have discussed three different mechanisms involving the following: i) existence of intermediate trapping states and ii) existence of a random distribution of donor-acceptor pairs.

Since at elevated temperatures there exists a competitive non-radiative process that causes the quenching of the signal, it is possible that the last mechanism proposed contributes to the temperature dependence of the exponent, p.

We can conclude that there also exist two sets of shallow trapping levels with energies ~5.7 meV from the conduction band, and ~15 meV from the donor level E_D. If the binding energy of donor, E_D, is ~6 meV, which is common for most donor states in GaAs, then this second trapping level is ~21 meV from the conduction band. The trapping donor level at ~21 meV is within the range of energies reported for a set of shallow donors related to EL2.

We suspect that the origin of the level at ~5.7 meV is related to silicon substituted at the gallium sites.

Bibliography

Ashen, D.J., Dean, P.J., Hurle, D.T.J., Mullin, J.B., and White, A.M. (1975). J. Phys. Chem. Solids 36, 1041

Dingle, R. (1969). Phys. Rev. 184, 788

Holmes, D.E., Chen, R.T., Elliott, K.R., and Kirkpatrick, C.G. (1982a). Appl. Phys. Lett. 40, 46

Hong, K.M., Noolandi, J., and Street, R.A. (1981). Phys. Rev. B 23, 2967

Jonscher, A.K., and de Polignac, A. (1984). J. Phys. C 17, 6493

Kamiya, T., and Wagner, E. (1976). J. Appl. Phys. 47, 3219

Kurita, S., Czaja, W., and Kinmond, S. (1979). Solid State Commun. 32, 879

Leverenz, H.W. (1950). *An Introduction to Luminescence of Solids*, p. 269 (Wiley, New York)

Levshin, V.L., Arapova, E. Ya., Blazhevich, A.I., Voronov, Yu. V., Voronova, I.G., Gutan, V.B., Lavrov, A.V., Popov, Yu. M., Fridman, S.A., Chikhacheva, V.A., and Shchaenko, V.V. (1963). In *Soviet Researches on Luminescence* (Acad. D.V. Skobel'tsyn, ed.)(English Translation), p. 98 (Consultants Bureau, New York, 1964)

Mott, N.F. (1978). Solid State Electron. 21, 1275

Ozeki, M., Nakai, K., Dazai, K., and Ryuzan, O. (1974). Jpn. J. Appl. Phys. 13, 1121

Street, R.A. (1981). Adv. Phys. 30, 593

Teh, C.K., Tin, C.C., and Weichman, F. L. (1986). J. Luminescence 35, 17

Thomas, D.G., Hopfield, J.J., and Angustyniak, W. M. (1965). Phys. Rev. 140, A202

Ulbrich, R. (1974). In *Proceedings of the Twelfth International Conference on the Physics of Semiconductors* (M.H. Pilkuhn, ed.), p. 376 (B.G. Teubner, Stuttgart)

Walukiewicz, W., Lagowski, J., and Gatos, H.C. (1983). Appl. Phys. Lett. 43, 112

Watts, R.K. (1977). *Point Defects in Crystals*, p. 206 (John Wiley & Sons)

Weiner, J.S., and Yu, P.Y. (1984). J. Appl. Phys. 55, 3889

6. FOURIER TRANSFORM INFRA-RED (FTIR) SPECTROSCOPY OF UNDOPED LEC SI GaAs

6.1 Introduction

The infra-red active localized vibrational modes (LVM) absorption is useful for identifying low atomic number impurities in GaAs. Each impurity gives rise to a characteristic frequency (Bellomonte, 1977) resulting from the LVM absorption, and the integrated intensity or absorption strength is proportional to the concentration of the impurity (Brozel *et al.*, 1978; Hunter *et al.*, 1984). We have measured the IR LVM absorption at 582 cm^{-1}, to detect the presence of carbon and to determine its concentration in samples of LEC SI GaAs.

The IR absorption spectra can be measured with a conventional IR spectrometer. However, due to some limitations that have been discussed in Chapter 1, we chose to use the FTIR technique for obtaining the IR spectra.

In addition, the optical constants, n, and k, for samples with different carbon concentrations, have also been computed using the Kramers-Krönig relation.

6.2 Theory: Fourier Transform Spectroscopy

A FTIR spectrometer or interferometer is basically a Michelson interferometer (Griffiths, 1975). When a continuum source of light is incident on an ideal beam splitter, it is split into two equal parts. Part of the beam is transmitted

and the other is reflected. Two plane mirrors situated at 45° to the beam splitter, and at right angles to each other, one with a fixed position while the other is movable, will reflect the two parts of the beam and will recombine them at the detector with varying optical path difference. If the mirror is moved by x cm, the optical retardation, δ, is 2x cm (the Bruker FTIR spectrometer used has been modified to give 4x cm). When the retardation is zero or an integral number of wavelengths, $n\lambda$ ($n=1,2,3,...$), the beam will interfere constructively, and the maximum intensity will be detected. When the optical retardation equals to $\frac{n\lambda}{2}$, there will be destructive intereference. If intensity is measured with the mirror moving at a constant velocity, then a sinusoidal signal will be detected. That is, the intensity of the signal at any point where $\delta = n\lambda$ is equal to the intensity of the source $\int_0^\infty I(\bar{\nu})\, d\bar{\nu}$, and at any value of δ (Griffiths, 1975):

$$I'(\delta) = \int_0^\infty 0.5\, I(\bar{\nu}) \{1 + \cos(2\pi\frac{\delta}{\lambda})\}\, d\bar{\nu} \,. \qquad (6.1a)$$

Since $\bar{\nu} = \frac{1}{\lambda}$

$$I'(\delta) = \int_0^\infty 0.5\, I(\bar{\nu}) \{1 + \cos(2\pi\delta\bar{\nu})\}\, d\bar{\nu} \,, \qquad (6.1b)$$

which consists of a constant d.c. term and a modulated a.c. component. The part that is important in spectroscopic measurements is the a.c. component, which is known as the *interferogram* given by:

$$I(\delta) = \int_0^\infty 0.5\ I(\bar{\nu})\ \cos(2\pi\delta\bar{\nu})\ d\bar{\nu}\ . \qquad (6.2)$$

For a non-ideal case, for example when the beam splitter is not 100% efficient, a correction factor, $H(\bar{\nu})$, must be introduced:

$$I(\delta) = \int_0^\infty B(\bar{\nu})\ \cos(2\pi\delta\bar{\nu})\ d\bar{\nu}\ , \qquad (6.3)$$

where $B(\bar{\nu}) = 0.5\ H(\bar{\nu})\cdot I(\bar{\nu})$.

If an interferogram is measured as a function of optical retardation, δ, information about the source intensity, $B(\bar{\nu})$, with instrumental correction, can be obtained by Fourier transformation of the interferogram. Thus,

$$B(\bar{\nu}) = \int_{-\infty}^\infty I(\delta)\ \cos(2\pi\bar{\nu}\delta)\ d\delta\ ,$$

$$= 2 \int_0^\infty I(\delta)\ \cos(2\pi\bar{\nu}\delta)\ d\delta\ . \qquad (6.4)$$

6.3 Data Analysis

6.3.1 Concentration Determination

It is known that the integrated intensity of the LVM absorption band is proportional to the concentration of the impurity, N_{imp} (Ulrici, 1984):

$$\int \alpha(\omega)\ d\omega \cong \alpha_{LVM}^{max}\cdot\Delta$$

$$= \sigma\cdot N_{imp}\ , \qquad (6.5)$$

where α_{LVM}^{max} is the absorption coefficient at the maximum of

the absorption with localized vibrational mode frequency ω_{LVM} of the impurity, Δ is the full width at half maximum (FWHM) of the peak, and σ is the absorption cross section of the center.

If the quantity αd is large enough, where d is the thickness of the sample, then the transmittance can be approximated as (Bourgoin and Lannoo, 1983):

$$T \cong (1 - R)^2 \cdot \exp(-\alpha d) \ , \qquad (6.6)$$

where R is the reflectivity of the sample. If T_o is the non-absorbing transmittance and T is the transmittance at the maximum absorption, then the absorption coefficient can be calculated as follows:

$$\alpha_{LVM}^{max} = \frac{1}{d} \cdot \ln\left(\frac{T_o}{T}\right) \ . \qquad (6.7)$$

The concentration of an impurity can then be determined if σ is known from a careful calibration. Many such calibrations have been reported for carbon impurity in GaAs (Hunter *et al.*, 1984; Homma *et al.*, 1985; Brozel *et al.*, 1986) and the values of $\frac{1}{\sigma}$ lie between 8±2 and 11 x 10^{15} cm^{-1}. In our calculations, we have used the value of 11 x 10^{15} cm^{-1} for our carbon concentration determinations.

The detection limit of impurity concentrations is given by (Ulrici, 1984):

$$DL \sim (\sigma \cdot d \cdot \frac{S}{N})^{-1} \ , \qquad (6.8)$$

where $\frac{S}{N}$ is the signal to noise ratio at the absorption peak.

For a value of $\frac{S}{N}$ = 300 and d ~3 mm, carbon concentrations as low as $\sim 10^{14}$ cm^{-3} can be detected. Measurements must be made at 77 K, because the two-phonon absorption in the GaAs lattice is reduced, as shown by Cochran *et al.* (1961), and the LVM absorption line is sharpened.

6.3.2 Computation of Optical Constants

The complex refractive index, $\hat{n}$, can be expressed by the sum of the real and imaginary refractive indices as follows (Heavens, 1955):

$$\hat{n} = n + ik \ . \tag{6.9}$$

The spectrum of the imaginary refractive index (also known as the extinction coefficient), $k(\bar{\nu})$, can be computed by an iterative process from the apparent k spectrum, $k_a(\bar{\nu})$, which is obtained from the experimental transmission spectrum, $T(\bar{\nu})$, using the relation (Cameron *et al.*, 1977):

$$k_a(\bar{\nu}) = - \frac{\ln T(\bar{\nu})}{4\pi\bar{\nu}d} \ . \tag{6.10}$$

The spectrum of the real refractive index, $n,(\bar{\nu})$ is then calculated from the extinction coefficients via the subtractive Kramers-Krönig transformation procedure during each iteration (Hawrenek *et al.*, 1976, 1976a). The equations cited are given as follows:

$$n_i = n_o + \frac{2}{\pi} (\bar{\nu}_i^2 - \bar{\nu}_o^2) \, P\int_0^{\infty} \frac{\bar{\nu} k(\bar{\nu})}{(\bar{\nu}^2 - \bar{\nu}_o^2)(\bar{\nu}^2 - \bar{\nu}_i^2)} \, d\bar{\nu} \ , \tag{6.11a}$$

which, when expanded, becomes

$$n_i = n_o + \frac{2}{\pi}\left[P\int_0^{\infty} \frac{\bar{\nu}k(\bar{\nu})}{(\bar{\nu}^2 - \bar{\nu}_i^2)}\, d\bar{\nu} - P\int_0^{\infty} \frac{\bar{\nu}k(\bar{\nu})}{(\bar{\nu}^2 - \bar{\nu}_o^2)}\, d\bar{\nu}\right], \tag{6.11b}$$

where P indicates that the principal value of the integral must be taken since there is a singularity at $\bar{\nu} = \bar{\nu}_i$.

In this subtractive Kramers-Krönig method, the computer program requires that the real refractive index, n_o, at some wavenumber $\bar{\nu}_o$ must be known. It is obtained by measuring the interference fringes of a thin sample (~0.5 mm) in a non-absorbing region in the wavenumber range that is transformed.

For all the thick samples (~3 mm) measured, the interference effects were not recorded. Hence a slight adjustment was made in the computer program to exclude these effects. Thus, the equation for transmittance is replaced by the expression:

$$T = \frac{(1 - R)^2 \cdot \exp(-\alpha d)}{1 - R^2 \exp(-2\alpha d)}, \tag{6.12a}$$

where $\alpha = \frac{4\pi k}{\lambda}$. (6.12b)

The computer program used is a modified version of the one obtained by the courtesy of Dr. J.E. Bertie of the Chemistry Department.

6.4 Experimental Procedure

We have measured the optical transmission spectra of undoped LEC SI GaAs in the wavenumber range 700–160 cm^{-1} (λ ~14–63 μm) at 80 K. These measurements were made on a Fourier transform infra-red spectrometer (Bruker IFS 113V) using a Globar source with 10 mm aperture, a black polyethylene filter, a 3 μm Mylar (polyethylene terephthalate) beam splitter and a DTGS (deuterated triglycine sulfate) detector. Details of the optics are shown in figure 6.1. The sample chamber, which was fitted with cesium iodide windows, was evacuated to ~10^{-2} Torr before the sample was cooled by liquid nitrogen.

Two interferograms, one each for the reference (empty cell) and the sample, were recorded at an optical velocity of 0.396 cm s^{-1} and averaging over 512 scans with a resolution of 0.5 cm^{-1}. The measurement of the optical retardation was provided by a He-Ne laser interferometer and a white light interferometer was used for registering the starting point. Four levels of zero-filling and a Happ-Genzel apodization were used in the computation. The interferograms were Fourier transformed, and the sample beam was then divided by the reference beam to yield the transmittance spectrum.

The LVM absorption due to C_{As} was identified; the absorption coefficient at the peak and FWHM were then measured.

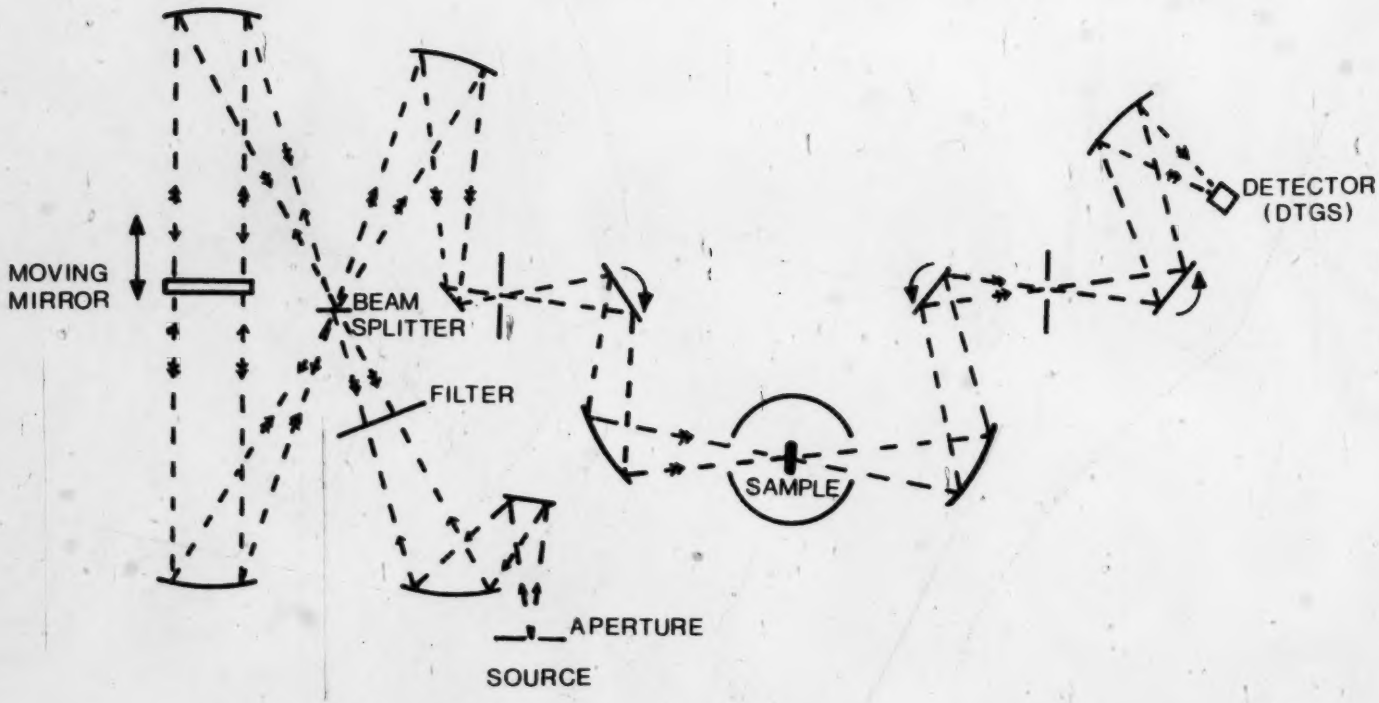

Figure 6.1 FTIR SPECTROMETER

The real and imaginary refractive indices were computed from the transmittance spectrum using program XLVI of Cameron *et al.* (1977).

The samples used for absorption measurements were carefully prepared such that the front and back surfaces were parallel and the thicknesses were appropriate for the wavelength region of interest.

All the sample thicknesses used for carbon analysis ranged from ~2.5 to 4.5 mm, and the cross-sectional area was 16 x 16 mm^2.

6.5 Results and Discussion

Figure 6.2 shows a typical transmission spectrum of an undoped LEC SI GaAs crystal. Two types of impurities, carbon and silicon, are identified by the LVM absorptions at 582.5±0.1 and 383.6±0.1 cm^{-1} similar to those discussed by Brozel *et al.* (1978), Newman *et al.* (1972), Thompson and Newman (1972), and Lorimor and Spitzer (1966).

Theis *et al.* (1982, 1983) and Leigh and Newman (1982) have shown that the carbon impurity is substituted at the arsenic site. Theis *et al.* (1982), were able to resolve the absorption peak near 582.5 cm^{-1} into five sub-bands. They have attributed the fine structure to contributions by the different isotopes of gallium, ^{69}Ga (60.4%) and ^{71}Ga (39.6%), acting as nearest neighbors to the carbon substituent. Ulrici (1984) has shown, from theoretical calculations, that the distribution of the phonon local density of states

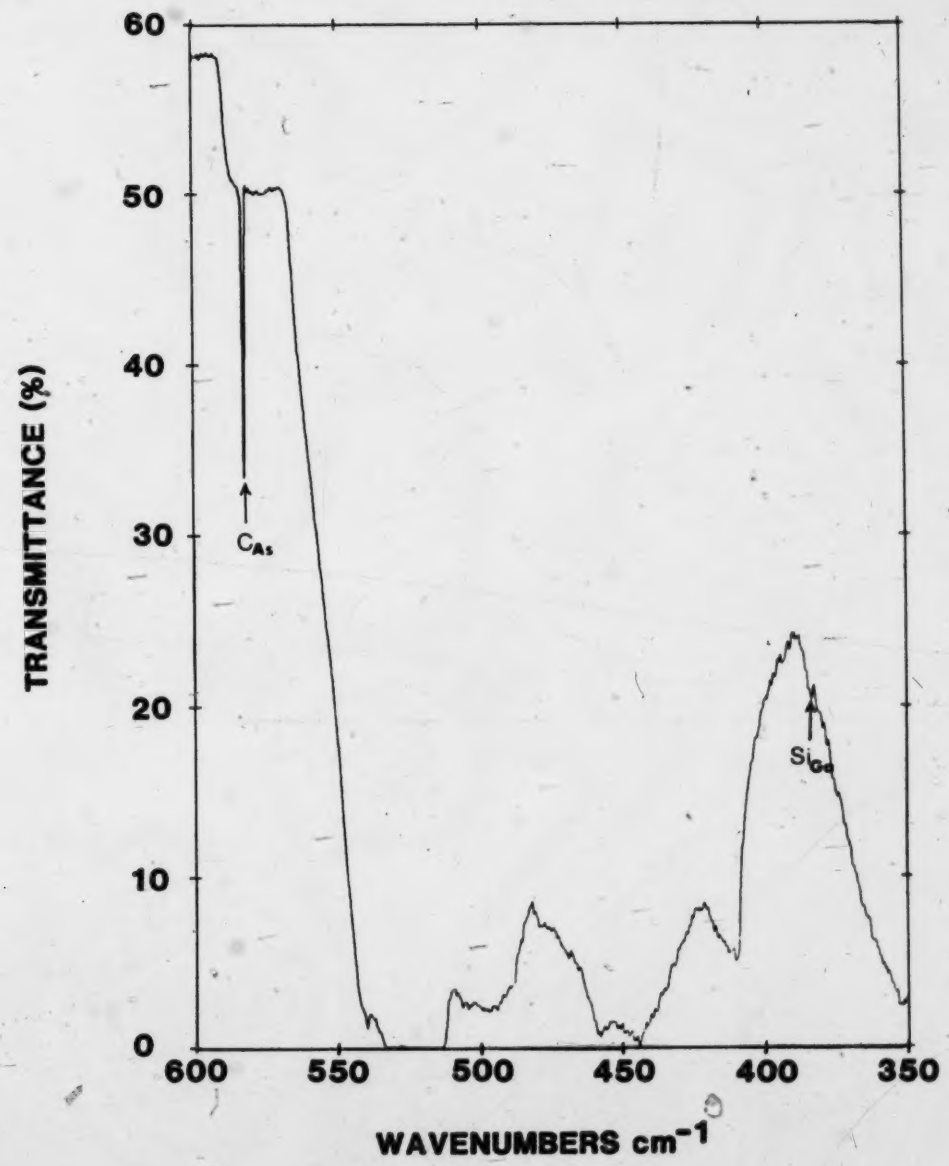

Figure 6.2 A typical transmission spectrum of LEC SI GaAs

(which is proportional to the absorption coefficient) resulting from the five different configurations of CGa_4, is in agreement with that of the experimental fine structure of Theis *et al.* (1982). All the above prove unambiguously that carbon atoms in GaAs are substituted at the arsenic sites.

Similar splitting effects for silicon substituted at the arsenic sites have also been observed (Theis *et al.*, 1982, 1983). For silicon substituted at the gallium sites, no such splitting was observed even under high resolution at 384 cm^{-1}. This is because there is only one isotope of ^{75}As as nearest neighbors to the silicon atoms at the gallium sites.

The concentrations of carbon have been determined from the absorption coefficient and FWHM of the LVM absorption peak of C_{As} using the relation in equation (6.5). Table 6.1 shows the concentrations of carbon for those samples that were chosen for the photoluminescence studies.

All the samples measured show weak absorption at 384 cm^{-1}, which is due to the Si_{Ga}. We have estimated a value in the neighborhood of $\sim 10^{15}$ cm^{-3} for Si_{Ga}, and no observable Si_{As} peak has been identified in any of the samples (>150 crystals) measured.

It is known that at low silicon concentration, the silicon atoms are incorporated predominantly at the gallium sites, which contribute to the shallow donor levels. When the concentration of silicon is increased beyond $\sim 10^{18}$ cm^{-3}, the silicon atoms begin to substitute at both the arsenic

Table 6.1 Carbon concentrations measured at LVM absorption.

Sample	Carbon concentration ($\times 10^{15}$ cm^{-3}) ± 0.08
825S	~0.06
914T	0.39
836T	1.08
866T	1.34
603T	4.15
862S	4.55
873T	6.45
977S	7.26
873S	11.60
813S	19.86
813T	29.71

sites and the gallium sites (Newman, 1973). Both Si_{Ga} and Si_{As} increase with increasing silicon impurity and always result in a net excess of Si_{Ga}.

The remaining absorption peaks are due to two-phonon absorptions, which are in agreement with observations of Koteles and Datars (1976) and Cochran *et al.* (1961).

In the region below the wavenumber 340 cm^{-1} ($\lambda > 29\ \mu m$), absorption is due to the Reststrahlen band. For frequencies below the Reststrahlen band, the transmittance becomes too low because of the thickness of the sample used. Hence no information could be extracted below 340 cm^{-1}.

The real refractive index, n, of SI GaAs was found to be 3.4, which is in excellent agreement with the documented value for GaAs. From the computed imaginary refractive index, k, at the frequency ω_{LVM}, α_{LVM}^{max} was calculated according to equation (6.12b). The calculated values of α agree very well with the measured values using equation (6.7) (table 6.2). However, if the absorption is too low the α values cannot be determined accurately. This shows that it is justified to use equation (6.6) to describe the transmittance for thicknesses ≥2.5 mm if the absorption is large enough such that the value αd is large.

6.6 Conclusion

Both carbon and silicon are found in undoped LEC SI GaAs. Although both impurities are amphoteric, they do not seem to be substituted at the same type of site in GaAs.

Table 6.2 Experimental and calculated α values.

Sample	Experimental ± 0.01 cm^{-1}	Calculated cm^{-1}
813T	3.10	2.8 ± 0.3
862T	2.15	2.0 ± 0.2
873S	1.32	1.2 ± 0.2
862S	0.54	0.6 ± 0.1
866T	0.15	0.26 ± 0.06
914T	0.05	0.20 ± 0.04
825S	~0.006	0.0

Carbon is preferentially substituted at the arsenic sites while silicon, when present in small concentrations, is mainly substituted at the gallium sites.

We also conclude that the carbon concentrations can be determined quite accurately from the estimated transmittance — without going through detailed calculations for the absorption coefficients if the absorption is large enough.

Bibliography

Bellomonte, L. (1977). J. Phys. Chem. Solids 38, 59

Bourgoin, J., and Lannoo, M. (1983). In *Point Defects in Semiconductors II* (M. Cardona, ed.), p. 113 (Springer-Verlag)

Brozel, M.R., Clegg, J.B., and Newman, R.C. (1978). J. Phys. D 11, 1331

Brozel, M.R., Foulkes, E.J., Series, R.W., and Hurle, D.T.J. (1986). Appl. Phys. Lett. 49, 337

Cameron, D.G., Hawranek, J.P., Neelakantan, P., Young, R.P., and Jones, R.N. (1977). *Computer Programs for Infrared Spectroscopy* National Research Council of Canada Bulletin No. 16, vol. VI, p. 93

Cochran, W., Fray, S.J., Johnson, F.A., Quarrington, J.E., and Williams, N. (1961). J. Appl. Phys. Supp. 32, 2102

Griffiths, P.R. (1975). *Chemical Infrared Fourier Transform Spectroscopy* (Wiley-Interscience, New York)

Hawrenek, J.P., Neelakantan, P., Young, R.P., and Jones, R.N. (1976). Spectrochim. Acta 32A, 85

Hawranek, J.P., and Jones, R.N. (1976a). Spectrochim. Acta 32A, 99

Heavens, O.S. (1955). *Optical Properties of Thin Solid Films* (Butterworths, London)

Homma, Y., Ishii, Y., Kobayashi, T., and Osaka, J. (1985). J. Appl. Phys. 57, 2931

Hunter, A.T., Kimura, H., Baukus, J.P., Winston, H.V., and Marsh, O.J. (1984). Appl. Phys. Lett. 44, 74

Koteles, E.S., and Datars, W.R. (1976). Can. J. Phys. 54, 1676

Leigh, R.S., and Newman, R.C. (1982). J. Phys. C 15, L1045

Lorimor, O.G., and Spitzer, W.G. (1966). J. Appl. Phys. 37, 3687

Newman, R.C. (1973). *Infrared Studies of Crystal Defects* (Taylor and Francis Ltd., London)

Newman, R.C., Thompson, F., Hyliands, M., and Peart, R.F. (1972). Solid State Commun. 10, 505

Theis, W.M., Bajaj, K.K., Litton, C.W., and Spitzer, W.G. (1982). Appl. Phys. Lett. 41, 70

Theis, W.M., Bajaj, K.K., Litton, C.W., and Spitzer, W.G. (1983). Physica 117B and 118B, 116

Thompson, F., and Newman, R.C. (1972). J. Phys. C 5, 1999

Ulrici, W. (1984). Czech. J. Phys. B34, 420

7. DISCUSSION AND CONCLUSION

Using photoluminescence spectroscopy, we have studied the effect of carbon impurity in samples of LEC SI GaAs with different carbon concentrations. From both the wavelength and the temperature scanning techniques, we have found results that have not been reported before, related to the residual carbon in LEC SI GaAs.

From the study of the energy distribution of the D-A pairs emissions, the value of R (separation between D-A pair) can be obtained. These values of R agree with those calculated from the concentration using the equation: $R = (2\pi N)^{-1/3}$ (Williams, 1968), only when the carbon concentration, N, is in the range of $\sim 10^{14} < N \leq 5 \times 10^{15}$ cm^{-3}. For concentrations $\geq 5 \times 10^{15}$ cm^{-3}, the emission energies tend to be higher than theoretical values, probably due to the coexistence of both D-A pairs and B-A transitions, which could not be resolved completely. At very low carbon concentration, $N < 10^{15}$ cm^{-3}, distant D-A pairs with very large R distances have a reduced probability of recombination; thus the dominating transition is B-A recombination. For samples with $N \geq 3 \times 10^{16}$ cm^{-3}, the main emission is near the B-A transition energy.

The separations, R, between distant D-A pairs are concentration dependent and the radiative recombinations are most probable for $200 < R < 1300$ Å.

At low temperatures, the main contribution to the emission spectrum comes from the D-A pairs emissions. The

B-A transition begins to dominate when the temperature is greater than 20 K.

From the study of the dynamics of the decay process, it was found that one of the samples that had a high carbon content ($N \simeq 3 \times 10^{16}$ cm^{-3}) had a very fast decay. Neither the power law nor the B component of the double exponential was detected. The luminescence efficiency was also found to be very low. Due to the fact that the emission peak corresponds to the B-A transition energy, we propose that the fast decay is influenced by the B-A transition.

Results from the studies of the temperature dependence of the decay process show that the ratio of the fast component (A) to the slow component (B) of the double exponential decay increases with temperature. At T ~ 34 K, only the A component remains.

These show that there exists a competitive process between the D-A and B-A recombinations. The B-A transition is more dominant at high temperatures. This B-A transition is also preferred for carbon concentrations that are either very high or very low.

We have developed a new method of analysis of photoluminescence decay curves that follow the Arrhenius relation. This method enables the extraction of the activation energy associated with the luminescence decay.

We have shown that the activation energy of ~5.7 meV from the conduction band could be related to the shallow donor states formed by Si_{Ga}, which has a well-documented

value of 5.85 meV (Watts, 1977). The second activation energy of ~15 meV could be due to a level at ~15 meV below a donor level. If the donor state has a binding energy of ~6 meV, which is common in GaAs (Watts, 1977), then this level would be about 21 meV from the conduction band. This level at ~21 meV could be related to the EL2 defects (Walukiewicz *et al.*, 1983).

The exponent, p, of the power law has a value of ~1.4 and is temperature independent for $T < 18$ K. For the temperature range $18 < T < 30$ K, we report for the first time in GaAs, that the exponent, p, is linearly temperature dependent and follows the expressions: $p(T) = -1 + \beta T$, where β is proportional to the concentration of acceptors, C_{As}.

We have discussed several mechanisms to explain the different temperature dependence of the exponent, p, for samples with different carbon contents. We believe that the most probable mechanism involves non-radiative states. This is supported by the observation that there is a great reduction in the luminescence intensity at temperatures > 20 K.

The mechanism proposed is only speculative and further detailed studies need to be done to conclusively determine the exact mechanism that is responsible for the power-law behavior of D-A emission involving carbon impurity in GaAs.

Since a higher excitation intensity is known to saturate the D-A pairs that are separated by large R distances (Maeda, 1965), further experiments using different

excitation intensity to study the temperature dependence of the decay process would shed some light on the decay mechanisms.

Bibliography

Maeda, K. (1965). J. Phys. Chem. Solids **26**, 595

Walukiewicz, W., Lagowski, J. and Gatos, H.C. (1983). Appl. Phys. Lett. **43**, 112

Watts, R.K. (1977). *Point Defects in Crystals* (John Wiley & Sons)

Williams, F. (1968). phys. status solidi **25**, 493

APPENDIX A

Hardware and software designs

The data acquisition system basically consists of a peak detector, an 8-bit analogue-to-digital converter (ADC), a monochromator drive unit, a parallel to serial interface (RS232), and an input/output (I/O) interface, all controlled by the TS1000 microcomputer and operating in conjunction with an Osborne 1 microcomputer. The block diagram is shown in figure 2.3. The use of the Osborne 1 microcomputer is optional. It can be replaced by a printer when necessary. The reason for using a microcomputer as a data storage device is that data can be conveniently written on floppy diskettes, and can be retrieved at a later time for plotting on a graphic plotter.

1. Input-output Interface

The circuit diagram for the I/O interface is shown in figure A1.

A 74LS138 decoder is used in the input-output (I/O) interface. The device addresses correspond to memory locations between 8192 and 8199 as tabulated below:

DEVICE	ADDRESS
Y1	8192
Y2	8193
Y3	8194
Y4	8195
Y5	8196
Y6	8197

Y7	8198
Y8	8199

Whenever a PEEK or POKE statement is executed using any one of the above addresses, a *trigger* pulse is sent to the specified device. The ROM (read-only memory) chip is disabled whenever a *PEEK* or *POKE* function is being carried out to prevent the computer from crashing.

2. Peak Detector

The signal from the photodetector (photomultiplier or photodiode with suitable preamplification) is fed into an amplifier with 52 dB gain. At the maximum of the signal, the peak detector stretches the signal considerably to allow time for the analogue to digital (A-D) conversion. The signal drops by less than 0.4 % of the maximum after a time elapse of 100 μs. That is, at the peak voltage of 5 V, the drop in voltage after 100 μs is less than 20 mV. Since the A-D conversion time is < 20 μs, the error is insignificant for an 8-bit ADC. The circuit diagram for the peak detector is shown in figure A2.

3. Analogue-to-digital converter

The circuit diagram for the analogue-to-digital converter (ADC) is shown in figure A1.

The ADC is based on the Analog Devices AD7574 with 8-bit resolution. This is connected in the static RAM interface mode. The start of the A-D conversion is initiated by part of the excitation laser pulse. Only pulses with intensity within a preset window are used to trigger the A-D

conversion. The trigger pulse is delayed by the 74LS123 dual retriggerable monostable multivibrator by 1 μs (variable) to allow for the rise time of the amplifiers. After the start of the conversion, the computer will check for the EOC (end of conversion) signal through a 74LS244 buffer. At the end of the conversion, the "busy" signal becomes high, and the data will be read by the computer. The ADC will then wait for the next conversion signal. The data can be accumulated for a preset number of laser triggers, hence an average signal for a particular wavelength setting can be obtained.

4. Monochromator Drive Unit

The monochromator drive unit is actually a pulse train generator. This unit consists of three 74LS193 presettable 4-bit binary up/down counters and a 555 timer which provides the pulses (figure A3). The interval between adjacent wavelength settings is determined by the number of pulses preset at the counters. A new wavelength setting is selected by sending a trigger pulse to the pulse train generator. That is, when the POKE instruction is executed (trigger pulse), the preset number is strobed into the counters, and a train of pulses, consisting of a predetermined number, will then be sent to the monochromator stepper motor.

5. RS232 Interface

The number representing the accumulated or averaged signal is sent to Osborne 1 or printer through the RS232 interface (figure A4). The RS232 interface consists of an AY-3-1015D UART (Universal Asynchronous

Receiver/Transmitter), and a AY-5-8116 dual baud rate generator, which is operating in conjunction with a 5.0688 MHz crystal to provide a baud rate of 1200.

At the end of the data transmission, the whole sequence is repeated at a new wavelength setting until the final wavelength setting is reached. The data at Osborne 1 are first stored in the buffer until the whole spectrum is completed, then are written on to a floppy diskette for storage. They can be retrieved for analysis, plotting or printing at a later time.

If a CW excitation source is used, a mechanical light chopper must be used in the path of the excitation light.

Software

The listing of the program is shown in figure A5.

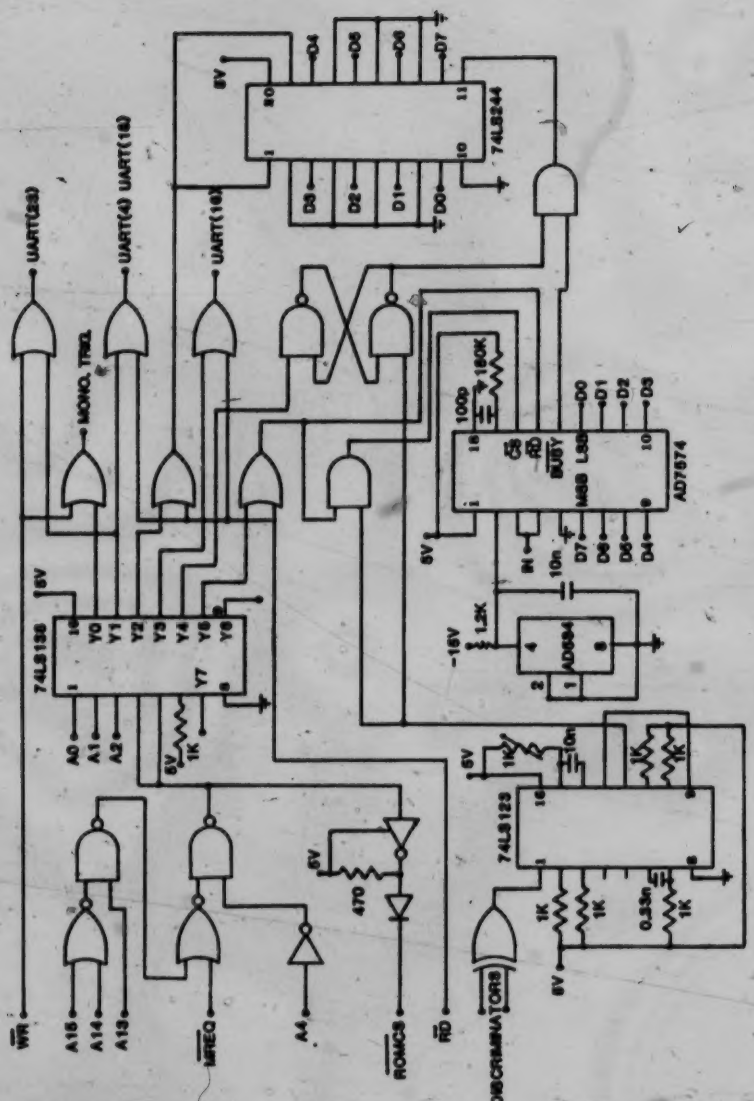

FIGURE A.1 TS1000 I/O INTERFACE AND A-D CONVERTER

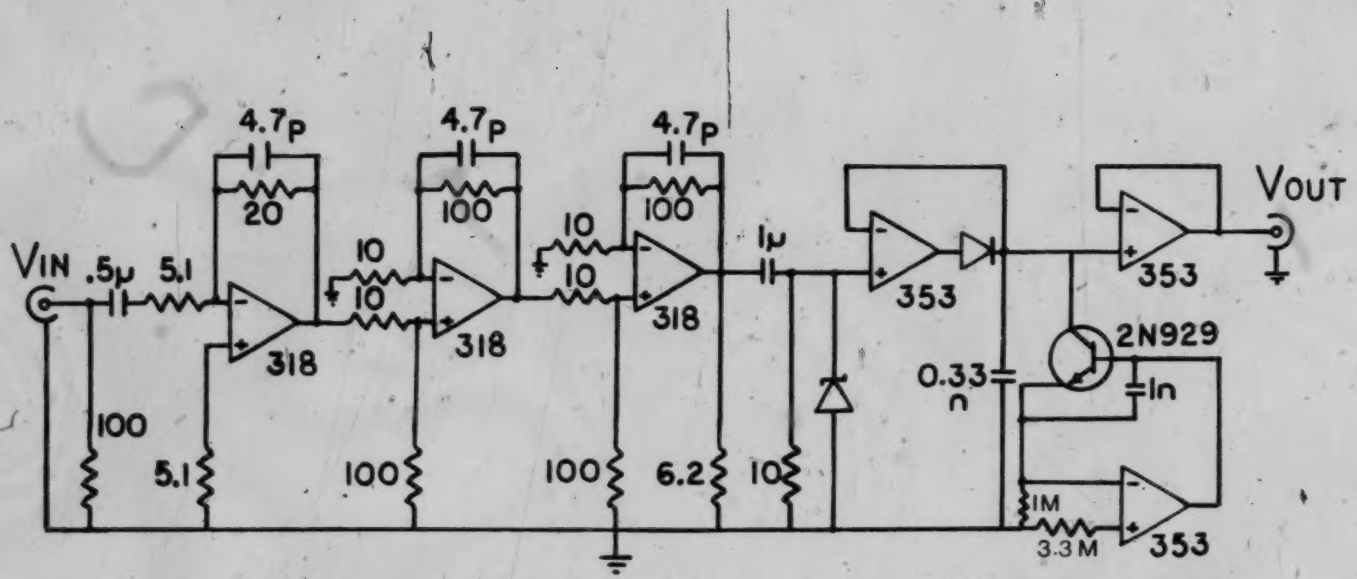

ALL RESISTANCES ARE IN KILO-OHMS
UNLESS OTHERWISE STATED

FIGURE A.2 PEAK DETECTOR

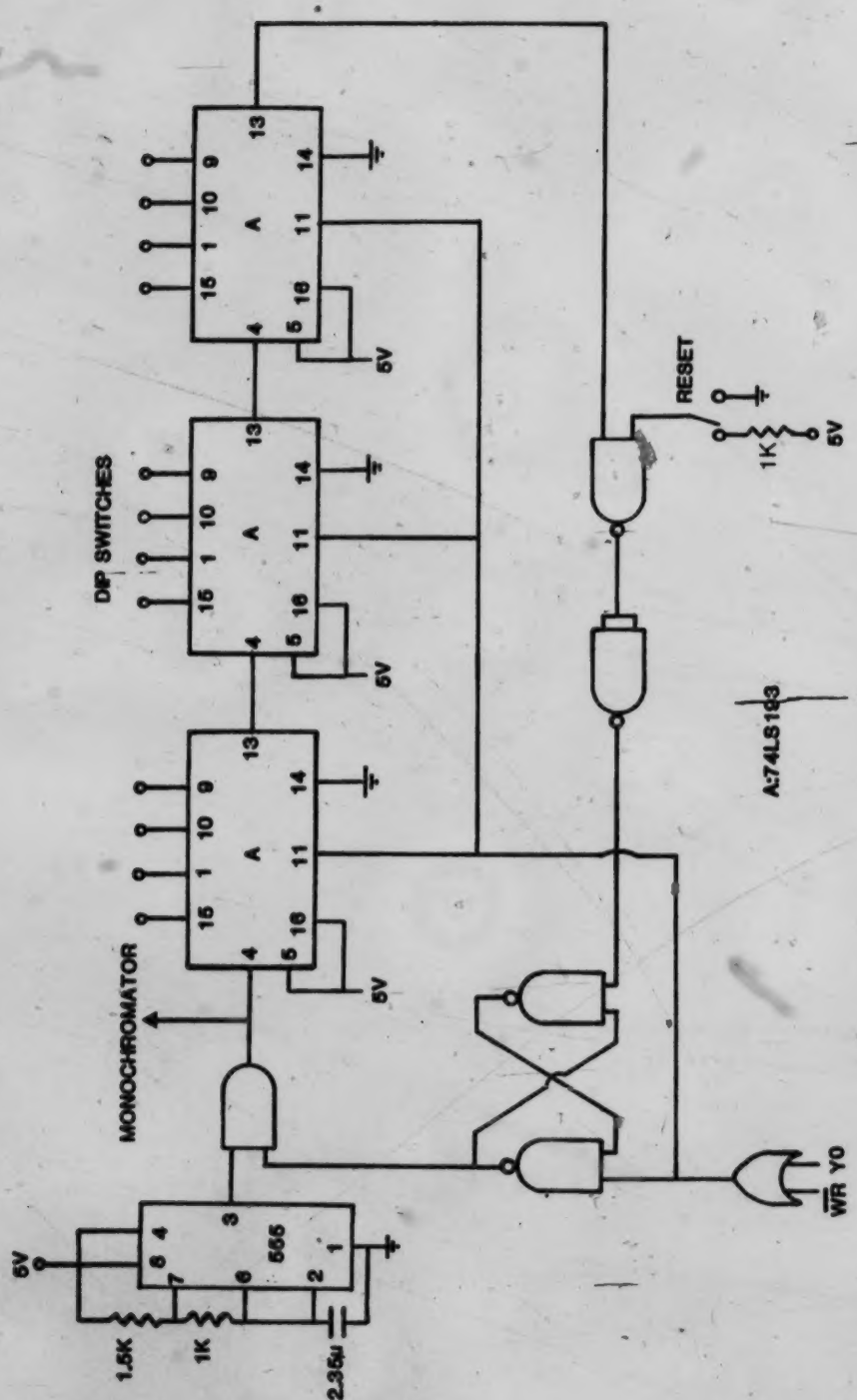

FIGURE A.3 MONOCHROMATOR DRIVER

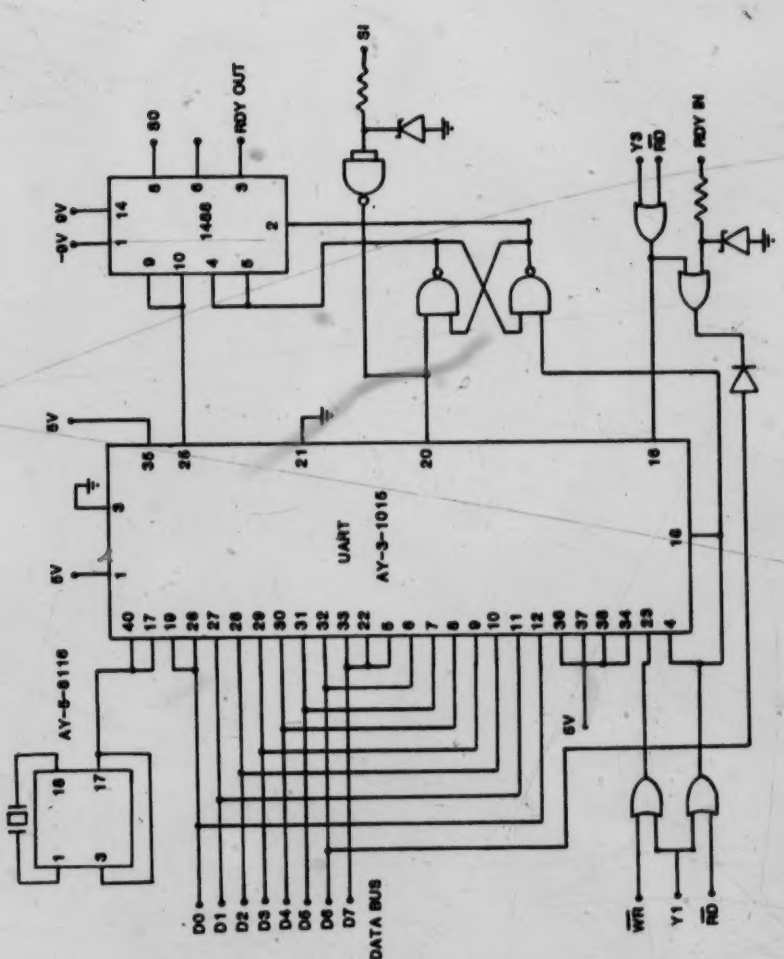

FIGURE A.4 RS232 SERIAL INTERFACE

Figure A5 Data acquisition program

```
10 REM: LUMINESCENCE (C.K.TEH)
15 REM: (JANUARY 1986)
17 SLOW
20 PRINT "STARTING WAVELENGTH (NM)?"
25 INPUT SW
30 PRINT SW
35 PRINT
40 PRINT "ENDING WAVELENGTH (NM)?"
45 INPUT EW
50 PRINT EW
55 PRINT
56 PRINT "WAVELENGTH INTERVALS (NM)?"
57 INPUT IV
58 PRINT IV
59 PRINT
60 PRINT "NO. OF LASER TRIGGERS REQUIRED?"
70 INPUT NR
75 PRINT NR
80 LET NW=1+INT(ABS(EW-SW)/IV)
90 LET AD=8193
100 GOSUB 610
110 LET Y=SW
120 GOSUB 500
130 GOSUB 780
140 LET Y=EW
150 GOSUB 500
160 GOSUB 230
162 GOSUB 865
164 GOSUB 900
166 GOSUB 830
168 POKE AD,41
170 GOSUB 580
180 LET Y=NW
190 GOSUB 500
200 GOSUB 580
205 FAST
210 FOR W=1 TO NW
215 LET CL=PEEK(8197)
220 LET SL=0
230 FOR R=1 TO NR
240 POKE 8196,0
250 LET LA=PEEK(8194)
```

```
260 IF LA=0 THEN GOTO 250
270 LET S=PEEK(8197)
280 LET SL=SL+S
290 NEXT R
295 IF W=NW THEN GOTO 310
300 POKE 8192,0
305 FOR D=1 TO 100
306 NEXT D
310 LET Y=SL
320 GOSUB 500
330 GOSUB 580
340 NEXT W
345 SLOW
350 FOR B=1 TO 10
360 POKE AD,7
365 PAUSE 40
370 NEXT B
380 STOP
490 REM: SUBROUTINES
500 LET DN=1E6
510 FOR N=1 TO 6
520 LET DN=DN/10
530 LET DT=INT(Y/DN)
540 POKE AD,DT+48
550 LET Y=Y-DN*DT
560 NEXT N
570 RETURN
580 POKE AD,13
590 POKE AD,10
600 RETURN
610 POKE AD,87
620 POKE AD,65
630 POKE AD,86
640 POKE AD,69
650 POKE AD,76
660 POKE AD,69
670 POKE AD,78
680 POKE AD,71
690 POKE AD,84
700 POKE AD,72
710 POKE AD,32
720 POKE AD,102
730 POKE AD,114
740 POKE AD,111
750 POKE AD,109
760 POKE AD,32
770 RETURN
```

```
780 POKE AD,32
790 POKE AD,116
800 POKE AD,111
810 POKE AD,32
820 RETURN
830 POKE AD,32
840 POKE AD,110
850 POKE AD,109
860 RETURN
865 POKE AD,32
868 POKE AD,40
870 POKE AD,115
875 POKE AD,116
880 POKE AD,101
885 POKE AD,112
890 POKE AD,58
895 RETURN
900 LET DT=INT(IV)
905 POKE AD,DT+48
910 POKE AD,46
915 LET DT=(IV-DT)*10
920 POKE AD,DT+48
925 RETURN
```

APPENDIX B

The complete non-linear least-squares curve fitting computer program written in Fortran is listed in figure B1.

The listed program is used to fit multiple-exponential curves. The same program can be modified to fit any non-linear function provided the function is differentiable with respect to the parameters.

Figure B1 Non-linear least-squares program

```
      IMPLICIT REAL*8(D)
      DIMENSION R(10,8),G(10,8),P(255),D(255,6),PS(6),DPS(6),C(6),
     1CFF(255),YWT(255),YCWT(255),ABF(255),BIT(255),DA(6),S(255),
     2QS(6),Q(6),X(255),Y(255),SIGN(6),SHGN(6),DS2(2,2),DS3(3,3),
     3DS4(4,4),DS5(5,5),DS6(6,6),DES2(2,2),DES3(3,3),DES4(4,4),
     4DES5(5,5),DES6(6,6),DR3(3,3),DR4(4,4),DR5(5,5),DR6(6,6),
     *DU(3),LL(6),ML(6),W(255,7),CHISQ(50),DR2(2,2),
     ASDEL(255),PARA(6),DSIG(6),PCENT(6),
     BSIG(6),U(3),DATE(3)
      READ(5,5)SAMPLE,RUN,DATE
    5 FORMAT(A4,A1,3A4)
      WRITE(6,7)SAMPLE,RUN,DATE
    7 FORMAT(1X,/1X,'SAMPLE= ',A4,6X,'RUN # ',A1,6X,'DATE: ',3A4/)
      WRITE(6,10)
   10 FORMAT(/9X,'TIME',10X,'COUNTS',/)
      READ(5,20)NP,N
   20 FORMAT(2I3)
      READ(5,30) (PARA(I),I=1,6)
   30 FORMAT(6F12.4)
      DO 37 I=1,N
   37 READ(5,40)X(I),Y(I)
   40 FORMAT(2F15.4)
      DO 50 I=1,N
   50 WRITE(6,40)X(I),Y(I)
      SDEG=0.01
      DEG=DBLE(SDEG)
      ZOT=0.4
      ZAP=0.2
      KUT=50
      TOL=0.001
      QUIT=6000
      NT=N
      LZ=0
      LS=0
      DO 52 I=1,6
   52 DPS(I)=0.0D0
      WRITE(6,53)
   53 FORMAT(/1H ,'INPUT PARAMETERS')
      WRITE(6,55)(PARA(I),I=1,NP)
   55 FORMAT(/1H ,5HPA1 =,F10.2/5HPA2 =,F10.2/5HPA3 =,F10.2/5HPA4 =,
     1F10.2/5HPA5 =,F10.2/5HPA6 =,F10.2/)
```

```
C
C  COMPUTE CURVE FROM INITIAL ESTIMATES AND EVALUATE FIT TO DATA
C
      DO 60 J=1,3
      K=2*J+J/2-1
      U(J)=1.0/PARA(K)
   60 DU(J)=DBLE(U(J))
      KOUNT=1
      IZ=0
      NU=1000
      DO 77 I=1,NP
      SHGN(I)=0.0
      DSIG(I)=10000.000
   77 PCENT(I)=10000.0
      DO 79 J=1,N
      SDEL(J)=1000.00
      Z=X(J)
      W(J,4)=SDECAY(NP,Z,PARA,U)
      IF(W(J,4).LT.1.0)W(J,4)=1.0
   79 P(J)=Y(J)-W(J,4)
      IFLAG=0
      JFLAG=0
      FLAMDA=POW
      LOUNT=1
      ABSUM4=0.0
      ALSUM=0.0
      DO 80 J=1,N
      IF(W(J,4).LT.1.0)W(J,4)=1.0
      BIT(J)=ABS(P(J)*P(J)/W(J,4))
   80 ALSUM=ALSUM+BIT(J)
      CHISQ(KOUNT)=ALSUM
      WRITE(6,85)KOUNT,CHISQ(KOUNT)
   85 FORMAT(1X,6HCHISQ(,I2,2H)=,F10.4/)
      WRITE(6,90)
   90 FORMAT(1X,20H      TITLE:   PARA1 ,5X,5HPARA2,6X,5HPARA3,5X,
     27H PARA4 ,5X,5HPARA5,5X,7H PARA6 )
      IF(CHISQ(KOUNT)/N.LT.QUIT)GO TO 110
   94 WRITE(6,97)
   97 FORMAT(1X/18X,37H- PARAMETERS INCOMPATIBLE WITH DATA -/)
      WRITE(6,100)N,(PARA(I),I=1,NP)
  100 FORMAT(1X,4HN  =,I2/5HPA1 =,F7.3/5HPA2 =,F8.2/5HPA3 =,
     3F8.2/5HPA4 =,F7.3/5HPA5 =,F8.2/5HPA6 =,F7.3/)
C
C  COMPUTE PARTIAL DERIVATIVES REQUIRED FOR NORMAL EQUATIONS,
C  ERROR ESTIMATES AND CHISQ-MINIMUM PROXIMITY INDICATOR
C
  110 DO 120 J=1,N
```

```
      Z=X(J)
      D(J,1)=U(1)*U(1)*Z*PARA(2)*DEXP(-Z*DU(1))
      D(J,2)=DEXP(-Z*DU(1))
      IF(NP.EQ.2)GO TO 120
      D(J,3)=1.0D0
      IF(PARA(4).NE.10000.0)D(J,3)=DEXP(-Z*DU(2))
      IF(NP.EQ.3)GO TO 120
      D(J,4)=U(2)*U(2)*Z*PARA(3)*DEXP(-Z*DU(2))
      IF(NP.EQ.4)GO TO 120
      D(J,5)=1.0D0
      IF(PARA(6).NE.10000.0)D(J,5)=DEXP(-Z*DU(3))
      IF(NP.EQ.5)GO TO 120
      D(J,6)=U(3)*U(3)*Z*PARA(5)*DEXP(-Z*DU(3))
  120 CONTINUE
      IF(IFLAG.EQ.1)GO TO 21
C
C  COMPUTE WEIGHTS
C
  166 YSPUD=0.0
      DO 170 J=1,N
      YWT(J)=1.0/ABS(W(J,4))
      IF(KOUNT.EQ.1)YWT(J)=1.0/(ABS(Y(J))+1.0)
  170 YSPUD=YSPUD+YWT(J)
      DO 180 J=1,N
  180 YWT(J)=YWT(J)/YSPUD
      IF(JFLAG.EQ.1)GO TO 673
C
C  COMPUTE COEFFICIENTS OF NORMAL EQUATIONS (FROM MINIMIZATION OF
C  SUMS OF SQUARES OF RESIDUALS), INCLUDING WEIGHTING FACTORS
C
C  SOLVE SYSTEM OF EQUATIONS
C  FORM INVERSE OF MATRIX OF COEFFICIENTS AND ITS PRODUCT
C  WITH MATRIX OF COEFFICIENTS WHEN REQUIRED FOR ERROR ESTIMATION
C
  190 GO TO (88,32,33,34,35,36),NP
   32 DO 230 L=1,2
      DO 220 K=L,2
      DSUM=0.0D0
      DSUM2=0.0D0
      DO 200 J=1,N
      DSUM=DSUM+D(J,K)*D(J,L)*YWT(J)
      IF(L.GT.1)GO TO 200
      IF(IZ.EQ.1)GO TO 200
      DSUM2=DSUM2+D(J,K)*P(J)*YWT(J)
  200 CONTINUE
      DS2(K,L)=DSUM
      IF(IZ.EQ.0)GO TO 210
```

```
      DES2(K,L)=DS2(K,L)
      DES2(L,K)=DES2(K,L)
  210 IF(L.GT.1)GO TO 220
      DPS(K)=DSUM2
  220 DS2(L,K)=DS2(K,L)
  230 CONTINUE
      IF(IZ.EQ.1)GO TO 240
      GO TO 250
  240 CALL DMINV(DES2,2,DET,LL,ML)
      IF(DET.EQ.0.0D0)WRITE(6,961)
      CALL DGMPRD(DS2,DES2,DR2,2,2,2)
      GO TO 800
  250 CALL DSIMQ(DS2,DPS,2,KS)
      GO TO 39
   33 DO 290 L=1,3
      DO 280 K=L,3
      DSUM=0.0D0
      DSUM2=0.0D0
      DO 260 J=1,N
      DSUM=DSUM+D(J,K)*D(J,L)*YWT(J)
      IF(L.GT.1)GO TO 260
      IF(IZ.EQ.1)GO TO 260
      DSUM2=DSUM2+D(J,K)*P(J)*YWT(J)
  260 CONTINUE
      DS3(K,L)=DSUM
      IF(IZ.EQ.0)GO TO 270
      DES3(K,L)=DS3(K,L)
      DES3(L,K)=DES3(K,L)
  270 IF(L.GT.1)GO TO 280
      DPS(K)=DSUM2
  280 DS3(L,K)=DS3(K,L)
  290 CONTINUE
      IF(IZ.EQ.1) GO TO 300
      GO TO 331
  300 CALL DMINV(DES3,3,DET,LL,ML)
      IF(DET.EQ.0.0D0)WRITE(6,961)
      CALL DGMPRD(DS3,DES3,DR3,3,3,3)
      GO TO 800
  331 CALL DSIMQ(DS3,DPS,3,KS)
      GO TO 39
   34 DO 430 L=1,4
      DO 400 K=L,4
      DSUM=0.0D0
      DSUM2=0.0D0
      DO 350 J=1,N
      DSUM=DSUM+D(J,K)*D(J,L)*YWT(J)
      IF(L.GT.1)GO TO 350
```

```
      IF(IZ.EQ.1)GO TO 350
      DSUM2=DSUM2+D(J,K)*P(J)*YWT(J)
  350 CONTINUE
      DS4(K,L)=DSUM
      IF(IZ.EQ.0)GO TO 351
      DES4(K,L)=DS4(K,L)
      DES4(L,K)=DES4(K,L)
  351 IF(L.GT.1)GO TO 400
      DPS(K)=DSUM2
  400 DS4(L,K)=DS4(K,L)
  430 CONTINUE
      IF(IZ.EQ.1)GO TO 410
      GO TO 431
  410 CALL DMINV(DES4,4,DET,LL,ML)
      IF(DET.EQ.0.0D0)WRITE (6,961)
      CALL DGMPRD(DS4,DES4,DR4,4,4,4)
      GO TO 800
  431 CALL DSIMQ(DS4,DPS,4,KS)
      GO TO 39
   35 DO 530 L=1,5
      DO 500 K=L,5
      DSUM=0.0D0
      DSUM2=0.0D0
      DO 420 J=1,N
      DSUM=DSUM+D(J,K)*D(J,L)*YWT(J)
      IF(L.GT.1)GO TO 420
      IF(IZ.EQ.1)GO TO 420
      DSUM2=DSUM2+D(J,K)*P(J)*YWT(J)
  420 CONTINUE
      DS5(K,L)=DSUM
      IF(IZ.EQ.0)GO TO 450
      DES5(K,L)=DS5(K,L)
      DES5(L,K)=DES5(K,L)
  450 IF(L.GT.1)GO TO 500
      DPS(K)=DSUM2
  500 DS5(L,K)=DS5(K,L)
  530 CONTINUE
      IF(IZ.EQ.1)GO TO 535
      GO TO 540
  535 CALL DMINV(DES5,5,DET,LL,ML)
      IF(DET.EQ.0.0D0)WRITE(6,961)
      CALL DGMPRD(DS5,DES5,DR5,5,5,5)
      GO TO 800
  540 CALL DSIMQ(DS5,DPS,5,KS)
      GO TO 39
   36 DO 570 L=1,6
      DO 560 K=L,6
```

```
      DSUM=0.0D0
      DSUM2=0.0D0
      DO 550 J=1,N
      DSUM=DSUM+D(J,K)*D(J,L)*YWT(J)
      IF(L.GT.1)GO TO 550
      IF(IZ.EQ.1)GO TO 550
      DSUM2=DSUM2+D(J,K)*P(J)*YWT(J)
  550 CONTINUE
      DS6(K,L)=DSUM
      IF(IZ.EQ.0)GO TO 551
      DES6(K,L)=DS6(K,L)
      DES6(L,K)=DES6(K,L)
  551 IF(L.GT.1)GO TO 560
      DPS(K)=DSUM2
  560 DS6(L,K)=DS6(K,L)
  570 CONTINUE
      IF(IZ.EQ.1)GO TO 580
      GO TO 590
  580 CALL DMINV(DES6,6,DET,LL,ML)
      IF(DET.EQ.0.0D0)WRITE(6,961)
      CALL DGMPRD(DS6,DES6,DR6,6,6,6)
      GO TO 800
  590 CALL DSIMQ(DS6,DPS,6,KS)
  961 FORMAT(1X//26X,22H- MATRIX IS SINGULAR -//)
C
C  ADJUST PARAMETER VALUES SUBJECT TO LIMITS ON INCREMENTS
C  IMPOSED BY NON-CONVERGENCE INHIBITORS:ZOT AND ZAP
C
   39 IF(KS.LT.1)GO TO 595
      WRITE(6,592)
  592 FORMAT(1X/16X,41H- SOLUTION OF NORMAL EQUATIONS ABNORMAL -)
      GO TO 88
  595 KOUNS=KOUNT
      KOUNT=KOUNT+1
      IF(KOUNT.EQ.2)GO TO 605
      DO 600 I=1,NP
  600 SHGN(I)=SIGN(I)
  605 DO 610 I=1,NP
      PS(I)=SNGL(DPS(I))
      SIGN(I)=PS(I)/ABS(PS(I))
      IF((SHGN(I)+SIGN(I)).EQ.0.0)PS(I)=PS(I)*ZOT
      ABF(I)=ABS(PS(I)/PARA(I))
      IF(ABF(I).GT.ZAP)PS(I)=ZAP*SIGN(I)*ABS(PARA(I))
      C(I)=PARA(I)
  610 PARA(I)=PS(I)+PARA(I)
```

```
C
C  TEST CHANGE IN CHISQ. IF INCREASE EXCESSIVE; QUIT
C
      DO 612 J=1,3
      K=2*J+J/2-1
      U(J)=1.0/PARA(K)
  612 DU(J)=DBLE(U(J))
      ALSUM=0.0
      DO 615 J=1,N
      Z=X(J)
      W(J,4)=SDECAY(NP,Z,PARA,U)
      IF(W(J,4).LT.1.0)W(J,4)=1.0
      P(J)=Y(J)-W(J,4)
      BIT(J)=ABS(P(J)*P(J)/W(J,4))
  615 ALSUM=ALSUM+BIT(J)
      CHISQ(KOUNT)=ALSUM
      ALPINC=(CHISQ(KOUNT)-CHISQ(KOUNS))/N
      IF(ALPINC.GE.QUIT)GO TO 94
C
C  WRITE RESULTS OF CURRENT ITERATION
C
  127 WRITE(6,620)KOUNT,CHISQ(KOUNT),(PARA(I),I=1,NP)
  620 FORMAT(1X/1X,6HCHISQ(,I2,2H)=,F10.4,10X/10HPARAMETER:,
     1F9.4,2X,F9.2,2X,F9.2,2X,F9.4,2X,F9.2,2X,F9.4)
      WRITE(6,625)(PS(I),I=1,NP)
  625 FORMAT(1X,10HINCREMENT:,F9.4,2X,F9.2,2X,F9.2,2X,F9.4,2X,
     1F9.2,2X,F9.4)
C
C  EXCESSIVE NUMBER OF ITERATIONS:WRITE
C
      IF(KOUNT.LE.KUT)GO TO 635
      SIGMA=1000000.0
      SUM5=100.0
      SKEW=100.0
      SUM4=100.0
      WRITE(6,630)
  630 FORMAT('1')
      GO TO 724
C
C  CHECK ACCURACY OF SOLUTIONS, REITERATE IF PARAMETERS'
C  CHANGES EXCEEDED 100*TOL%
C
  635 TEL=TOL
   72 DO 640 I=1,NP
      IF(ABF(I).LE.TEL)GO TO 640
      LOUNT=1
      GO TO 110
  640 CONTINUE
```

```
C
C  IF INCREMENT CRITERION SATISFIED COMPUTE AND
C  WRITE PARTIAL DERVIVATIVES OF CHISQ
C
      IFLAG=1
      GO TO 110
   21 DO 650 J=1,N
  650 S(J)=Y(J)/W(J,4)*Y(J)/W(J,4)-1.0
      DO 660 K=1,NP
      DSUM6=0.0D0
      DO 655 I=1,N
  655 DSUM6=DSUM6-S(I)*D(I,K)
  660 DA(K)=DSUM6
      IFLAG=0
      WRITE(6,662)(DA(I),I=1,NP)
  662 FORMAT(1X,10HDCHISQ/DP:D9.2,2X,D9.2,2X,D9.2,2X,D9.2,
     12X,D9.2,2X,D9.2)
C
C  TEST DERIVATIVES OF CHISQ, REITERATE IF SLOPE
C  EXCEEDS DEG (5 SUCH ITERATIONS ALLOWED)
C
      DO 665 I=1,NP
      IF(DABS(DA(I)).LE.DEG)GO TO 665
      LOUNT=LOUNT+1
      IF(LOUNT.LE.5)KOUNT=KOUNT-1
      IF(LOUNT.GT.5)GO TO 670
      GO TO 166
  665 CONTINUE
C
C  ESTIMATE STD DEVNS AND %ERRORS IN PARAMETERS
C  COMPUTING STATISTICAL PARAMETERS OF FIT
C
  670 JFLAG=1
      GO TO 166
  673 NU=N-NP
      SUM5=0.0
      SUM7=0.0
      JFLAG=0
      DO 675 J=1,N
      SUM7=SUM7+P(J)*P(J)*P(J)*YCWT(J)
  675 SUM5=SUM5+P(J)*YCWT(J)
      VAR=(CHISQ(KOUNT)/YSPUD-SUM5*SUM5)*N/NU
      SIGMA=SQRT(VAR)
      SKEW=(SUM7-3.0*SUM5*NU*VAR/N+2.0*SUM5*SUM5*SUM5)*N/
     1(VAR*SIGMA*NU)
      REDCHI=CHISQ(KOUNT)/NU
      IZ=1
```

```
      GO TO 190
  800 WRITE(6,810)
  810 FORMAT(/5X,53H- PRODUCT OF MATRIX OF COEFFICIENTS AND ITS INVERSE
     1-,/)
      GO TO(88,811,816,821,826,835),NP
  811 DO 815 I=1,2
      DSIG(I)=DSQRT(DES2(I,I)/YSPUD)
      SIG(I)=SNGL(DSIG(I))
      PCENT(I)=ABS(SIG(I)*100.0/PARA(I))
      WRITE(6,812)(DR2(I,J),J=1,2)
  812 FORMAT(1X,2(D9.2,3X)/)
  815 CONTINUE
      GO TO 850
  816 DO 820 I=1,3
      DSIG(I)=DSQRT(DES3(I,I)/YSPUD)
      SIG(I)=SNGL(DSIG(I))
      PCENT(I)=ABS(SIG(I)*100.0/PARA(I))
      WRITE(6,817)(DR3(I,J),J=1,3)
  817 FORMAT(1X,3(D9.2,3X)/)
  820 CONTINUE
      GO TO 850
  821 DO 825 I=1,4
      DSIG(I)=DSQRT(DES4(I,I)/YSPUD)
      SIG(I)=SNGL(DSIG(I))
      PCENT(I)=ABS(SIG(I)*100.0/PARA(I))
      WRITE(6,823)(DR4(I,J),J=1,4)
  823 FORMAT(1X,4(D9.2,3X)/)
  825 CONTINUE
      GO TO 850
  826 DO 830 I=1,5
      DSIG(I)=DSQRT(DES5(I,I)/YSPUD)
      SIG(I)=SNGL(DSIG(I))
      PCENT(I)=ABS(SIG(I)*100.0/PARA(I))
      WRITE(6,827)(DR5(I,J),J=1,5)
  827 FORMAT(1X,5(D9.2,3X)/)
  830 CONTINUE
      GO TO 850
  835 DO 840 I=1,6
      DSIG(I)=DSQRT(DES6(I,I)/YSPUD)
      SIG(I)=SNGL(DSIG(I))
      PCENT(I)=ABS(SIG(I)*100.0/PARA(I))
      WRITE(6,837)(DR6(I,J),J=1,6)
  837 FORMAT(1X,6(D9.2,3X)/)
  840 CONTINUE
  850 SUM3=0.0
      DO 870 J=1,N
      CFF(J)=SQRT(ABS(W(J,4)))
```

```
  870 SUM3=SUM3+P(J)/CFF(J)
      SUM4=SUM3/N
      SQMEAN=SUM4*SUM4
      SIGSQ=(CHISQ(KOUNT)-SQMEAN*N)/(N-1)
      SEGMA=SQRT(SIGSQ)
      DO 875 J=1,NT
  875 SDEL(J)=P(J)/(CFF(J)*SEGMA)
  724 WRITE(6,880)(PARA(I),I=1,NP)
  880 FORMAT(1X,10HPARAMETER:,1X,7H PARA1 ,5X,5HPARA2,6X,5HPARA3,5X,
     17H PARA4 ,5X,5HPARA5,5X,7H PARA6 //5X,6HVALUE:,F8.4,1X,
     2F10.2,1X,F10.2,2X,F9.4,1X,F10.2,2X,F9.4)
      IF(KOUNT.GT.KUT)GO TO 88
      WRITE(6,885)(DSIG(I),I=1,NP)
  885 FORMAT(/2X,9HST. DEVN:,2X,F6.4,4X,F7.2,4X,F7.2,4X,F7.4,4X,
     1F7.2,4X,F7.4)
      WRITE(6,890)(PCENT(I),I=1,NP)
  890 FORMAT(2X,9HPER CENT:,2X,F6.1,5(5X,F6.1))
      WRITE(6,892)CHISQ(KOUNT),SIGMA,SUM4,SKEW
  892 FORMAT(/2X,5HCHISQ,2X,5HSIGMA,2X,5HDVBAR,3X,4HSKEW,
     1/1X,F7.3,3X,F9.3,1X,F7.4,1X,F6.3/)
   88 STOP
      END
C
      FUNCTION SDECAY(I,Z,PARA,U)
      DIMENSION PARA(6),U(3)
      GO TO (7,2,3,4,5,6),I
    2 SDECAY=PARA(2)*EXP(-Z*U(1))
      RETURN
    3 SDECAY=PARA(2)*EXP(-Z*U(1))+PARA(3)
      RETURN
    4 SDECAY=PARA(2)*EXP(-Z*U(1))+PARA(3)*EXP(-Z*U(2))
      RETURN
    5 SDECAY=PARA(2)*EXP(-Z*U(1))+PARA(3)*EXP(-Z*U(2))+PARA(5)
      RETURN
    6 SDECAY=PARA(2)*EXP(-Z*U(1))+PARA(3)*EXP(-Z*U(2))+PARA(5)*EXP(-Z*U
     *(3))
    7 RETURN
      END
C
      SUBROUTINE DSIMQ(A,B,N,KS)
C
C  DECLARE ALL VARIABLES STARTING WITH LETTERS (A-H OR O-Z) TO BE DOUBLE
C  PRECISION.
C
      IMPLICIT REAL*8(A-H,O-Z)
      DIMENSION A(1),B(1)
      TOL=0.0D0
```

```
      KS=0
      JJ=-N
      DO 65 J=1,N
      JY=J+1
      JJ=JJ+N+1
      BIGA=0.0D0
      IT=JJ-J
      DO 30 I=J,N
      IJ=IT+I
      IF(DABS(BIGA).GE.DABS(A(IJ)))GO TO 30
      BIGA=A(IJ)
      IMAX=I
   30 CONTINUE
      IF(DABS(BIGA).GT.TOL)GO TO 40
      KS=1
      RETURN
   40 I1=J+N*(J-2)
      IT=IMAX-J
      DO 50 K=J,N
      I1=I1+N
      I2=I1+IT
      SAVE=A(I1)
      A(I1)=A(I2)
      A(I2)=SAVE
   50 A(I1)=A(I1)/BIGA
      SAVE=B(IMAX)
      B(IMAX)=B(J)
      B(J)=SAVE/BIGA
      IF(J.EQ.N)GO TO 70
      IOS=N*(J-1)
      DO 65 IX=JY,N
      IXJ=IOS+IX
      IT=J-IX
      DO 60 JX=JY,N
      IXJX=N*(JX-1)+IX
      JJX=IXJX+IT
   60 A(IXJX)=A(IXJX)-(A(IXJ)*A(JJX))
   65 B(IX)=B(IX)-(B(J)*A(IXJ))
   70 NY=N-1
      IT=N*N
      DO 80 J=1,NY
      IA=IT-J
      IB=N-J
      IC=N
      DO 80 K=1,J
      B(IB)=B(IB)-A(IA)*B(IC)
      IA=IA-N
```

```
   80 IC=IC-1
      RETURN
      END
C
      SUBROUTINE DMINV(A,N,D,L,M)
      IMPLICIT REAL*8(A-H,O-Z)
      DIMENSION A(1),L(1),M(1)
      D=1.0D0
      NK=-N
      DO 80 K=1,N
      NK=NK+N
      L(K)=K
      M(K)=K
      KK=NK+K
      BIGA=A(KK)
      DO 20 J=K,N
      IZ=N*(J-1)
      DO 20 I=K,N
      IJ=IZ+I
   10 IF(DABS(BIGA).GE.DABS(A(IJ)))GO TO 20
      BIGA=A(IJ)
      L(K)=I
      M(K)=J
   20 CONTINUE
      J=L(K)
      IF(J.LE.K)GO TO 35
      KI=K-N
      DO 30 I=1,N
      KI=KI+N
      HOLD=-A(KI)
      JI=KI-K+J
      A(KI)=A(JI)
   30 A(JI)=HOLD
   35 I=M(K)
      IF(I.LE.K)GO TO 45
      JP=N*(I-1)
      DO 40 J=1,N
      JK=NK+J
      JI=JP+J
      HOLD=-A(JK)
      A(JK)=A(JI)
   40 A(JI)=HOLD
   45 IF(BIGA.NE.0.0D0)GO TO 48
      D=0.0D0
      RETURN
   48 DO 55 I=1,N
      IF(I.EQ.K)GO TO 55
```

```
      IK=NK+I
      A(IK)=A(IK)/(-BIGA)
   55 CONTINUE
      DO 65 I=1,N
      IK=NK+I
      HOLD=A(IK)
      IJ=I-N
      DO 65 J=1,N
      IJ=IJ+N
      IF(I.EQ.K)GO TO 65
      IF(J.EQ.K)GO TO 65
      KJ=IJ-I+K
      A(IJ)=HOLD*A(KJ)+A(IJ)
   65 CONTINUE
      KJ=K-N
      DO 75 J=1,N
      KJ=KJ+N
      IF(J.EQ.K)GO TO 75
      A(KJ)=A(KJ)/BIGA
   75 CONTINUE
      D=D*BIGA
      A(KK)=1.ODO/BIGA
   80 CONTINUE
      K=N
  100 K=(K-1)
      IF(K.LE.O)GO TO 150
      I=L(K)
      IF(I.LE.K)GO TO 120
      JQ=N*(K-1)
      JR=N*(I-1)
      DO 110 J=1,N
      JK=JQ+J
      HOLD=A(JK)
      JI=JR+J
      A(JK)=-A(JI)
  110 A(JI)=HOLD
  120 J=M(K)
      IF(J.LE.K)GO TO 100
      KI=K-N
      DO 130 I=1,N
      KI=KI+N
      HOLD=A(KI)
      JI=KI-K+J
      A(KI)=-A(JI)
  130 A(JI)=HOLD
      GO TO 100
  150 RETURN
      END
```

```
C
      SUBROUTINE DGMPRD(A,B,R,N,M,L)
      IMPLICIT REAL*8(A-H,O-Z)
      DIMENSION A(1),B(1),R(1)
      IR=0
      IK=-M
      DO 10 K=1,L
      IK=IK+M
      DO 10 J=1,N
      IR=IR+1
      JI=J-N
      IB=IK
      R(IR)=0.0D0
      DO 10 I=1,M
      JI=JI+N
      IB=IB+1
   10 R(IR)=R(IR)+A(JI)*B(IB)
      RETURN
      END
```

VITA

NAME: TEH CHIN KHUAN

PLACE OF BIRTH: Kulim, Kedah, Malaysia.

YEAR OF BIRTH: 1954

POST-SECONDARY EDUCATION:

1. B.Sc.(Honours) in Physics and Chemistry
   University of London, London, England
2. M.Sc. in Solid State Physics
   University of London, London, England

PUBLICATIONS:

1. Photoluminescence and optical absorption studies of the effects of heat treatment on cuprous oxide, C.K. Teh and F.L. Weichman, Canadian Journal of Physics, 61, 1423 (1983)
2. A mechanism for induced surface degradation of high-resistive GaAs during device fabrication, A.C. Rastogi, C.K. Teh and F.L. Weichman, Canadian Journal of Physics, 63, 740 (1985)
3. A new method of analysis of photoluminescence decay curves, C.K. Teh, C.C. Tin and F.L. Weichman, Journal of Luminescence, 35, 17 (1986)
4. Optical and electrical studies of LEC SI GaAs with different carbon concentrations, C.K. Teh, C.C. Tin and F.L. Weichman
   (Canadian Journal of Physics, May 1987)

Paper submitted for publication:

1. PITS and Photoluminescence studies of copper-

contaminated LEC SI GaAs, C.C. Tin, C.K. Teh, and F.L. Weichman (submitted to Journal of Applied Physics)